UNIVERSITY OF LEÓN

Spectral Mixture Analysis and Object-based Image Analysis for Forestry Applications

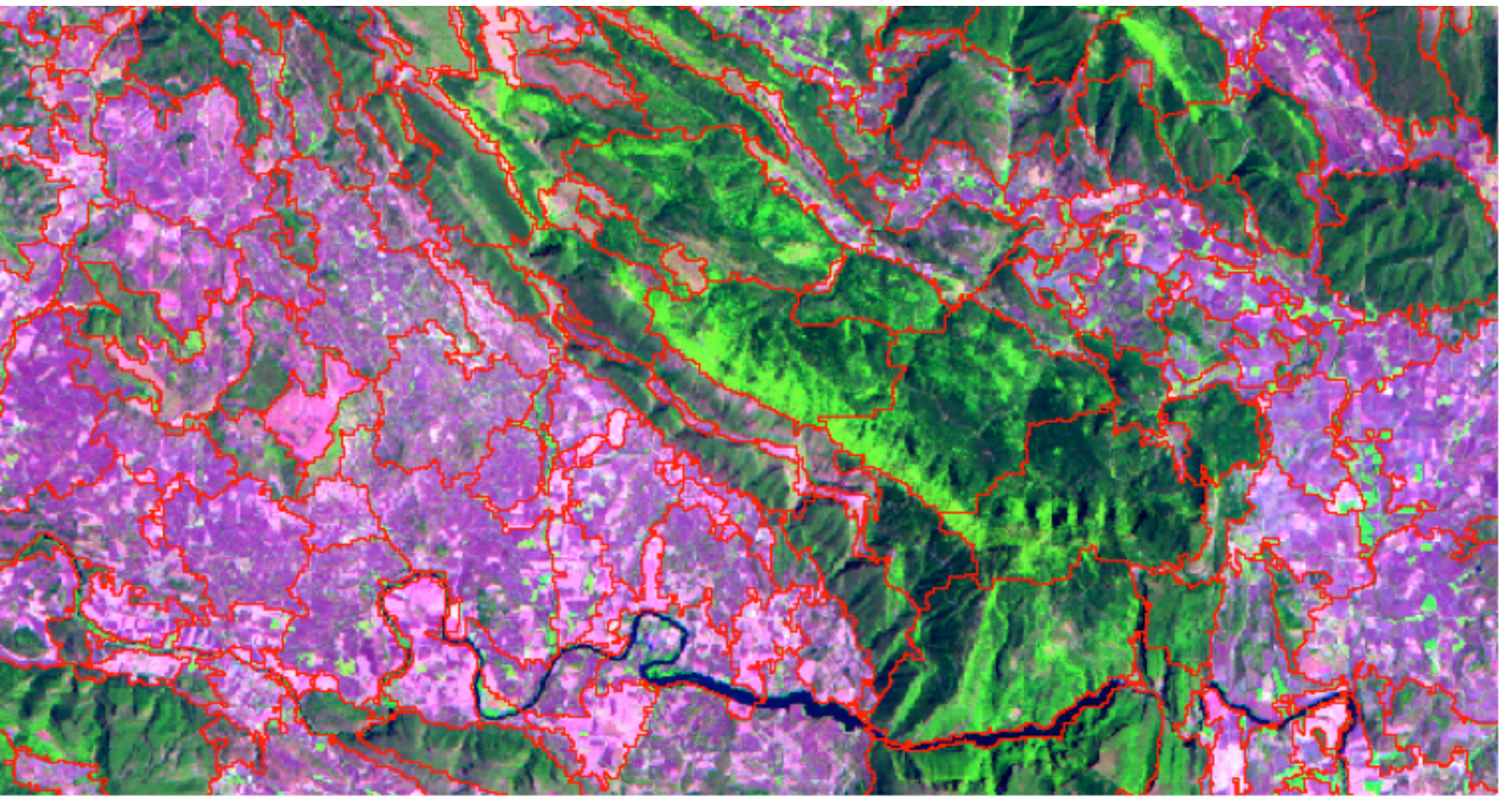

Doctoral Thesis
Óscar Fernández Manso
León, 2015

UNIVERSITY OF LEÓN

UPPER SCHOOL OF AGRICULTURAL ENGINEERING

Spectral Mixture Analysis and Object-based Image Analysis for Forestry Applications

Doctorate programme on Agrarian Technologies

The present thesis fulfils the necessary requisites to obtain the
International Doctorate Mention through the University of León

Academic dissertation

Óscar Fernández-Manso

CONTENTS

ÍNDICE

FOREWORD

This doctoral thesis consists of a series of original research papers. Details for identification of these publications are listed in the paragragh List of Original Papers.

An extended introduction is included in this dissertation for contextualization and linkage of the original research publications, and to help understanding the relevance of the findings. A brief description of the main methods provides an overview of the range of techniques applied, and **it is not intended to give exhaustive details of the work done, which is properly related in specific chapters (publications)**. Likewise, the compilation of specific objectives, summary of results and discussion, provide just a synthesized version of the entire work related in the publications.

ABSTRACT

Remote sensing constitutes a tool of acquiring and processing data and information in forestry applications. Advanced satellite image analysis techniques have potential to be used for monitoring and managing forest. Presently, optical satellite image analysis can be used for a variety of different purposes, and the number of new approaches are constantly increasing.

This doctoral thesis examined the use of optical remote sensing for estimating aboveground biomass (AGB), for mapping wildfire severity, stand conifer volume and forest cover changes by mining activities in Mediterranean forests in Spain. The work focused on studying the usability of linear spectral mixture analysis (LSMA) and/or object-based image analysis (OBIA) as main satellite image processing techniques. The reference data consisted of field measurements and forest inventories. Advanced Spaceborne Thermal Emission and Reflection Radiometer (ASTER), Landsat Thematic Mapper and Landsat Enhanced Thematic Mapper (ETM+) image products are the principal satellite data.

Results indicated that using ASTER fraction images in regression models improve the AGB estimation in Mediterranean pine forests. Similarly, LSMA and regression techniques can be used for quantifying the volume of Scots pine stands in Mediterranean environments. Besides, using a combined-approach based in LSMA and OBIA models for evaluating and mapping fire severity classes achieved higher accuracy, even improving accuracy of individual classes. Those remote sensing techniques demonstrated that can be integrated into the monitoring process, allowing the regulatory agencies responsible for monitoring surface mining and reclamation to do so more efficiently and help avoid or minimize the adverse effects of mining.

The produced digital maps can be integrated as a new source of information in the regional administration geographic information system (GIS) (forestry, civil protection). Although the methods applied were useful for estimating and mapping forest attributes and forest damage, further research incorporating new remote sensing data should be done.

Keywords: aboveground biomass, wildfire severity, forest stand volume, spectral mixure analysis, multiresolution segmentation, object-based classification, multiple linear regression, forest inventory, Mediterranean pine, Scots pine, Landsat ETM+, ASTER, forest-cover changes, mining activities

RESUMEN

La teledetección constituye una herramienta para adquirir y procesar datos e información en aplicaciones medio ambientales. Las técnicas avanzadas de procesamiento digital de imágenes tienen el potencial de ser utilizadas para el seguimiento y gestión de los bosques. En la actualidad, el análisis de imágenes ópticas de satélite puede ser empleado en multitud de estudios, incrementando constantemente el número de nuevos enfoques.

Esta tesis doctoral examinó la aplicación de la teledetección óptica a la estimación de biomasa aérea forestal, a la cartografía de severidad de incendios forestales, a la cartografía de masas de pino silvestre y a la de cambios de cobertura de bosques producida por minería a cielo abierto, en bosques mediterráneos españoles. El trabajo se centró en el estudio de la utilidad del análisis de mezclas espectrales lineales (LSMA) y del análisis de imágenes basado en objetos (OBIA) como principales técnicas para el procesado de imágenes de satélite. Medidas en el terreno e inventarios forestales fueron utilizados como datos de referencia. Imágenes de satélite de los sensores ASTER, Landsat TM y Landsat ETM+ fueron los principales datos satelitales empleados.

Los resultados indicaron que la utilización de imágenes de fracción ASTER en modelos de regresión mejoran la estimación de la biomasa aérea en pinares mediterráneos. Del mismo modo, el análisis de mezclas espectrales junto a técnicas de regresión pueden ser empleados para la cuantificación de volumen en masas forestales de pino silvestre en entornos de transición mediterráneos. Además, a la hora de evaluar y cartografiar los diferentes niveles de severidad de un incendio forestal, la utilización conjunta de LSMA y OBIA consiguieron una mayor precisión, incluso mejorando la de los niveles o clases individuales de severidad. Estas técnicas de teledetección mostraron que pueden ser integradas dentro de procesos de seguimiento, permitiendo a las agencias responsables de la regulación y restauración de explotaciones mineras a cielo abierto, hacer de forma más eficiente sus trabajos y ayudar para evitar o minimizar los efectos adversos de este tipo de minería.

Esta cartografía digital puede ser integrada como nueva fuente de información en los sistemas de información geográfica (SIG) de la administración regional (forestal y protección civil). Aunque los métodos testados presentaron buenos resultados a la hora de estimar y cartografiar atributos y daños forestales y/o medioambientales, es necesario abordar investigaciones adicionales incorporando datos de nuevos sensores.

Palabras clave: biomasa forestal aérea, severidad incendio forestal, volumen masa forestal, análisis de mezclas espectrales, segmentación mutiresolución, clasificación basada en objetos, regresión múltiple lineal, inventario forestal, pino resinero, pino silvestre, Landsat ETM+, ASTER, cambios cubierta forestal, impacto medioambiental, actividades mineras.

ACKNOWLEDGEMENTS

While sitting here the day before I hand in my thesis and looking back all of these years of PhD studies, a lot of memories and thoughts pass by. The device 'the goal is nothing, the road is everything' seems today more true than ever. However, I guess I should start doing what this section is for, namely thanking all the people who have helped me all along this road.

First and foremost I would like to give the credit to my supervisors, Dr. Carmen Quintano and Prof. Dr. Antonio Alfonso Fernández for their unreserved guidance, encouregement and moral support throughout the research work. It was a real opportunity and pleasure to work under their supervision.

I am very grateful to Prof. Dr. Håkan Olsson and Dr. Mats Nilsson for accepting and arranging the possibility to spend nine months at the Dept. of Forest Resource Management and Geomatics, Remote Sensing Laboratory at Swedish University of Agricultural Sciences (SLU) in Umeå (Sweden). I am also very grateful to Prof. Dr. Maggie Kelly for the kindness during my stay at the Dept. of Environmental Sciences, Policy and Management at University of California Berkeley (USA).

I would like to thank the Ministry of Environment of the Castilla y León regional government for its collaboration in this work. This work was in part done under the framework of the L25-04 project: Application of new satellite image processing methodologies to estimate forest resources in Castilla y León, Spain, which is supported by funding of Junta de Castilla y León (Spain). Field inventory data were kindly provided by Servicio Territorial de Medio Ambiente de la Consejería de Fomento y Medio Ambiente de la Junta de Castilla y León, and Ministerio de Agricultura, Alimentación y Medio Ambiente (Government of Spain).

Lastly, my heartfelt appreciation goes to my family, the encouragement from you makes the accomplishment of my work possible. Really, nothing else matters to me.

LIST OF ORIGINAL PAPERS

- Fernández-Manso, O., Fernández-Manso, A., Quintano, C., 2014. **Estimation of aboveground biomass in Mediterranean forests by statistical modelling of ASTER fraction images**. *International Journal of Applied Earth Observation and Geoinformation*, 31, 45–56.
  (DOI: http://dx.doi.org/10.1016/j.jag.2014.03.005)

- Fernández-Manso, O., Quintano, C., Fernández-Manso, A., 2009. **Combining spectral mixture analysis and object-based classification for fire severity mapping**. *Forest Systems,* 18 (3), 296-313.
  (DOI: http://dx.doi.org/10.5424/fs/2009183-01070)

- Fernández-Manso, O., Fernández-Manso, A., Quintano, C., Álvarez, F., 2005. **Mapping forest cover changes caused by mining activities using spectral mixture analysis and object oriented classification**. *ForestSat 2005 -Scientific workshop in operational tools in forestry using remote sensing techniques. May 31 - June 3, 2005, Borås -Sweden-. In Håkan Olsson (ed.) Proceedings of ForestSat 2005 -Scientific workshop in operational tools in forestry using remote sensing techniques*, 8c, 77-81. (ISSN 1100-0295).

- Fernández-Manso, A., Quintano, C., Fernández-Manso, O., dos Santos, J.R., Maldonado, F.D., 2005. **Spectral Mixture Modeling to estimate wood volume in the north of Spain from optical satellite data**. *Ambiência,* 1 (2), 213-222. (ISSN 1808-0251).

1. INTRODUCTION

1.1. Forest and Remote sensing overview

Forests are an important element of the biosphere and a source of many products. New data and non-traditional approaches are needed for monitoring forest condition and dynamics under natural and anthropogenic influences. Earlier research shows that information from satellite images can be used to assess a number of important forest characteristics. Remote sensing technologies have developed at accelerating rates for the past few decades (Boyd and Danson, 2005). The availability of remotely sensed data from different sensors of various platforms with a wide range of spatiotemporal, radiometric and spectral resolutions has made remote sensing as, perhaps, the best source of data for large scale applications and studies. It offers powerful capabilities for understanding, forecasting, managing and decision making about resources (e.g. wood, water, wildlife, recreation, timber management, maintenance and improvement of existing forest stands and fire control and detecting signs of damage of forests by fire, insects or disease, etc). Remotely sensed image data from earth observation sensor systems is widely used in a range of terrestrial and atmospheric applications, such as land cover mapping, environmental modelling and monitoring and updating of geographical databases.

Digital remote sensing data of large regions of the earth's surface became routinely available to a wide range of research institutes, which greatly increased the interest in and development of digital image analysis techniques. Over last decades, numerous algorithms to extract environmental information from remotely sensed images have been designed. Being a well-known statistical technique in other scientific disciplines, pixel-based classification was the first method to be applied to the multispectral digital image data and nowadays still remains as an important tool (Tso and Mather, 2001). In contrast to this method that classify individual pixels directly, more advance algorithms have been developed in order to estimate the abundances of the ground cover types in a mixed pixel, such as spectral umixing technique. Interest in spectral unmixing has greatly increased, which resulted in a wide variety of decomposition techniques and application areas. In remote sensing data applications, linear spectral analysis has been used extensively in past studies for determining urban vegetation abundance (e.g. Demarchi *et al*., 2012; Michishita *et al*., 2012; Deng and Wu, 2013), estimating biophysical parameters such as leaf area index, biomass and net primary productivity (e.g. Zheng *et al*., 2004; Huang *et al*., 2009), mapping burned areas (Quintano *et al*., 2006, 2013; Fernández-Manso *et al*., 2009), mapping surface coal affected areas (Fernández-Manso *et al*., 2012), aboveground biomass estimation (e.g. Soenen *et al*., 2010; Cutler *et al*., 2012; Morel *et al*., 2012; Fernández-Manso *et al*., 2014). Besides, recently, considerable advancements have been made in the development of object-based image analysis (OBIA) (Blaschke *et al*., 2014; Blaschke, 2010; Hay and Blaschke, 2010). The interest of this method has increased with the improvements in image segmentation techniques (Neubert *et al*., 2008; van der Werff and van der Meer, 2008; Wuest and Zhang, 2009), and it has been used for mapping of forest burned areas using Landsat Thematic Mapper (TM) (Mitri and Gitas, 2004), mapping forest fire severity (Mitri and Gitas, 2008; Fernández-Manso *et al*., 2009), mapping land cover for coal fire research (Yan, 2003), forest vegetation studies (Addink *et al*., 2007; Mallinis *et al*., 2008; Pascual *et al*., 2008), land cover/land use (Chen *et al*., 2007; Lackner and

Conway, 2008; Johansen *et al*., 2007), change detection (Desclée *et al*., 2006; Duveiller *et al*., 2008).

1.2. Remote sensing of forest attributes (stand volume, aboveground biomass)

Forest attributes such as volume and biomass have long been estimated using extensive in-field inventory methods or aerial photography volume tables (Avery and Burkhart, 1994). Although field-based methods are typically unbiased, both approaches are time-consuming and expensive. Digital, large-scale remote sensing could provide a less expensive option for estimation of forest biophysical parameters over large tracts, while potentially also providing accurate and unbiased estimates.

Satellite imagery can be used to meet, at various scales, the information requirements of forest managers (Sayn-Wittgenstein, 1986). Satellite imagery has been especially valuable as a source of information for estimating forest conditions across broad landscapes (Maselli *et al*., 2011). The spectral reflectance values contained in the smallest component of a digital image (the pixel), along with other synthetic combinations of these, can be of value in estimating stand-level forest characteristics. These stand-level estimates of forests can then facilitate strategic planning of forested areas where field-based forest inventories are too expensive to obtain (Holmgren *et al*., 2000). Some stand-level forest characteristics, such as timber volume and average tree age, are important for planning and management purposes, while others, aboveground biomass (AGB), are perhaps more important for sustainability and carbon sequestration, carbon accounting, and carbon dynamics purposes. Over the last fifteen years, timber volume, stand age, forest density, tree crown closure, and average tree height have all been estimated to some reasonable degree of accuracy for various parts of the world using Landsat satellite imagery (Trotter *et al*., 1997; Reese *et al*., 2002; Kajisa *et al*., 2008).

Estimating stand-level forest characteristics can be challenging from remotely sensed imagery because as some studies have found, each type of vegetation can emit or reflect different levels of electromagnetic energy. Large set of published research from around the world has focused on AGB estimation. Some examples of these include work performed for forests in India (Roy and Ravan, 1996; Manna *et al*., 2014), Sweden (Fazakas *et al*., 1999; Shendryk, 2014), Brazil, Malaysia, and Thailand (Foody *et al*., 2003; Hamdan *et al*., 2011), the United States (Zheng *et al*., 2004), China (Zheng *et al*., 2007), Canada (Wulder *et al*., 2008) and Spain (Fernández-Manso *et al*., 2014). Hall *et al*. (2006) have observed a non-linear relationship between stand attributes such as AGB and reflectance values from satellite imagery, perhaps due to the typical successional growth trend for most tree species. A number of modeling techniques or analytical tools can be used in conjunction with satellite imagery to estimate stand-level forest characteristics, and in some cases it may be difficult to conclude that one technique is superior to others (Powell *et al*., 2010).

Correlation analysis and various forms of regression have been widely used for estimating forest characteristics (Zheng *et al*., 2007; Ji *et al*., 2012; Ghasemi *et al*., 2013). It seems that regression analyses will generally require as independent variables some transformation (e.g. logarithmic) of the original spectral data or synthetic data (i.e., a composite, or a specific combination of data) derived from various Landsat spectral bands. The k-Nearest Neighbor (kNN) technique of image classification

(Moeur and Stage, 1995) and assignment of stand-level forest characteristics to raster database pixels has been used extensively in Scandinavia for at least 15 years (Gjertsen, 2007), and in North America for nearly a decade (McRoberts, 2012).

Various other analytical techniques have been used in an attempt to estimate stand-level forest characteristics. Conversion tables, for example, that relates a classification (unsupervised, supervised, etc.) of satellite imagery to stand-level forest characteristics, can be employed (Labrecque *et al*., 2006; Luther *et al*., 2006), neural network classification technique has been employed for AGB estimation (Cutler *et al*., 2012; da Silva *et al*., 2014; Lu *et al*., 2014), alternatively, decision trees (Liu *et al*., 2008), object-based process (Chubey *et al*., 2006; Kajisa *et al*., 2009) and regression kriging (Viana *et al*., 2012) have reported promising results. Regarding AGB, previous studies (e.g. Peddle *et al*., 2001; Soenen *et al*., 2010; Morel *et al*., 2012; Fernández-Manso *et al*., 2014) showed the superiority of fraction images derived from LSMA compared to original bands or vegetation indices to estimate biomass from medium spatial resolution imagery. The estimation of AGB seems to benefit greatly with the introduction of field-based measurements even though at times the process can be challenging (Hall *et al*., 2006), and the estimation of timber volume seems to benefit from prior knowledge of average stand heights (Magnusson and Fransson, 2005), since tree height is a key component in many equations for estimating timber volume. Further, ancillary information, such as broad land cover classes (Avitabile *et al*., 2012), inventory plots, or LiDAR data (Lefsky *et al*., 2005; Clark *et al*., 2011; Zolkos *et al*., 2013) may be of value in increasing the accuracy of stand-level forest characterization, particularly in areas that contain a mixture of coniferous and deciduous tree species (McRoberts, 2009). It seems especially useful for estimating forest structures and stand height. Though LiDAR data are limited in terms of coverage over large areas.

1.3. Remote sensing of forest fires

Wildfires as a natural or a human-induced phenomenon has gained importance at regional and global levels. Wildfire activity and intensity has increased in the last decades, as a result of both human influences shaping land use/land cover of the landscape and climate change expressed through extremes and climate shifts. In southern Europe wildfires can be a key factor for the ecosystem dynamics and they can seriously threaten human lives and infrastructures (Scarascia-Mugnozza *et al*., 2000). It is important therefore, to dispose of techniques to efficiently evaluate fire effects in burned areas. Effective fire management strategies are necessary to minimize fire hazard and the consequences of fire spread such as environmental (land degradation, biodiversity loss, desertification), economic and human losses. Monitoring can support post-fire management (e.g. to identify the location and assess the extent of the burned surfaces, to evaluate the damage to the forest stands, to follow vegetation recovery and to plan restoration interventions) and remotely sensed data are a key source of information for supporting these tasks (Chirici and Corona, 2005). Remote sensing and GIS are today, more than ever before, common tools for fire monitoring at local, regional and global levels. Remote sensing technologies can provide useful data for fire management, from fire risk estimation (Gabban *et al*., 2006; Manzo-Delgado *et al*., 2009), fuel mapping (Van Wagtendonk and Root, 2003; Lasaponara and Lanorte, 2006), fire detection (Calle *et al*., 2009; He and Li, 2012; Miettinen *et al*., 2013), to post fire monitoring (Palandjian *et al*, 2009; Huesca *et al*., 2013), including burn area and severity estimation (Gitas and Desantis, 2009; Quintano *et al*., 2013; Fernández-Manso *et al*., 2009).

Methods generally used to estimate fire severity from satellite are based on spectral indices, due to their conceptual simplicity and computational efficiency (Veraverbeke *et al*., 2011), obtained as a combination of bands which emphasize changes induced by fire in vegetation spectral behaviour. Many studies rely on the Normalized Difference Vegetation Index (NDVI) as a spectral index (Veraverbeke *et al*., 2010; Harris *et al*., 2011). Numerous modifications of the NDVI have been derived to reduce atmospheric sensitivity and background variability (Veraverbeke *et al*., 2011). Other spectral indices have been developed specifically to detect post-fire effects: the Burned Area Index (BAI) (Chuvieco *et al*., 2002), the Char Soil Index (CSI) (Smith *et al*., 2005), the Mid Infrared Burn Index (MIRBI) (Trigg and Flasse, 2001) and the Normalized Burn Ratio (NBR) (Key and Benson, 2006; Soverel *et al*., 2010). As well as spectral indices, linear transformation techniques have been used for the multi-temporal mapping of burn severity. Patterson and Yool (1998) compared two linear transformation techniques, the Kauth–Thomas (KT) and principal components (PC) transforms, for mapping burn severity. The KT or "Tasselled Cap" transform is sensitive to fire-induced changes in the moisture content of soil and vegetation and, in this study, produced betters result than the PC transform. Other approaches to retrieve burn severity from satellite imagery have been proposed. Some of them are based on radiative transfer models, which provide a more physical basis to estimate this variable (Chuvieco *et al*., 2007; de Santis and Chuvieco, 2007, 2009; de Santis *et al*., 2009, 2010). Recent research has highlighted subpixel-based methods as one such alternative (Hudak *et al*., 2007; Lentile *et al*., 2006, 2009; Smith *et al*., 2007). Chuvieco (2002) and Caetano *et al*. (1994) concluded that LSMA proved to be efficient in detecting the charcoal signal even in lightly burned areas that kept a strong vegetation signal, a situation that is typically considered to be problematic. LSMA was considered advantageous over vegetation index-based methods, due to its improved capability to distinguish burns from other bare or sparsely vegetated areas (Caetano *et al*., 1996; Díaz-Delgado *et al*., 2001). This technique was also successful applied by Díaz-Delgado and Pons (1999) and Rogan and Franklin (2001) to carry out the burn severity classification. A few burn severity studies have been carried out in the Mediterranean Basin (e.g. de Santis and Chuvieco, 2007; Fernández-Manso *et al*., 2009; Veraverbeke *et al*., 2010; Quintano *et al*., 2013).

1.4. Remote sensing of forest cover changes by mining activities

Land cover refers to the observed (bio)physical cover of the Earth's surface, the description of vegetation being a key component of it (Di Gregorio, 2005). Land cover and vegetation have a central role in the climate, hydrology and biogeochemical cycling. They also provide humans with a vast natural resource base. Information on land cover and land use change (LCLUC) is required to understand and manage the environment at variety of spatial and temporal scales. It is essential for monitoring global change and for sustainable management of natural resources. It is also input data for a range of environmental models (Jiang *et al*., 2014; Song *et al*., 2014). Furthermore, policy-driven needs, particularly the international agreements, motivate the production of land cover information for the climate models, quantification of carbon cycle and biodiversity assessments (Rosenqvist *et al*., 2003; Turner *et al*., 2004).

Satellite remote sensing provides capabilities for gathering land cover information over large areas in a synoptic and spatially explicit manner. The science- and policy-driven needs for land cover information, the unprecedented variety of remotely sensed data, and improved computing resources and data analysis tools have created new opportunities for major improvements in the global and regional land cover

characterization (Townshend *et al*., 2012; Tan *et al*., 2013). Remote sensing also provides information to assess the state of forests and to manage forest resources in a sustainable manner (Franklin, 2010).

Information about mining activities location is essential for environmental applications, specifically the temporal and spatial patterns of LCLUC. Surface mining in particular may lead to severe environmental degradation. From an environmental point of view, it is a transforming activity with a high number of detrimental consequences, namely soil erosion, acid-mine drainage and increased sediment load as a result of abandoned and un-reclaimed mined lands (Parks *et al*., 1987; Rathore and Wright, 1993; Latifovic *et al*., 2005).

Quantification of the effects that mining activities have on ecosystems is a major issue in sustainable development and resources management (Latifovic *et al*., 2005). Generating an environmental database for carrying out environmental surface mining impact assessment is a difficult task by conventional methods. Due to its synoptic coverage and repetitive data acquisition capabilities, remote sensing has become an effective alternative to conventional methods for monitoring surface mining. Advancements in satellite imagery analysis provide possibilities to investigate new approaches for LCLUC detection caused by surface mining. Compared to other environmental land cover changes studies, such as forest fires, fewer studies (e.g. Rathore and Wright, 1993; Schmidt and Glaesser, 1998; Lévesque and Staenz, 2008; Schroeter, 2011) have evaluated the potential of remote sensing for monitoring environmental impacts in mining areas.

Various techniques have been used in an attempt to study land cover changes caused by surface mining activities, such as, Support Vector Machine (SVM) (Townsend *et al*., 2009), Artificial Neural Networks (ANN) (Charou *et al*., 2010), LSMA (Fernández-Manso *et al*., 2005a; Lévesque and Straenz, 2008; Ritcher *et al*., 2008; Shang *et al*., 2009), and multiple endmember spectral mixture analysis (MESMA) (Fernández-Manso *et al*., 2013).

2. OBJECTIVES

Given the advantages of using remotely sensed data for forestry applications, the integration of image analysis techniques such as LSMA and OBIA is a possible approach to generating maps over large areas. Bearing in mind this question the final goal of the thesis was to evaluate the potential of LSMA and/or OBIA techniques for improving the result's accuracy for forestry applications.

Once having revised some preliminary works related to LSMA and/or OBIA as main satellite image techniques, it appeared that to start from, the following questions that should be answered:

1) How can the study of forest attributes such as AGB be estimated in a regional scale in a cost-effective way?. How much biomass is stored in a Mediterranean pine forest?.

2) How can be estimated fire severity in large forest fires in a cost-effective way?. What would be one of the most adequate ways to estimate fire severity in large Mediterranean fire scars using remote sensing techniques?. Are there any synergies combining LSMA and OBIA as main image analysis techniques?.

3) How can be monitored surface mining activities in large areas at low cost?. Which role does play remote sensing techniques for quantifying forest cover changes caused by mining activities?. Could this approach be considered for monitoring effective reclamation?.

4) How do remote sensing techniques estimate wood volume in conifer stands?. How do fraction images improve the results?. How much volume is stored in Scots pine forests in Mediterranean areas?.

Accordingly, this thesis focuses on four targets which are approached in the corresponding chapters:

1) Quantification of Mediterranean pine (*Pinus pinaster* Ait.) AGB at compartment level using fraction images from LSMA as independent variables in multiple linear regression models using Advanced Spaceborne Thermal Emission and Reflection Radiometer (ASTER) satellite data.

2) Estimating fire severity classes of large forest fires with medium spatial resolution satellite imagery, using a combined approach based in a LSMA and OBIA, and comparing with other approaches in order to evaluate the suitability to distinguish between the fire severity classes into the fire scars.

3) Mapping human-induced lanscape transformation in mined sites by means of Landsat ETM+, using a combined approach based in a LSMA and OBIA, ancillary data was useful for distinguishing with other land use classes.

4) Combining National Forest Inventory field plots and remotely sensed data, improving results using fraction images from unmixing Landsat TM satellite data and, quantifying Scots pine stands volume by means of regression models.

3. OUTLINE OF THE THESIS

The *first block* of this doctoral thesis serves as introduction and describes information about data (ground, satellite imagery and auxiliary) and, the main image analysis techniques applied on Chapters I to IV, focusing on LSMA, OBIA models and image regression in order to understand how work those main methods.

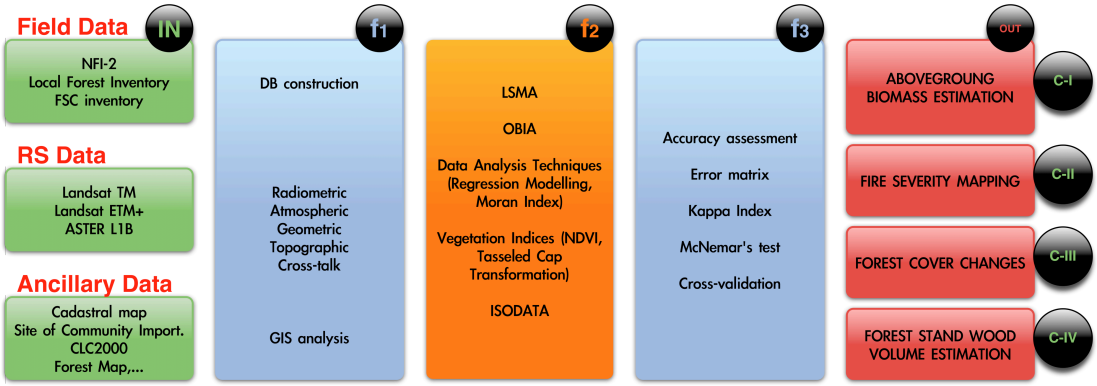

IN: input dataset; f1: dataset preparation; f2: image analysis; f3: analysis validation process; OUT: outputs; SMA: Spectral Mixture Analysis; OBIA: Object-based Image Analysis; CLC2000: Corine Land Cover 2000; NFI: National Forest Inventory; FSC: Fire Severity Classes; NDVI: Normalized Difference Vegetation Index; ISODATA: Iterative Self-Organizing Data Analysis Technique; C-I...IV: Chapter I...IV.

Figure 1. Overall thesis diagram

The *second block* of the thesis summarises the results, discussion and conclusions.

The *last block* aims specifically at the use of LSMA and/or OBIA for forestry applications (Chapters I to IV). Specifically, Chapter I corresponds to a paper published on the *International Journal of Applied Earth Observation and Geoinformation* based on the estimation of aboveground biomass in Mediterranean forests by statistical modelling of ASTER fraction images (Fernández-Manso *et al*., 2014). In Chapter II, synergies between LSMA and OBIA methods were found for fire severity mapping. This study is based on the paper published on the scientific journal *Forest Systems* by (Fernández-Manso *et al*., 2009). Next, Chapter III is the paper published in the proceedings of *FORESTsat'05* (Operational tools in forestry using remote sensing techniques) related with mapping forest cover changes caused by mining activities using mixture analysis and object oriented classification (Fernández-Manso *et al*., 2005a). Finally, in Chapter IV, it is discussed an unmixing method of Landsat TM data for wood volume estimation in conifer stands. It is based in the paper published on *Ambiência* (Fernández-Manso *et al*., 2005b).

A basic diagram of the development of this thesis, datasets used, tools and analysis carried out is shown in Figure 1. In the corresponding chapters, a more detailed scheme of specific procedures is shown.

4. GENERAL DESCRIPTION OF STUDY AREAS

Castilla y León autonomous community (Spain) is the place where are located the four studies carried out along this thesis (Figure 2).

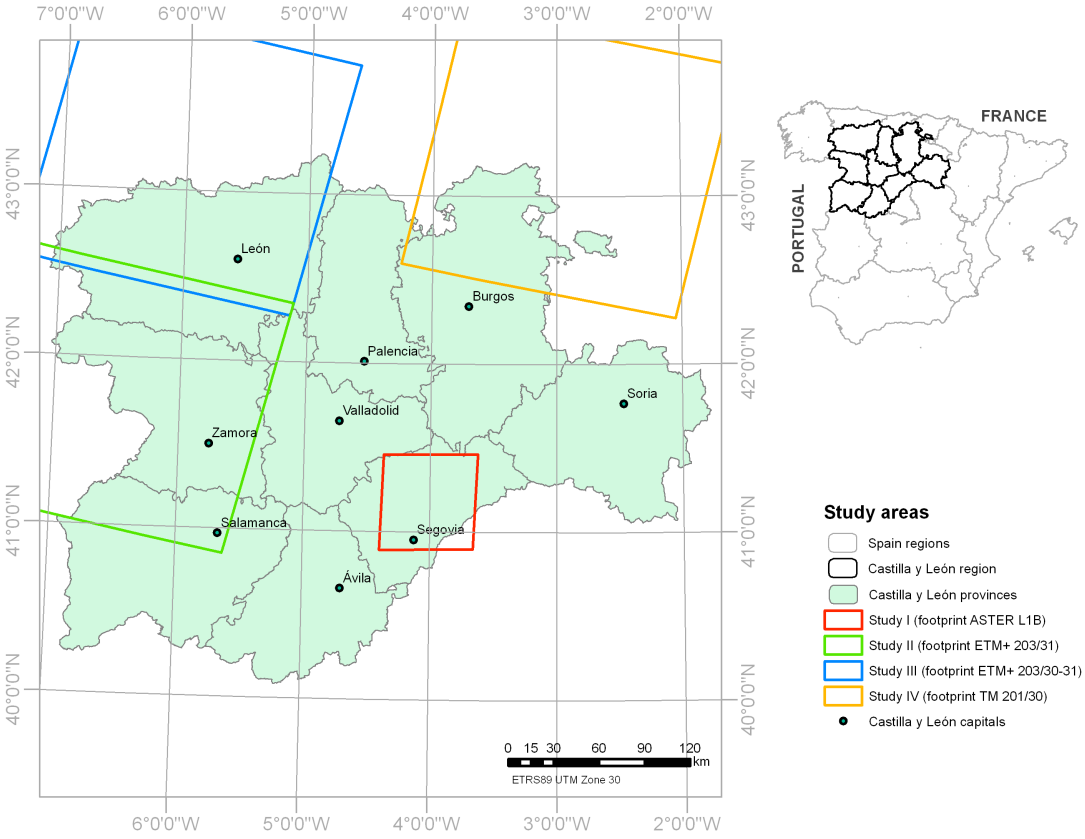

Figure 2. Location of study areas

This region is placed as the largest in Spain (94 225 km²) and one of the largest of the European Union. (Figure 3). It is located at the north side of the Iberian Plateau and is compound by nine provinces (Ávila, Burgos, León, Palencia, Salamanca, Segovia, Soria, Valladolid and Zamora). Castilla y León is surrounded by impressive mountain chains and by generous plains. With an average altitude over the sea level of 830 m, the higher peaks are over 2 500 m.

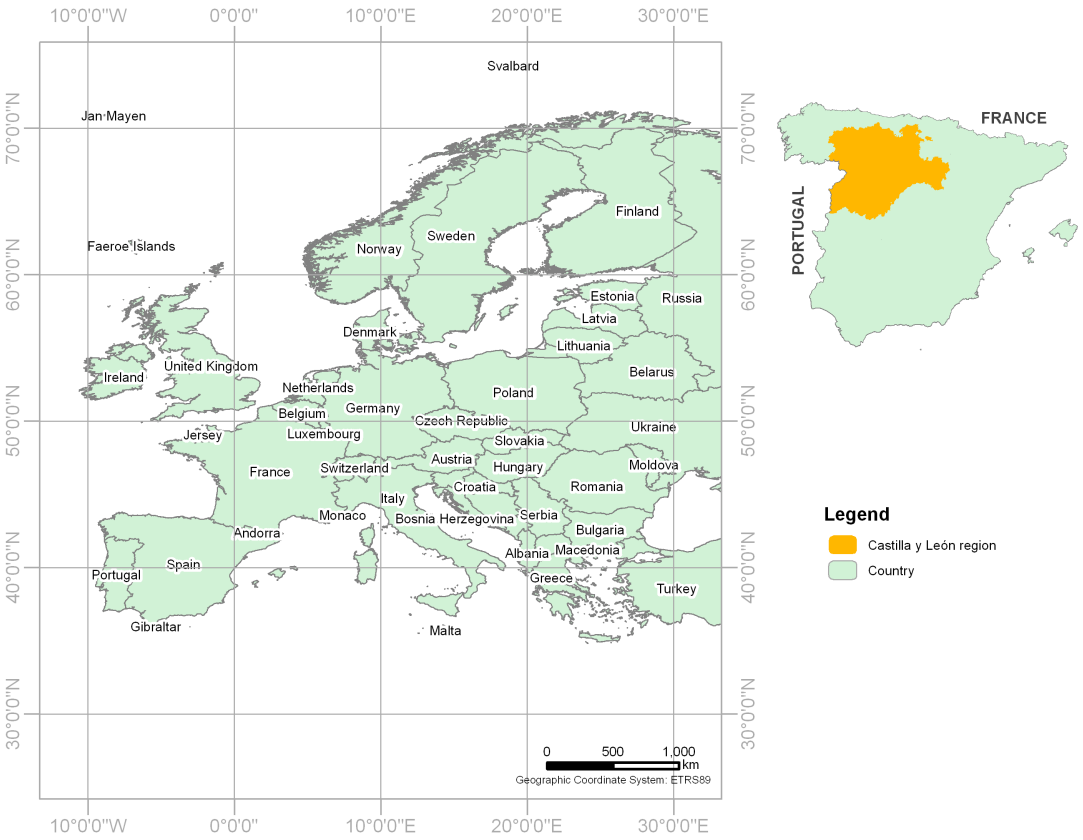

Figure 3. Castilla y León location

The region is located in the Duero basin that is, with no doubt, the most important river in Castilla y León (near 600 km crossing it from east to west). Castilla y León has an oceanic continental climate, characterised by cold winters and hot summers with short periods of spring and autumn. The maximum temperatures range from 39 ºC in the hot months to 12 ºC below zero in winter months, being the average temperature of almost 12 ºC. Total rainfalls are running from 371 mm/year (Salamanca province) to 698 mm/year (Burgos province) (AEMET, 2014).

The diversity of natural spaces to be found in Castilla y León single it out as one of the most complete regions of nature in the whole of Western Europe. Castilla y León contains 40 Natural Parks managed within the programme "Parques Naturales de Castilla y León", under the shelterhood of the "Red de Espacios Naturales" ("Natural Areas Network"). In this extraordinary mosaic of environmental diversity and quality, the mountains, plains and river valleys provide home to a wide range of ecosystems of wildlife and, above all, an environment where human population centres can continue to coexist within the Natural Areas .

5. DATA SOURCES

5.1. Field data

Field measurements were carried out using objective unbiased inventory methods. In the Chapters I and IV the inventories were performed by sample plots allocated systematically in a quadratic grid (200 m and 1 000 m, respectively) with a random starting-point. On Chapter I, field data were taken from a forest inventory carried out by Castilla y León Forest board and on Chapter IV the ground data from the Second National Forest Inventory (NFI2) was used. Plots from the Spanish National Forest Inventory (SNFI) were selected with BasIFor 2.0 (Bravo *et al*., 2005), software dedicated to handle the SNFI provincial databases for research, management, and planning (Bravo *et al*., 2002). It enables selection of data based on location, species, or structural parameters, calculates volumes and growth, and facilitates SNFI2 and SNFI3 data comparison. Spatial location of data is facilitated by identification of plot coordinates. GIS tools assisted in location and geo-processing for analysis of inventory data. The inventory conducted in the study of Chapter II was designed for estimating qualitative degree of fire severity, where sample plots were placed randomly positioned across the entire fire scar. The field survey plots were sized, with an average area of 0.78 ha (100 m diameter). Non-field measurements were performed for the identification of places with mining affectation since they were taken from digital photographies and other ancillary data (Chapter III).

5.2. Satellite image data

The analyses were based on optical satellite images from sensors TM and ETM+ of Landsat satellite program and from ASTER sensor onboard of TERRA satellite.

Landsat program

The Landsat program was the first to launch an Earth-observing satellite with the express intent to study and monitor our planet's landmasses (Lauer *et al*., 1997). Back in 1972 when Landsat 1 was launched, it was called Earth Resources Technology Satellite (ERTS). With seven satellites successfully launched, the program has acquired imagery covering all but the highest polar latitudes during more than forty years, contributing to the longest and most geographically comprehensive record of the Earth's surface ever assembled (Wulder *et al*., 2012). Technical characteristics of all segments (spacecraft, sensors, ground station, and data transfer) have evolved over the years, improving the spectral, spatial, temporal, and radiometric resolution of the data, refining the instruments' calibration (Irons and Masek, 2006), and establishing an optimized plan called Long Term Acquisition Plan for acquisition of global imagery (Arvidson *et al*., 2006). Landsat 8 was launched in February 2013, assuring the continuity of monitoring programs. Further operational missions (Landsat 9 and 10) are intended to follow (Loveland and Dwyer, 2012) and will provide continuity of comparable measures.

The spectral, radiometric, and spatial characteristics of the optical components of sensors onboard all Landsat satellites (Multi Spectral Scanner (MSS), TM, ETM+, and Operational Land Imager (OLI)) are presented in Table 1.

Table 1. Landsat sensors characteristics

	MSS			TM			ETM+			OLI		
	#Band	Width (µm)	GSD (m)	#Band	Width (µm)	GSD (m)	#Band	Width (µm)	GSD (m)	#Band	Width (µm)	GSD (m)
Visible										1	0.43-0.45	30
				1	0.45-0.52	30	1	0.45-0.52	30	2	0.45-0.51	30
	4 (1)	0.5-0.6	68x83	2	0.52-0.60	30	2	0.52-0.60	30	3	0.52-0.60	30
	5 (2)	0.6-0.7	68x83	3	0.63-0.69	30	3	0.63-0.69	30	4	0.63-0.68	30
NIR	6 (3)	0.7-0.8	68x83	4	0.76-0.90	30	4	0.76-0.90	30	5	0.84-0.88	30
	7 (4)	0.8-1.1	68x83									
SWIR				5	1.55-1.75	30	5	1.55-1.75	30	6	1.56-1.66	30
				7	2.08-2.35	30	7	2.09-2.35	30	7	2.10-2.30	30
Pan							8	0.50-0.68	30	8	0.50-0.68	15
SWIR										9	1.36-1.39	30

Terra satellite

TERRA is the flagship of the Earth Observing System (EOS), a series of spacecraft that represents a step in NASA's role to observe Earth from the unique vantage point of space. It was launched into sun-synchronous Earth orbit on December 18, 1999, and started sending data back to earth in February 2000. Terra carries five scientific instruments: ASTER, CERES, MISR, MODIS, and MOPITT, and it is being used to obtain detailed maps of land surface temperature, reflectance and elevation.

The ASTER instrument consists of three separate instrument subsystems: Visible and Near Infrared (VNIR), Shortwave Infrared (SWIR) and, Thermal Infrared (TIR). (Figure 4). The *VNIR subsystem* operates in three spectral bands at visible (green and red) and near-IR wavelengths, with a resolution of 15 m and provides 8-bit data (Band 1 to 3). The *SWIR subsystem* operates in six spectral bands in the near-IR region through a single, nadir-pointing telescope that provides 30 m resolution and 8-bit data (Band 4 to 9). The *TIR subsystem* operates in five bands in the thermal infrared region using a single, fixed-position, nadir-looking telescope with a resolution of 90 m and provides 12-bit data (Band 10 to 14). (Abrams and Hook, 2002).

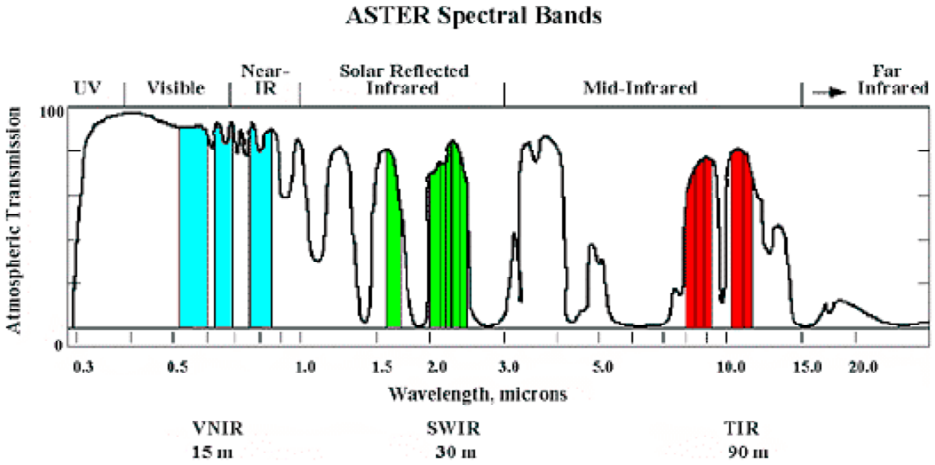

Figure 4. The spectral range of each band (courtesy NASA)

5.3. Ancillary data

5.3.1. Digital aerial orthophotography

The orthoimages employed were acquired from the 'Vitivinícola' (1999-2001) and 'SIGPAC' (2002) plans (prior to National Plan of Aerial Orthophotography, PNOA (2004- nowdays). These images have a spatial resolution of 0.7-0.5 m/pixel and 3 spectral bands: red (R), green (G) and blue (B).

5.3.2. National Topographic Map

The cartographic series of the National Topographic Map at a scale of 1:50 000 (MTN50), these days produced through software procedures, it is successor to the Map of Spain at a scale of 1:50 000, the publication of which was initiated in 1875 by what was then the Geographic and Statistical Institute.

Currently, the MTN50 project is based on digital data provided by the National Topographic Map at a scale of 1:25 000 (MTN25), which is composed by the basic state cartography. The four fourths that form the sheet of the MTN50 are merged to exploit the layered information structure. Codes identify each geographic element and there must be continuity in the adjoining sheets. Software is used that allows content to derive from one scale to another, selecting, extracting and adapting the original information by a process of cartographic generalization that is partly automatic and partly manual, and that produces the MTN50.

5.3.3. Digital Elevation Model

It is a representation of a surface's topography stored in a numerical format. Each pixel is has been assigned coordinates (UTM 30N) and an altitude. Digital Elevation Model (DEM) is the preferred term. Generated from the National Topographic Base by altimetry of 25-grid.

5.3.4. Cadastral information

The modern Spanish Land (Rural) Cadastre has been built using othophotos as basic cartography. Conventional ones were at scales 1:2 000 and 1:5 000, depending on the land division in each area, and digital ones pixel 0.5 or 1 m. The land parcels are drawn on the orthophotos and checked on the spot, taking field information on owners and crops. The lines are vectorized and parcel areas are calculated as a result of the digital process.

The Spanish Land (Rural and Urban) Cadastre was primarily designed for taxation purposes. However, other uses became more and more important, especially for the Rural Cadastre. When it was time to renew our cadastres, the use of cadastral information by the Agrarian Administration for the control and monitoring of EU CAP subsidies had become very important, so it was taken into account in the design of the new cadastral system.

Now, the Spanish Rural Cadastre is a modern GIS currently available in more than 80% of territory, being the remains in conventional maps.

5.3.5. National Forest Inventory

SNFI is based on permanent plots (Continuous Forest Inventory, CFI) and it has been performed since 1986 (Second SNFI). The CFI consists of regularly spaced permanent sample plots. It has a stratified systematically sampling design, in which the strata are derived from existing maps by grouping polygons of the forest map. Principal criteria for the stratification are species and forest types (Martínez-Millán, 1997).

The design is efficient for estimating both current values and rates of change. It is also expensive, however, since the permanent plots must be well maintained in the field, and the same plots are located and measured on every occasion. Another disadvantage is that the system can not easily be adapted to future estimates of different precision (Cunia, 1981). Others European countries such as Austria, Belgium, Germany, Italy and Netherlands have widely applied it for more than 40 years.

5.3.6. Spanish National Forest Map

Spanish National Forest Map at 1:50 000 (MFE50) is presented as a map for using in a wide range of applications in the field of environmental management, national forest inventory (it participates as a thematic and cartographic base), inventory of habitats and species, protection against forest fires, combating erosion and desertification, etc.

Like the SNFI has a term of ten years, covering five provinces on average per year.

5.3.7. Corine Land Cover

Corine Land Cover 2000 (CLC2000) was a project jointly managed by the Joint Research Centre (JRC) and the European Environment Agency (EEA). Its aim is to update the Corine Land Cover (CLC) database in Europe for the year 2000. Landsat ETM+ satellite images were used for the update and were acquired within the framework of the Image2000 project. The first CLC inventory for the EU-15 and most of the new Member States was implemented between 1985 and 1996. It was carried out in order to characterise the land surface. A uniform nomenclature across Europe at scale 1:100 000 was used. The CLC nomenclature basically includes land cover items though land elements can also be found. This is especially the case for built-up environments (Heymann *et al*., 1994; Bossard *et al*., 2000). The CLC database is a digital map covering countries with a seamless polygon database with 25 ha minimum mapping unit (MMU). The CLC nomenclature includes 44 categories in five major groups. In addition to the updated CLC2000 there are also other national deliverables: land cover changes between the 1990s and 2000 (CLC-Change), revised first CLC inventory (revised CLC90) and metadata (EEA-ETC/TE, 2002).

5.3.8. Site of Community Importance

The continuing deterioration of natural habitats and the threats posed to certain species are one of the main concerns of EU environment policy. The Habitats Directive, is intended to help maintain biodiversity in the Member States by defining a common framework for the conservation of wild plants and animals and habitats of Community interest. A Site of Community Importance (SCI) is defined in the European Commission Habitats Directive (92/43/EEC) as a site which, in the biogeographical region or regions to which it belongs, contributes significantly to the maintenance or restoration at a favourable conservation status of a natural habitat type or of a species

and may also contribute significantly to the coherence of Natura 2000, and/or contributes significantly to the maintenance of biological diversity within the biogeographic region or regions concerned. They are proposed to the Commission by the State Members and once approved, they can be designed as Special Areas of Conservation (SACs) by the State Member. No later than six years after the selection of a site of Community importance, the Member State concerned must designate it as a special area of conservation.

6. SATELLITE IMAGE PREPROCESSING

The use of digital satellite image data for a spatial database requires several preprocessing procedures. These procedures include, but are not limited to: radiometric correction, geometric correction, terrain correction, image enhancement, and feature selection. The goal of digital image preprocessing is to increase both the accuracy and the interpretability of the digital data during the image-processing phase (Peddle *et al*., 2003).

The main preprocessing techniques applied to the optical satellite images used in the studies are the following.

6.1. Subsetting the image

In some cases, satellite image scenes are much larger than a project study area. In these instances it is beneficial to reduce the size of the image file to include only the area of interest. This not only eliminates the extraneous data in the file, but it speeds up processing due to the smaller amount of data to process. This is important when utilizing multiband data such as TM, ETM+ or ASTER. This reduction of data is known as subsetting. This process cuts out the preferred study area from the image scene into a smaller more manageable file.

Subsetting of the image was applied on satellite images of Chapter I, Chapter II, Chapter III and Chapter IV.

6.2. Geometric correction

Remotely sensed raw images contain geometric distortions specific to the acquisition system, mainly related to sensor orientation and viewing angle, sun elevation, and atmospheric effects. Every system geometric distortions require a particular correction approach prior to analysis or integration with other spatial data. Systematic distortions introduced by the instrumentation (e.g. skew caused by Earth rotation effects, variation in ground resolution cell size due to the scanning system) are corrected at ground receiving stations or image distributors, but distortions related to specific acquisition time and location (e.g. topographic relief) require correction by the user.

In this work Landsat TM, ETM+ and ASTER images were rectified to the local and accurate spatial reference system using a set of ground control points (GCPs). A first-order polynomial warp function was applied and a nearest-neighbour resampling protocol was used. This method has the advantage of simplicity and the ability to preserve original values in the unaltered scene (Jensen, 2005), and compared to bilinear interpolation and cubic convolution, it is computationally the most effective, although it may create perceptible positional errors (Campbell, 2002). Geometric correction involves the reorientation of the image data to selected parameters. This includes the selection of a map projection system and the co-registration of satellite image data with other data layers that may be used in a GIS. This will allow for accurate spatial assessments and measurements of the data generated from the satellite imagery. All satellite images were reprojected to Universal Transverse Mercator (UTM) map projection and co-registered by image-to-image rectification with a National Topographic Map. The map coordinate system used was Datum European 1950 UTM 30N.

Geometric correction was applied on satellite images of Chapter I, Chapter II, Chapter III and Chapter IV.

6.3. Radiometric correction

Radiometric image processing is aimed to transform raw data (i.e. radiant energy coded by intensity and spectral character) as captured by the sensor into at surface reflectance suitable for applications. Radiometric processing includes sensor radiometric calibration, surface reflectance retrieval based on atmospheric corrections, image normalization to provide radiometric consistency across multiple scenes and/or dates, and specialized corrections for surface terrain induced variations (Peddle *et al*., 2003). A robust radiometric calibration of images is essential in change detection applications (Coppin *et al*., 2004; Lu *et al*., 2004), and it is crucial if images are to be related with biophysical phenomena (Gong and Xu, 2003) like forest structure, health, biomass, or successional development. This task becomes especially challenging when various sensors are included in the analysis (Roder *et al*., 2005).

The radiometry of satellite sensors is evaluated periodically to account for changes produced after pre-launch calibration. Onboard systems, pseudo-invariant targets and cross-sensor approaches are used for calibration, and coefficients to transform digital numbers into radiance and at sensor (top of atmosphere-TOA) reflectance are provided in user manuals (Chander *et al*., 2009). The reduction in scene-to-scene variability is an advantage of reflectance over radiance, due to the removal of the cosine effect of different solar zenith angles, the compensation for different values of the exoatmospheric solar irradiance, and the correction for variation in the Earth-Sun distance between different data acquisition dates.

An atmospheric radiation transfer model was used to produce and estimate of the true surface reflectance (Lu, 2006). To accurately compensate for atmospheric effects, the atmospheric correction model applied was the MODTRAN-based Fast line-of-sight Atmospheric Analysis of Spectral Hypercubes (FLAASH) (Matthew *et al*., 2000). Thermal infrared data were not used.

Radiometric correction was applied on satellite images of Chapter I, Chapter II, Chapter III and Chapter IV.

6.4. Topographic normalization

Topographic effects hinder the use of remote sensing of mountainous terrain (Colby, 1991). Depending on the elevation of the sun and the orientation of the terrain, shadows cause a loss of information in satellite images. Topographic normalization, or topographic correction, refers to the compensation of the different solar illuminations due to the irregular shape of the terrain. This effect causes a high variation in the reflectance response for similar vegetation types: shaded areas show less than expected reflectance, whereas in sunny areas the effect is the opposite (Riaño *et al*., 2003).

The main difficulty in applying topographic corrections is related to the lack of standard and generally accepted models. A wide variety of methods have been proposed in the literature (e.g. cosine correction, spectral rationing, empirical-statistical method of Teillet, Minnaert correction or, C-correction) however, there is no clear consensus on methods that may be universally applicable (Minnaert, 1941; Short, 1982; Teillet *et al*., 1982; Civco, 1989; Colby, 1991; Conese *et al*., 1993; Meyer *et al*., 1993).

C-correction had been developed from the cosine illumination correction but introduces an adjusted offset derived from the regression of the digital number against the calculated sun incidence angle which should model the diffuse sky radiation (Teillet *et al*., 1982; Meyer *et al*., 1993). The application of these method required the use of a high resolution (25 metre in *x* and *y* and 0.1 m for elevation) Digital Elevation Model (DEM) provided by IGN. A C-correction model was developed using ERDAS Imagine® Model Maker and applied on satellite images of Chapter II (Figure 5).

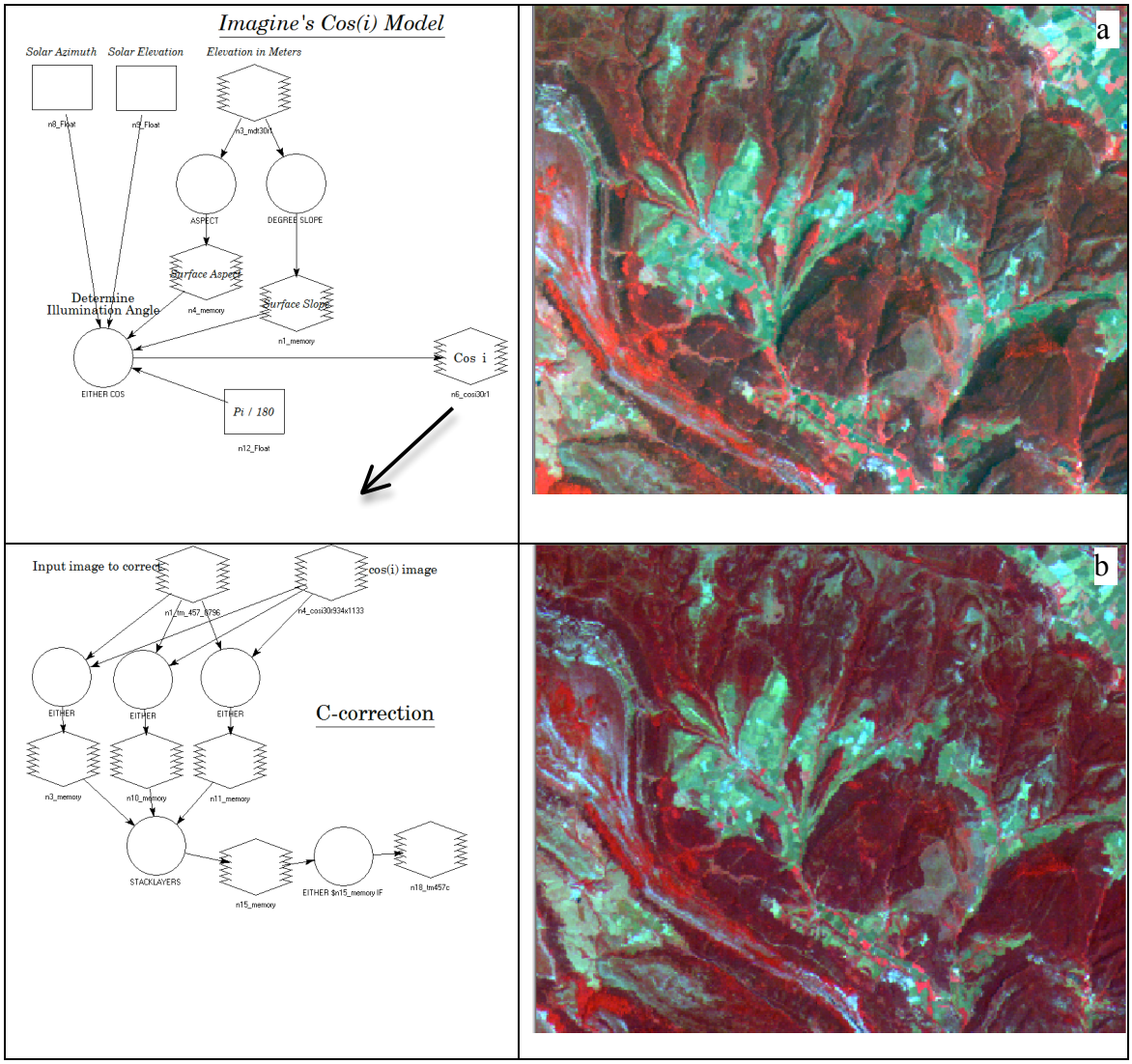

Figure 5. Terrain illumination correction by means of C-correction algorithm developed using ERDAS Imagine® Model Maker; (a) Original TM image, (b) Topographic corrected TM image

Teillet *el al*. (1982) describe the possibility of bringing the original data into the form LT= m cos(i) + b. This corresponds to a regression line used in the statistical-empirical approach with the reflectance on the ordinate and *cos (i)* on the abscissa. Teillet *et al*. (1982) now introduce a parameter *c* which is the quotient of *b* and *m* of the regression line (Equation 1). Parameter *c* is built in the cosine law as an additive term (Equation 2):

$$c = \frac{b}{m} \qquad [1]$$

$$L_H = L_T \left[\frac{\cos(sz) + c}{\cos(i) + c} \right] \quad [2]$$

where: c = correction parameter; m = inclination of regression line; b = intercept of regression line; LH = reflectance observed for horizontal surface; LT = reflectance observed over sloped terrain; sz = sun's zenith angle; i = sun's incidence angle in relation to the normal on a pixel (Figure 6).

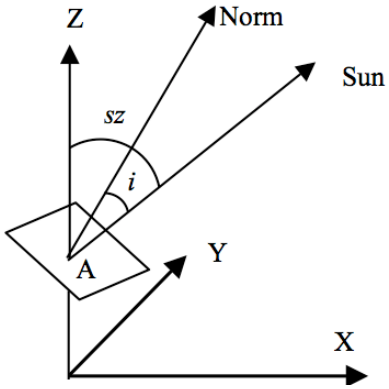

Figure 6. Terrain illumination diagram (source: Teillet *et al*., 1982)

According to Teillet *et al*. (1982) the parameter *c* might emulate the effect of path reflectance on the slope-aspect correction, but the physical analogies are not exact. Mathematically, the effect of *c* is similar to that of the Minnaert constant (Minnaert, 1941). It increases the denominator and weakens the overcorrection of faintly illuminated pixels as a consequence. Parameter *c* is determined with the same regression that used in the statistical-empirical approach (Ekstrand, 1996).

6.5. Crosstalk correction

Originally, the word "crosstalk" came from telecommunication, referring to the phenomenon that signals of other lines get mixed. In remote sensing, the word refers to the phenomenon that the electrical or optical signals of a band leaks into another band.

In some images observed by ASTER SWIR sensor, weak ghosts appear near border of water and land areas (Iwasaki *et al*., 2002).

The ASTER SWIR sensor is affected by a crosstalk signal scattering problem, a phenomenon discovered after the launch of ASTER aboard the TERRA platform in December 1999. The source of the crosstalk problem is the ASTER Band 4 detector, whose incident light is reflected by the detectors aluminum-coated parts (especially from the area between the detector plane and band-pass filter), and it is then projected on to the other detectors. The problem is further worsened by the band-to-band parallax effect and the distance between the CCD array pairs. Bands 9 and 5 are most affected because of their closeness to the Band 4 detectors. The spectral range of Band 4 is between 1.6 and 1.7 microns (0.092 μm bandwidth), which is not only the widest

bandwidth of the SWIR bands (average of 0.052 μm bandwidth for Bands 5 through 9), but is also the strongest in its reflectivity component (Tonooka and Iwasaki, 2003).

The Japanese Science team developed the original crosstalk correction algorithm that is used to correct an ASTER Level-1B data set. The original model is based on the fundamental understanding that incident radiation to Band 4 that is reflected or leaked to the other bands will follow a certain pattern of line-shifts in the along-track direction. The kernel function used in the convolution (in the original algorithm) is not considered symmetrical in the cross-track direction. Improved kernel functions are used in the updated algorithm. The radiometric sensitivity coefficients are statistically derived to ensure that a calibration consistency is maintained in both pre- and post-crosstalk correction. Using the Japanese crosstalk correction algorithm, the ASTER Project at Jet Propulsion Laboratory (JPL) has implemented a crosstalk-correction process that is applied to ASTER Level-1B data before deriving the reflectance product (Iwasaki and Tonooka, 2005).

Crosstalk correction was applied on satellite image of Chapter I.

7. SATELLITE IMAGE ANALYSIS TECHNIQUES

7.1. Spectral Mixture Analysis technique

While multispectral sensing has largely succeeded at classifying whole pixels, further analysis of the constituent substances that comprise a pixel is limited by a relatively low number of spectral measurements. The recognition that pixels of interest are frequently a combination of numerous disparate components has introduced a need to quantitatively decompose, or "unmix," these mixtures.

Multi- and hyperspectral sensors have demonstrated the capability of performing spectral unmixing. Mixed pixels are a mixture of more than one distinct substance, and they exist for one of two reasons. First, if the spatial resolution of a sensor is low enough that disparate materials can jointly occupy a single pixel, the resulting spectral measurement will be some composite of the individual spectra. This is the case for remote sensing platforms flying at a high altitude or performing wide-area surveillance, where low spatial resolution is common. Second, mixed pixels can result when distinct materials are combined into a homogeneous mixture. This circumstance can occur independent of the spatial resolution of the sensor, thus the mixed pixel problem is not solved simply by increasing the spatial resolution (Keshava and Mustard, 2002). Besides, the number of mixed pixels usually decreases as the spatial resolution increases. However, in some cases this number can increase because the finer detail resolves features not recorded before, thus introducing new spectral classes (Campbell, 2002).

In this manner, the pixel reflectance cannot be simply interpreted in terms of properties of a single cover type and the conventional classification (hard classification) of mixed pixels leads to errors that make the subsequent area estimation inaccurate. These errors are caused mainly by the premise of classification that all pixels are pure, i.e. consisting of a single ground cover type, while in fact they are not. Alternatively, spectral unmixing can be applied, after which a mixed pixel can be assigned to several categories proportionally to the fraction of its area covered by each class. Therefore, spectral unmixing may reduce the mixed pixel problem (Adams *et al*., 1995; Shimabukuro *et al*., 1998; Lu *et al*., 2003). On the other hand, spectral unmixing cannot be only considered as a classifier but also as a data transformation. This process can reduce the bands number of satellite data in a similar way that Principal Components Analysis (PCA) does, and furthermore the new bands have a physic meaning so can be interpreted more easily.

7.1.1. Linear versus Nonlinear Mixing

The mixing process can be considered linear or nonlinear. The combination will be basically linear if endmembers in a pixel appear in spatially segregated patterns. In this case, the scattering and absorption of incident electromagnetic radiation for any region on the surface is dominated by a single component on the surface, and thus the spectrum of a mixed pixel is a linear combination of the endmember spectra weighted by the fractional area coverage of each endmember in the pixel. However, if the components of interest are in an intimate association (the endmember materials are mixed on spatial scales smaller than the path length of photons in the mixture, like sand grains of different composition in a beach deposit) light will typically interact with more than one

component as it is multiply scattered, and the mixing process between these different components will be nonlinear. There are some important implications of these differences for spectral unmixing. If a linear mixing model is used on data where the combination is nonlinear, the calculated fractions will be significantly in error (Borel and Gerstl, 1994; Ray and Murray, 1996). However, despite the obvious advantages of using a nonlinear approach for intimate mixtures, this has not been widely applied to remotely acquired data of particulate surfaces, the most important obstacle to implementing nonlinear models is that the particle size, composition, and alteration state of the endmembers are very important controlling parameters of the solutions, and the linear approach has been demonstrated in numerous applications to be a useful technique for interpreting the variability in remote sensing data and a powerful means for converting spectral information into data products that can be related to the physical abundance of materials on the surface (Keshava and Mustard, 2002).

The LSMA is usually written in matrix-vector notation as (Equation 3):

$$X = Mf + e \qquad [3]$$

If the number of spectral bands and ground cover types are given by *n* and *c* respectively, then *X* represents a (*n*x1) pixel vector or multispectral observation, while, *f* denotes the (*c*x1) fractions vector with the proportions of the different ground cover types. Each column of (*n*x*c*) matrix *M* contains an endmember spectrum, which is the reflectance typical for a pixel containing nothing but the cover type of interest. *e* represent the error term.

These mixing equations are usually accompanied by two constraints that should be satisfied explicitly when estimating *f*. The full additivity constraint is that a pixel is well defined by its components, whose proportions should therefore add up to unity: $\Sigma f_i = 1$. The other constraint that should be satisfied is the nonnegativity constraint, which says that no component of a mixed pixel can make a negative contribution: $f_i \geq 0$. Satisfaction of the latter constraint is often difficult and may require some specialised techniques.

Together, the mixing equations and the constraints describe a model that must be solved for each mixed pixel that is to be decomposed, i.e. given *X* and *M*, it is necessary to determine *f* and *e* subject previous equations. Two alternatives can be basically used to solve the mixing equations: numerical methods and statistical methods. However, different authors (Shimabukuro, 1987; Kalluri *et al*., 1997) affirmed that the algorithm employed to perform unmixing had little influence in results.

7.1.2. Algorithms for Linear Unmixing

As mentioned before, LSMA allows decomposing each pixel of the image in its basic components from the endmembers spectra. The endmembers spectra must have recognizable characteristics in the scene and must be significant for the observer, since they constitute abstractions of real objects that have the same or similar properties. In many cases, the number of components and its composition are unknown, and the problem is to unmix spectrally the data in a number supported by the data dimension.

The estimation of the endmember spectra is not an easy work, since they change with the scale and the purpose of study. These spectra are also influenced by processes as for example the material surface dispersion and the illumination geometry, which could be considered additional noise sources of the model. Nevertheless, and as it is affirmed by Tompkins *et al*. (1997), all the advantages of LSMA depend on how accurately the endmembers spectra are defined. If the endmembers are incorrect in physical sense, the proportions or fractions will be also incorrect, and potentially without meaning, and spectral mixture analysis will contribute just like any other method of statistical analysis.

In order to be able to distinguish completely two endmember spectra, it is necessary that they are orthogonal; in this manner, they will be linearly independent and completely spectrally separable. If these vectors are almost linearly dependent, some vectors will be linear combinations of other ones and, therefore, spectrally inseparable. Nevertheless, as indicated by Sohn and McCoy (1997), endmembers spectra are habitually non-orthogonal, although they are sufficiently distant to be distinguished. Van der Meer and De Jong (2000) studied also the spectral unmixing dependency with the endmembers spectra orthogonality. These authors observed that error disappears when all the endmembers existing in the image are considered and correctly characterized. Their experiments demonstrated that the amount of information in selected endmembers (standard deviation) in relation with the duplicated information (correlation among them) affects the unmixing error. Since it is impossible to improve the amount of information in image data, they recommended achieving some decorrelation of the data using readily available transformations (as the Minimum Noise Fraction (MNF) transformation).

In general, it is advisable to reduce the dimension of the data in the scene although this step is optional using multispectral data. Dimension reduction algorithms do not reduce the dimension of data with the goal of reconstructing an approximation to the original signal. Instead, they seek a minimal representation of the signal that sufficiently retains the requisite information for successful unmixing in the lower dimension. Dimension reduction algorithms are designed to minimize errors in the procedures performed in the lower dimension. The more habitually employed reduction algorithms are PCA and MNF.

PCA is used to guide image endmember selection because it puts almost 90% of the variances on the first two or three components and minimizes the influence of band to band correlation (Smith *et al*., 1985). However, noise variance in one band may be larger than signal variance in another band in terms of unequal scaling in different bands (Small, 2001). Therefore, PCA cannot necessarily order components according to signal information. Unlike PCA, MNF transformation orders components according to signal to noise ratios (Green *et al*., 1988). MNF transformation can be considered two cascaded PC transformations given the following steps: 1) a PC transformation is performed to diagonalize the noise covariance matrix; 2) the noise covariance matrix is converted to an identity matrix by scaling the transformed dataset; and 3) a second PC transformation is conducted on the scaled dataset. Among these steps, a difficult task is to estimate the error covariance matrix. Some sensor calibration measurements or ground reflectance measurements may provide the error covariance matrix (Lee *et al*., 1990). However, these measurements are not generally available. Green *et al*. (1988) provided a Minimum/Maximum Autocorrelation Factors (MAF) procedure to estimate the noise covariance matrix directly from images assuming that noise is spatially uncorrelated while signal is highly correlated over space.

Once decided the bands used in the unmixing process, it is necessary to fix the number and the characteristics of endmembers. The key to linear unmixing is to define a set of spectral endmembers that are representative of physical components on the surface and that encompass the spectral variability inherent in a given scene. The number of endmembers that can be distinguished by the sensor is therefore constrained by the number of spectral channels available as well as the wavelengths spanned by the bands. Dimensionality is ultimately limited by the number of spectral bands but noise and redundancies in the bands information content may result in a dimensionality that is less than the full potential dimensionality implied by the number of bands (Small, 2004). Thus, the number of endmembers that may be practically identified and used is far fewer than the number of bands plus one, typically ranging from three to seven, depending on the number of channels and the spectral variability of the scene components. (Keshava and Mustard, 2002).

None of the existing methods to obtain endmembers spectra is perfect. Some methods simply extract them from the satellite image using the spectral signature of the ground cover considered (Bierwith, 1990). Other techniques assume that endmembers spectra are enclosed within a geometric figure whose vertices number agrees with the dimension of the scene. Nevertheless, although these methods guarantee that fractions will be suitably obtained, they presuppose that endmembers are contained in the data set. This last fact is not always realistic, since it is difficult to find pure zones (covered by an only material) in images of low spatial resolution. For this reason, other methods to obtain endmembers spectra have been developed when they cannot be extracted from the image. For example: spectral matching; using an expert system, Qmodel, fuzzy logic algorithms, parallel coordinates representations, etc.

Settle and Campbell (1998) indicated that two work schemes to obtain endmembers spectra exist. The first one uses reflectance values extracted from spectral libraries, this kind of endmember is called *reference endmember*. The main disadvantage of this option is that image correction is not trivial and errors are always introduced. The second option uses information from own image to define endmembers spectra and it is refering to *image endmembers*. Image endmembers presents two advantages: 1) they are easily obtained and, 2) they have the same scale of measurement as the data.

Each alternative presents its advantages and disadvantages and it will be necessary to choose the most suitable option in each situation. According to Drake *et al*. (1999), reference endmembers has the advantage of being pure and therefore fractions obtained will be absolute. Besides, Settle and Drake (1993) indicated that image endmembers contain image noise, which allows calculating the error associated with that noise, impossible calculation with reference endmembers. Gong *et al*. (1994) also made comparisons between reference and image endmembers. When employing image endmembers, the root mean square error (RMSE), was uniformly distributed indicating that all image had the same accuracy level. However, when using reference endmembers, certain linearity in distribution of error term was observed.

Reference endmembers utilization forces to calibrate the image, which not always is simple. For this reason, image endmembers are preferred in many cases. Nevertheless, reference endmembers employment can be advisable in some occasions like changes analysis. Adams *et al*. (1995) affirmed that it is essential to have endmembers invariant in the time when detecting temporal changes and therefore, they recommend reference endmembers use in that case. Also Roberts *et al*. (1997) analyzed temporal changes and unmixing, and recommend reference endmembers adoption.

Different alternatives exist to select endmembers from spectral libraries. Van der Meer (1995) identified twelve candidate endmembers and stored them in a spectral library specially constructed taking measurements from field. Next, he used Spectral Angle Mapper (SAM) technique (Kruse *et al*., 1993), to select the five definite endmembers. This technique calculates the spectral similarity between a candidate reflectance spectra and a reference reflectance spectra in terms of the angle between both spectra. Drake *et al*. (1999) used spectral matching method to select endmembers from a spectral library. Schmid *et al*. (2004) also performed an identification of the image endmembers by matching field spectra from the spectral library with the image endmember spectra. Thus, the spectral curve matching allowed soil properties and ancillary data to be associated with the final identification of a wetland component. In occasions, spectral libraries are employed primarily to identify the composition of image endmembers. Roberts *et al*. (1993) used the two steps technique described by Smith *et al*. (1990). In the first stage, the original image is modelled as a mixture of image endmembers. In the second step, image endmembers are modelled as mixtures of reference endmembers, after calibration terms were calculated.

Image endmember selection is achieved through an educated trial-and-error approach. An analyst has some knowledge of the field site or data set, and a set of objectives for conducting the analysis. For example, results should be repeatable, and the fraction images should describe realistic physical variables or components in the scene. It is advisable to choose them as the extreme values of the scatter diagram of two bands of the considered image. This allows assuring that endmembers are spectrally distinguishable and that the chosen bands present a sufficiently low correlation. Different methods to obtain image endmember exist: from scatter plots (Carpenter *et al*., 1999; Peterson and Stow, 2003), using regression techniques (Metternicht and Fermont, 1998) and finer spatial resolution imagery, etc. In many situations, however, an automated method of determining these essential components is desired. Several techniques have been developed to estimate endmembers that do not require specific assumptions on the probabilistic densities of the data. Examples of automated methods are: Clustering Algorithms, Modified Spectral Mixture Analysis (MESMA), Geometric Perspective, etc. The Pixel Purity Index (PPI®) is a common one (Boardman, 1993) due to its publicity and availability in the Environment for Visualizing Images (ENVI) software (ENVI, 2000). This algorithm uses the MNF as a pre-processing step to reduce dimensionality and to improve the Signal-to-Noise Ratio (SNR). The algorithm then projects every spectral vector onto "skewers" (large number of random vectors). The points corresponding to extremes, for each "skewer" direction, are stored. A cumulative account records the number of times each pixel is found to be an extreme. The pixels with the highest scores are the purest ones. Chang and Plaza (2006) proposed a fast iterative algorithm to implement the PPI, referred to as Fast Iterative PPI (FIPPI) which is an unsupervised algorithm as opposed to the PPI, which requires human intervention to manually select a final set of endmembers. The experiments showed that both the FIPPI and the PPI produce very close results, but the FIPPI converges very rapidly with significant savings in computation.

Finally, it is also possible to use unsupervised algorithms to define the endmembers. García-Haro *et al*. (1999) tried three new methods to identify the number and the spectral signature of endmembers. Two of the methods consist in different optimization procedures based on objective functions defined from the coordinate axes of the dominant factors. The third one consists in the design of a neural network whose architecture implements the spectral mixture analysis principles. Results indicated that

the three methods provide accurate estimations of the spectral endmembers, especially the third one. Moreover, the second method, based on the exploration of the mixture positions in the factor space, demonstrated to be the most appropriate when the dimensionality of the data is reduced. Bateson *et al*. (2000) presented a new approach to image endmembers definition where endmember variability is incorporated into mixture analysis by representing each endmember by a set or bundle of spectra, each of which could reasonably be the reflectance of an instance of the endmember.

The class of inversion algorithms based on minimizing squared-error start from the simplest form of least squares inversion and increase in complexity as further assumptions and parametric structure are imposed on the problem. Variations of the least squares concept have been adopted to reflect the unique circumstances associated with hyperspectral data. The *Least Squares solution* is the method most often used for solving the linear mixture model (Smith *et al*., 1990; Shimabukuro and Smith, 1991; García-Haro *et al*., 1996) due to its simplicity and ease of implementation. The statistical method analogue of least squares estimation minimizes the variance of the estimator and it is called *Minimum Variance Method* (Manolakis *et al*., 2000).

In the dissertation' study cases, the root mean square error (RMSE) was used to assess the fit of the model (Adams *et al*., 1993; Roberts *et al*., 1998) and it is shown in Equation 4, where *m* is the number of bands.

$$RMSE = \sqrt{\left(\sum_{b=1}^{m} \varepsilon_b^2\right) / m} \qquad [4]$$

LSMA was applied in Chapter I to obtain the fraction images and using them as independent variables in multiple linear regression models to estimate aboveground biomass. Fraction imagery was employed in Chapter II and Chapter III as input in a object-based image classification model and used for segmentation process. And, in Chapter IV, fraction image was used as independent variable in a regression equation and for estimating wood volume.

7.2. Object-based Image Analysis technique

OBIA is a technique used to analyze digital image that was developed reletively recently compared to traditional pixel-based image analysis (Burnett and Blaschke, 2003). It is based to partitioning remote sensing imagery into meaningful image-objects (segments), and assessing their characteristics through spatial, spectral and temporal scale. Those image objects are the basic processing units, and not single pixels as in a pixel-based image analysis approach (Benz *et al*., 2004). (Figure 7).

Figure 7. Pixels versus objects image analysis (source: Benz *et al*., 2004)

At its most fundamental level, OBIA requires image segmentation, attribution, classification and the ability to query and link individual objects (segments) in space and time. In order to achieve this, OBIA incorporates knowledge from a vast array of disciplines involved in the generation and use of GIS. It is this unique focus on remote sensing and GIS that distinguishes OBIA from related disciplines such as Computer Vision and Biomedical Imaging, where outstanding research exists that may significantly contribute to OBIA (Hay and Castilla, 2006). Hay and Castilla (2008) argue that Geographic space is intrinsic to this analysis, and as such, should be included in the name of the concept and, consequently, in the abbreviation: ‘‘Geographic Object-Based Image Analysis’’ (GEOBIA). The acronyms OBIA and GEOBIA, which stand for geospatial object based image analysis, are both herein used interchangeably.

OBIA aims at scene representations at several levels of resolution, thus relying on segmentation results at multiple scales. Multiscale denotes the multiple spatial dimensions at which entities, patterns and processes can be observed and measured (Hay *et al*., 2005). A crucial point is the appropriateness of object generation, which is a matter of choosing the ‘right’ scale. This scale has to be translated to appropriate segmentation parameters (typically based on spectral homogeneity, size, or both) for the varying sized, shaped, and spatially distributed image-objects composing a scene, so that segments can be generated that satisfy user requirements (Hay *et al*., 2005; Lang 2005; Mallinis *et al*., 2008).

Object-based image techniques have opened the door to technically implement the way of human perception. Common region-based segmentation algorithms are limited in delineating higher-level objects that consist of high contrast, but regularly appearing objects. Those arrangements which are characterised by regularity in their heterogeneous structure are hardly captured by segmentation algorithms, whereas readily detectable for humans (Lang and Langanke, 2006). As stated by Navon (1977), a scene is rather decomposed than built-up: since segmentation routine is starting usually working in either direction (bottom-up or top-down), it can hardly mimic the way of visual processing, namely to start from a global analysis of the overall pattern and to proceed to finer structures. The segmentation of the image data at fine and coarse scales is important in the object-based multiscale analysis, in order to extract boundaries of the dominant objects occurring at the corresponding scales (Hall *et al*., 2004). The resulting objects of the segmentation can then be described and classified by an extensive variety of its features related to the color, texture, form, and horizontal and vertical context properties. The OBIA classifiers using eCognition™ software (Definiens imaging) are soft classifiers that are based on fuzzy logic, using membership to express

an object's assignment to a class. A simple Nearest Neighbour (NN) classifier might be used as well (Figure 8).

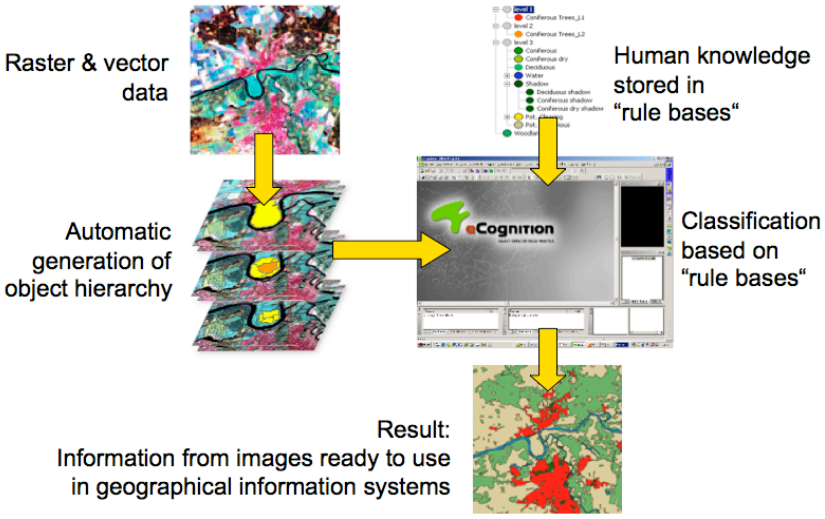

Figure 8. Object-based image analysis process summary (source: Baatz *et al*. (2004))

The object-based approach has the advantanges over the pixel-based approach in twofold (Liu and Xia, 2010): (1) the change of classification units from pixels to image objects reduces within-class spectral variation and generally removes the so-called salt and pepper effects that are typical in pixel-based classification and, (2) a large set of features characterizing objects' spatial, textural, and contextual properties (neighbour, super-object) can be derived as complementary information to the direct spectral observations to potentially improve classification accuracy (Baatz *et al*., 2004; Guo *et al*., 2007).

OBIA approach has its own limitations as well. Two types of errors often exist in image segmentation including over-segmentation and under-segmentation (Möller *et al*., 2007; Kampouraki *et al*., 2008) and these segmentation errors could affect the subsequent classification process in two ways: (1) under-segmentation results in image objects that cover more than one class and thus introduce classification errors because all pixels in each mixed image object have to be assigned to the same class and (2) features extracted from mis-segmented image objects with over-segmentation or under-segmentation errors do not represent the properties of real objects on the Earth surface (e.g. shape and area), so they may not be useful and could even reduce the classification accuracy if not chosen appropriately (Song *et al*., 2005). Therefore, the final performance of object-based classification is determined by both positive and negative effects due to the use of image objects as classification units and the addition of objects' features in classification.

7.2.1. Multiresolution segmentation (Multiscale)

For many years, procedures for image segmentation have been a main research focus in the area of image analysis. Many different approaches have been followed. However, few of them lead to qualitatively convincing results which are robust and applicable under operational settings. To obtain useful information from an image, the segmentation process splits an image into unclassified 'object primitives' that form the basis for the image objects and the rest of the image analysis. Objects, formed by grouping pixels according to a certain criterion of heterogeneity and homogeneity by

image segmentation, are the basic processing units in object-based image analysis approach (Benz *et al*., 2004). This segmentation can be realized as an optimization process. Regions of minimum heterogeneity given certain constraints have to be found. Criteria for heterogeneity, definition of constraints and the strategy for sequence of aggregation determine the final segmentation result (Figure 9).

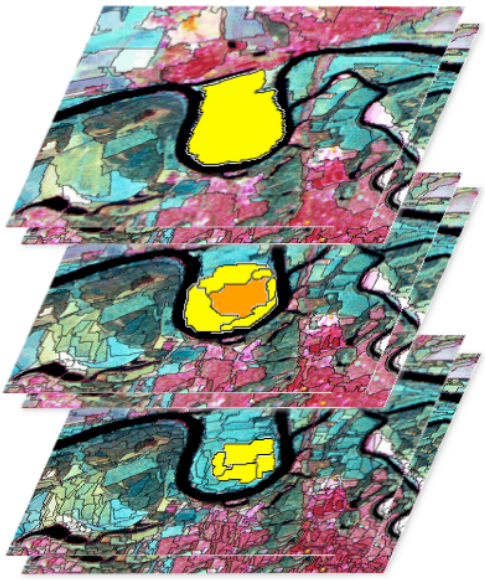

Figure 9. Context and hierarchical relation in multiresolution segmentation (source: Baatz et al. (2004))

Image segmentation methods are split into two main domains (Baatz *et al*., 2004): knowledge driven (top-down) methods and data driven (bottom-up) methods. On the one hand, in top-down approach it is known what to extract from the image, but not how to perform the extraction. By formulating a model of the desired objects, the system tries to find the best methods of image processing to extract them. On the other hand, bottom-up methods are kind of data abstraction or data compression, because in the beginning the generated segments are only 'image object primitives' (as with clustering methods). It groups pixels to spatial clusters that meet certain criteria of homogeneity and heterogeneity and the user determines what kind of real world objects the generated image objects represent. The basic difference between both approaches is that top-down methods usually lead to local results because they just mark pixels/regions that meet the model description, whereas bottom-up methods perform a segmentation of the complete image.

Two of the most common bottom-up approaches to image segmentation are (1) region growing algorithms and (2) knowledge-based approaches (Baatz *et al*., 2004):

(a) *Region growing algorithms* cluster pixels starting from a limited number of single seed points. These algorithms basically depend on the set of given seed points and often from a lack of control in the break-off criterion for the growth of a region.

(b) *Knowledge-based approaches* try to incorporate knowledge derived from training areas or other sources into the segmentation process. These approaches mostly perform a pixel-based classification, based on clustering in a global feature space. Segments are produced implicitly after classification, simply by merging all adjacent pixels of the same class. These approaches are typically not able to separate different units or objects of interest of the same classification. Further, the information on which classification can act typically is limited to spectral and filter derivates.

The method used in this dissertation is a bottom-up advanced region growing and knowledge-based multi-resolution segmentation approach implemented in eCognition™ software (Baatz *et al*., 2004). The algorithms are based on the conceptual idea that important semantic information required to interpret an image is not represented in single pixels but in meaningful image objects and their mutual relations, i.e. the context. The segmentation algorithm starts with one-pixel objects, and in many subsequent steps smaller image objects are merged into larger ones.

Throughout this pair-wise clustering process, the underlying optimization procedure minimizes the weighted heterogeneity $n \cdot h$ of resulting image objects, where n is the size of a segment and h a parameter of heterogeneity. In each step, that pair of adjacent image objects is merged which results in the smallest growth of the defined heterogeneity. If the smallest growth exceeds the threshold defined by the scale parameter, the process stops.

Definition of heterogeneity

Heterogeneity in eCognition™ considers as primary object features color and shape. The increase of heterogeneity f (Equation 5) has to be less than a certain threshold. The weight parameters (w_{color}, w_{shape}) allow adapting the heterogeneity definition to the application.

$$f = w_{color} \cdot \Delta h_{color} + w_{shape} \cdot \Delta h_{shape} \qquad [5]$$

$$w_{color} \in [0,1]; \qquad w_{shape} \in [0,1]; \qquad w_{color} + w_{shape} = 1$$

where w_{color} is the weight of color parameter, w_{shape} is the weight of shape parameter, Δh_{color} is the difference in spectral heterogeneity, and Δh_{shape} is the difference in shape heterogeneity.

Difference in spectral heterogeneity (Δh_{color}) is defined in Equation 6 (Benz *et al*., 2004). The spectral heterogeneity allows multi-variant segmentation by adding a weight w_c to the 'C' image channels.

$$\Delta h_{color} = \sum_c w_c (n_{merge} \cdot \sigma_{c,merge} - (n_{obj\_1} \cdot \sigma_{c,obj\_1} + n_{obj\_2} \cdot \sigma_{c,obj\_2})) \qquad [6]$$

where Δh_{color} is the difference in spectral heterogeneity, w_c is the weight to the image channels c, n_{merge} is the number of pixels within merged object, n_{obj_1} is the number of pixels in object 1, n_{obj_2} is the number of pixels in object 2, and σ_c is the standard deviation within object of channel c. Subscripts merge refer to the merged object, object 1 and object 2 prior to merge, respectively.

The shape heterogeneity (Δh_{shape}) is a value that describes the improvement of the shape with regard to smoothness and compactness of an object's shape, and it is calculated using Equation 7 (Benz *et al*., 2004). Thus, the smoothness heterogeneity (Δh_{smooth}) (Equation 8) equals the ratio of the factor border length l and the border length b given by the bounding box of an image object parallel to the raster (Benz *et al*., 2004). The compactness heterogeneity (Δh_{compt}) equals the ratio of the border length l and the square root of the number of pixels forming this image object (Equation 9) (Benz *et al*., 2004). The weights (w_i) are parameters which can be selected in order to get suitable segmentation results for a certain image data stack and a considered application.

$$\Delta h_{shape} = w_{compt} . \Delta h_{compt} + w_{smooth} . \Delta h_{smooth} \quad [7]$$

with

$$\Delta h_{smooth} = n_{merge} . \frac{l_{merge}}{b_{merge}} - \left(n_{obj\_1} . \frac{l_{obj\_1}}{b_{obj\_1}} + n_{obj\_2} . \frac{l_{obj\_2}}{b_{obj\_2}} \right) \quad [8]$$

$$\Delta h_{compt} = n_{merge} . \frac{l_{merge}}{\sqrt{n_{merge}}} - \left(n_{obj\_1} . \frac{l_{obj\_1}}{\sqrt{n_{obj\_1}}} + n_{obj\_2} . \frac{l_{obj\_2}}{\sqrt{n_{obj\_2}}} \right) \quad [9]$$

where Δh_{shape} is the shape heterogeneity, Δh_{compt} is the compactness heterogeneity, Δh_{smooth} is the smoothness heterogeneity, w_{compt} is the compactness parameter weight, w_{smooth} is the compactness parameter weight, n_{merge} is the number of pixels within merged object, l_{merge} is the border length of the merged object, n_{obj_1} is the number of pixels in object 1, n_{obj_2} is the number of pixels in object 2, l_{obj_1} is the perimeter of object 1,l_{obj_2} is the perimeter of object 2, b_{obj_1} is the perimeter of object 1's bounding box, and b_{obj_2} is the perimeter of object 2's bounding box.

Scale parameter

The scale parameter is the stop criterion for optimization process. Prior to the fusion of two adjacent objects, the resulting increase of heterogeneity *f* is calculated (Equation 5). If this resulting increase exceeds a threshold *t* determined by the scale parameter, $t = \Psi$ (scale parameter), then no further fusion takes place and the segmentation stops. It is an abstract term, which determines the maximum allowed heterogeneity for the resulting image objects. The larger the scale parameter, the more objects can be fused and the larger the objects grow. Details can be found in Baatz *et al*. (2004).

Hierarchical object network

Objects created on different scales can be linked together to a hierarchical object network like the one displayed in Figure 10. The levels of image objects are generated by the described multi-resolution segmentation described above. All segmentation procedures operate on arbitrary levels in a strong hierarchical network. To guarantee a definite hierarchy over the spatial shape of all objects the segmentation procedures follow two rules (Benz *et al*., 2004):

1) Object borders must follow borders of objects on the next lower level.
2) Segmentation is constrained by the border of the object on the next upper level.

Since the level of pixels and the level of the whole image always exist by definition, each segmentation of a new level is a construction in between a lower and an upper level.

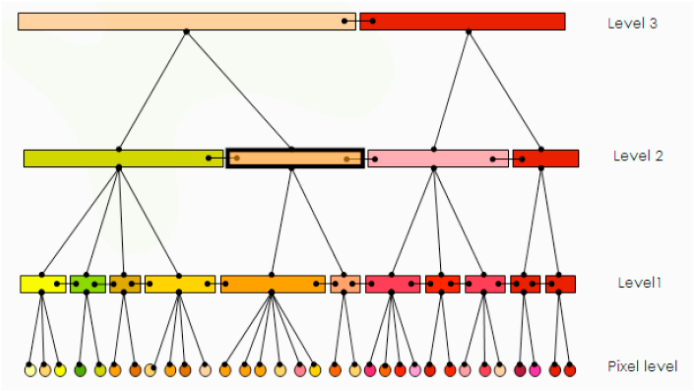

Figure 10. Four-level hierarchical network of image objects (source: Baatz *et al*. (2004))

This hierarchical network allows structures of different scales to be represented simultaneously and thus classified in relation to each other. Moreover, classifying the upper level, each register object can be analyzed based on the composition of its classified sub-objects. By means of this technique different data types can be analyzed in relation to each other, and object shape correction based on regrouping of sub-objects is possible (Cho, 2002).

7.2.2. Object-Based Classification

For OBIA usually is employed a soft classifier, which uses a degree of membership to express an object's assignment to a class. The membership value is usually between 1 and 0, where 1 expresses full membership (a complete assignment) to a class and 0 expresses absolutely non-membership. The degree of membership depended on the degree to which the objects fulfill the class-describing conditions. The main advantage of this soft classifier lies in their possibility to express uncertainties about the classes' descriptions. It makes it also possible to express each object's membership in more than just one class or the probability of belonging to other classes, but with different degrees of membership (Baatz *et al*., 2004). Each class of a classification scheme contains a class description and each class description consists of a set of fuzzy expressions allowing the evaluation of specific features and their logical operation. The output of the system is twofold (Yan, 2003): (1) a fuzzy classification with detailed information of class mixture and reliability of class assignment, and (2) a final crisp classification where each object is assigned to exactly one class (or none, if no assignment was possible). A fuzzy rule can have one single condition or consist of a combination of several conditions that have to be fulfilled for an object to be assigned to a class. The conditions are defined by expressions which are inserted into the class descriptions. Expressions can be membership functions, similarities to classes, or a NN. The output of fuzzy rules can be the input to the next fuzzy rule. Thus a well-structured hierarchy is created.

Classification results can be differentiated and improved by using semantic context information: as soon as objects are classified according to their intrinsic and topological features, classification can be refined using semantic features – mostly by describing neighborhood relationships or the composition of sub-objects. The class hierarchy supports semantic grouping of classes. This can be used to assign classes of different attributes to a common class of superordinated semantic meaning.

With these possibilities the class hierarchy allows the efficient creation of a well-structured knowledge base of a semantic richness. Together with fuzzy classification this adds a lot of power to OBIA approach.

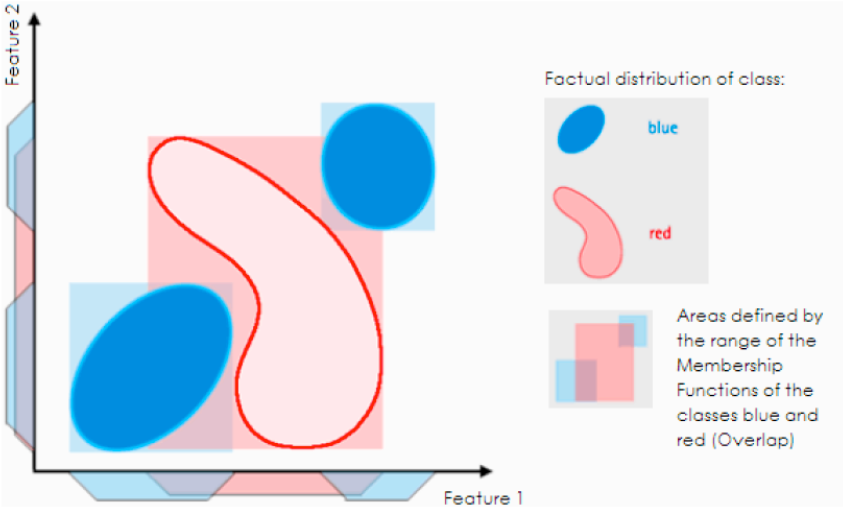

Figure 11. Overlap of class descriptions based on membership functions in a two-dimensional features space (source: Hofmann (2003))

For instance, when using two features to describe the classes red and blue, the areas defined by the range of one dimensional membership functions produce an enormous overlap (Figure 11). This overlap can be reduced if multidimensional membership functions are directly designed because the actual distribution of the class red can be approximated much better. The application of a NN to define these multidimensional membership functions is advisable if several object features will be used to describe a class. The reasons for this are that:

1) NN evaluates the correlation between object features favourably.
2) Overlaps in the feature space increase with its dimension and can be handled much easier with NN.
3) NN allows very fast and easy handling of the class hierarchy for the classification.

Therefore, if a class can be separated from other classes by just a few features or only one feature, the application of membership functions is recommended; otherwise the NN be suggested (Baatz *et al*., 2004).

When using fuzzy classification methods, objects can belong to several classes but with different degrees of membership, which is the case when class descriptions overlap. Thus, to evaluate the reliability or stability of classes it is necessary to survey the different degrees of membership of the classified objects. Objects whose feature values are within these overlapping ranges can be seen as ambiguous objects, since they fulfil the criteria of more than one class. Although fuzzy concepts make it possible to describe these ambiguities, the main aim of each classification should be to define classes as unambiguously as possible.

OBIA was used in two approaches in Chapter II for mapping fire severity classes. OBIA was empoloyed in Chapter III for identificating surface mining affectation.

7.3. Data analysis techniques for exploration, characterization and modelling

Statistics and techniques for data analysis were fundamental tools in most stages of this work, for exploration and description of datasets, in determining relations among data, and for modelling. A brief description of the main statistical and data analysis methods employed follows, oriented to the specific application made in this work.

7.3.1. Statistical modelling

The traditional method applied in remote sensing has been discriminant analysis and its different versions. This method is relevant when the goal is to estimate a limited number classes, e.g., vegetation types or land cover classes. Regression analysis has been used estimating quantitative variables, e.g., tree stem volume and biomass. Non-parametric methods, e.g., k-nearest neighbour estimation (k-NN estimation) and artificial neural networks have the advantages that they can be used for estimating simultaneosuly all inventory variables. Particularly, k-NN method is under intensive research in Europe and North America and has also been applied in operative inventories.

Statistical modelling was applied in Chapter I and Chapter IV.

7.3.2. Moran Index for analysis of spatial correlation

Moran's Index (Moran, 1948) is one of the most commonly used statistical measures for spatial autocorrelation (Anselin, 1992), and it can be expressed as (Equation 10):

$$I = \frac{N}{\sum_i \sum_j w_{ij}} \cdot \frac{\sum_i \sum_j w_{ij}(x_i - \mu)(x_j - \mu)}{\sum_i (x_i - \mu)^2} \qquad [10]$$

where x_i is the variable of interest x measured at location i, N the number of observations, μ the mean of the variable, and w_{ij} are the elements of the spatial weights matrix, which expresses the membership of observations in the neighbourhood set for each location (Anselin, 1992). For easiness of interpretation, a standardized z-value is reported instead of the index itself; z-value is calculated by subtracting the expected value for the statistic, and dividing the result by the standard deviation (Equation 11). When interpreted as a global measure, positive z-values point to positive spatial correlation and negative z-values point to negative spatial correlation; a zero value indicates there is no spatial association in the dataset. Moran's I can be interpreted as a spatially weighted form of Pearson's correlation coefficient (Goovaerts *et al*., 2005) and its significance is assessed against a null hypothesis of no correlation with a permutation procedure (Anselin, 2003).

$$z_i = \frac{I_i - E(I_i)}{\sqrt{V(I_i)}} \qquad [11]$$

Moran Index was applied in Chapter I for testing spatial autocorrelation of the work database before applying non-spatial statistical analysis.

7.3.3. McNmear Test

In many remote sensing studies the same set of sites are used in the assessment of the accuracy of the thematic maps to be compared. Consequently, the samples are not independent, and an alternative approach to that outlined above that is suitable for related samples is required. For related samples, the statistical significance of the difference between two proportions may be evaluated using McNemar's test (Bradley, 1968; Agresti, 1996). This is a non-parametric test that is based upon confusion matrices that are 2 by 2 in dimension. The constraint on the size of the matrices is often not a problem because larger matrices can be collapsed to this size because attention is, in effect, focused on the binary distinction between correct and incorrect class allocations. The McNemar test is based upon the standardized normal test statistic (Equation 12).

$$z = \frac{f_{12} - f_{21}}{\sqrt{f_{12} + f_{21}}} \qquad [12]$$

in which f_{ij} indicates the frequency of sites lying in confusion matrix element i, j.

Commonly in the literature, some discussions of this technique, including its use within remote sensing to compare accuracy statements (e.g., Chan *et al*., 2003), bases the evaluation upon a chisquare ($\chi 2$) distribution; the square of z follows a chi-squared distribution with one degree of freedom (Agresti, 1996). In such circumstances, the test equation may be expressed as (Equation 13).

$$\chi^2 = \frac{(f_{12} - f_{21})^2}{f_{12} + f_{21}} \qquad [13]$$

with the derived value compared against tabulated chi-squared values to indicate its statistical significance. This approach cannot, however, be used for testing a one-sided hypothesis because the rejection region for the chi-squared test is one-tailed.

McNemar Test was employed in Chapter II for determining significant differences among classifications.

7.4. Vegetation indices

A vegetation index is a dimensionless, radiation based measurement that indicates relative abundance and activity of green vegetation (Jensen, 2005) by isolating its contribution from other materials (Asner *et al*., 2003). Vegetation indices are simple, reduce data dimensionality, and can easily be applied to different scenes. Vegetation indices take advantage of the unique spectral signature of vegetation, characterized by a large difference in reflectance between the visible (high absorption) and near-infrared (reflectance). Typical indices use the ratio or difference of NIR (near infrared) and VIS (visible) reflectance, and most commonly are defined with VIS in the red region of the visible spectrum (630-690 nm).

Vegetation indices are frequently used in forestry applications, capitalizing on a strong relationship with structural attributes like Leaf Area Index (LAI) and canopy cover, to estimate, map, and monitor forest health, biomass content, and landscape disturbances (i.e. fire, windstorms). When used for discrimination of land cover and characterization

of vegetative condition, vegetation indices must normalize effects such as sun angle or atmospheric effects for consistent comparisons in time and space.

7.4.1. Normalized Difference Vegetation Index

One of the most widely used vegetation indices is the Normalized Difference Vegetation Index (NDVI) developed by Rouse *et al*. (1973). NDVI is defined as (Equation 14).

$$NDVI = \frac{\rho_{nir} - \rho_{red}}{\rho_{nir} + \rho_{red}} \quad [14]$$

where ρ_{nir} and ρ_{red} are the reflective values in the NIR and red bands for each pixel.

NDVI values vary between 0 and 1 and are directly related to the vigour of vegetation. NDVI is extensively used to monitor seasonal and annual global changes in vegetation communities, and as a component of particular models. NDVI has demonstrated useful for evaluation of forest biomass and structure (Dong *et al*., 2003; Piao *et al*., 2005). Chuvieco (2002) noted as a weakness of the NDVI its inability to discriminate between areas with different proportion of vegetation/soil: an area with vigorous canopy and scarce density can show the same NDVI value as other area with higher density but less vitality.

NDVI was employed in Chapter I.

7.4.2. Tasseled Cap Transformation

The Tasseled Cap transformation (TC) (Kauth and Thomas, 1976; Crist and Cicone, 1984; Crist, 1985; Huang *et al*., 2002) is a linear transform for reduction of the Landsat spectral space that was initially developed by Kauth and Thomas (1976) for understanding of crop spectral behaviour. The TC has been broadly employed in forestry studies of structure (Cohen *et al*., 2001; Hansen *et al*., 2001), condition (Healey *et al*., 2006; Wulder *et al*., 2006), successional state (Peterson and Nilson, 1993; Helmer *et al*., 2000) and change detection (Lea *et al*., 2004; Jin and Sader, 2005) in a range of forest environments. The first three components of the TC were named Wetness (TC-W), Greenness (TC-G), and Brightness (TC-B), in relation with their physical interpretation, and have received special attention for forest applications. TC-B and TC-G components form the vegetation plane (Crist and Cicone, 1984), where the spectral behaviour of forest stands provides insights into forest cover densities and forest development stages.

TC transformations and NDVI were employed in Chapter I.

8. RESULTS

The performance and main outcomes of the implemented techniques are mentioned here, and the most important results are summarized. Detailed results are described in each chapter.

Chapter I: Estimation of aboveground biomass in Mediterranean forests by statistical modelling of ASTER fraction images.

* Fraction images showed differentiation in abundances between Green Vegetation (GV), shade and exposed soil. Shade was well predicted over the scene. High shade fractional values were most evident along the river and well distributed throughout the forest stands. The soil fractional endmember showed localized areas of high soil abundances, particularly in the continental sand-dune areas.

* Spatial autocorrelation of the work datatabase was checked out with the Moran´s *I* test. It evidenced that feature values were randomly distributed across the study area. The *Z*-score was -2.15, *p*-value was 0.05, indicating statistical significance and Moran's *I* index was -0.53, indicating a tendency toward dispersion.

* A strong positive correlation was found between GV fraction values and ground measured AGB (Pearson´s correlation of 0.729). This strong relationship showed that GV fraction was suitable for AGB estimation. The relationship between GV fraction image and AGB was stronger than the rest of independent variables (ASTER original bands, NDVI and TC components).

* Regression model #5 (three independent variables, first order polynomial) using the combination of GV fraction image and ASTER bands 2 and 8 as independent variables improved the regression performance (R^2_{adj} value=0.632) and RMSE=12.84 Mg ha^{-1}, 13.3 Mg ha^{-1} from cross-validation, and relative RMSE=36.3% and 37.7% resulting form cross-validation.

* Spatial distribution of the AGB was produced based on the multiple linear regression model #5, generating the estimated/predicted mean value of 42.4 Mg ha^{-1} (SD=11.9 Mg ha^{-1}).

Chapter II: Combining spectral mixture analysis and object-based classification for fire severity mapping.

* The image endmembers picked up from the study area have produced robust and representative image fractions of burned areas, soil and two kinds of vegetation. The RMSE image showed areas poorly modelled by the least squares algorithm represented by crops at the time of image acquisition and the rest of the image presented a random error distribution.

* The fraction imagery performed better than the original Landsat ETM+ bands into a combined-based approach using LSMA and OBIA to capture fire severity classes (high,

moderate and low) into a fire scar. The applied model had two different levels of image objects representing different scales.

* Fuzzy membership functions used to apply fuzzy range to selected features (fraction image-abundance values, contextual information and relation to super-objects) allowed separate fire severity classes to the rest of image objects and severity classes each other.

* Among the models tested, object-based approaches showed the highest accuracies, in opposite relation with the pixel-based approaches. As happened in overall accuracy, Kappa Index of Agreement (KIA) values displayed better values when fraction images were introduced.

* The advantage of the approach using LSMA and OBIA over the rest of the approaches tested was significant. McNemar´s test permited to revise the differences among KIA statistics and showed that the classification accuracy derived from the considered approaches was different with statistical significance.

Chapter III: Mapping forest cover changes caused by mining activities using spectral mixture analysis and object oriented classification.

* The combined approach using LSMA and OBIA allowed to discriminate surface mining activities in a forested area and to map the areas affected by those mining exploitations.

* The applied model permited to identify what surface mines were into the Site of Community Importance (Habitats Directive 92/43/EEC) and the land use affected by this kind of mining activities. The largest areas affected were shrubs and broadleaved forests (57% and 25%, respectively, of the total area occuped by mining exploitations).

* Among the three kind of mining exploitations into the study area, it was only possible to distinguish between two groups: coal-slate and limestone. Later it was possible to discriminate them by using geologic maps.

Chapter IV: Spectral Mixture Modeling to estimate wood volume in north of Spain from optical satellite data.

* The LSMA model performed well using the Landsat bands (3, 4, 5 and 7) commonly used in vegetation studies. The fraction imagery obtained were shade, soil and vegetation.

* The analysis between over bark volume (OBV) and the fraction images was attempted by several approaches. The most accurate results were reached by defining the relation between variables considering the different levels of existing OBV, analyzing the behaviour of each OBV group defined independently. The groups were defined by percentiles of 25%, 50%, 75% and 99% (low, medium, high and very high OBV, respectively).

* There were good estimations when the volume not exceeded of 200 m^3 ha^{-1} (very high volume) and the worst estimations were observed when the volume belonged to the very high OBV group. These results agree with findings of other researchers.

* In spite of the good results obtained, this expression has practical limits as it does not allow the volume of a specific forest stand to be estimated unless certain knowledge of it is available. This problem is minimized when the stand is stratified by identification on digital orthophotographs of different development levels. The application to the different strata of the model developed allowed an estimated volume map to be prepared.

9. DISCUSSION

The work performed in this doctoral thesis covered a range of satellite image techniques for forestry applications. Methods were developed in each chapter, which in turn contributed to the advance of scientific knowledge on the field. Remakably, estimation of aboveground biomass in Mediterranean forests by statistical modelling of ASTER fraction images, combining fraction images and object-based classification for fire severity and for forest cover changes by surface mining mapping, and wood volume estimation in conifer forests by Landsat TM fraction images.

Regarding satellite fraction images on forest attributes, in our work, inclusion of fraction imagery from LSMA as independent variables improved the statistical modelling of aboveground biomass as function of ASTER data in Mediterranean ecosystems. GV fraction was strongly positively correlated with AGB (r=0.729) that indicated that this variable was a good candidate for AGB estimation (Lu *et al*., 2005). The suitability of GV fraction image to aboveground biomass estimation has been shown in different ecosystems, mainly boreal and tropical biomes (Lu *et al*., 2005; Poulain *et al*., 2012). Accuracy test levels were comparable to vegetation studies of other biomes (Muukkonnen and Hesikanen, 2005; Xie *et al*., 2009) and we reported better results than other studies carried out in boreal coniferous and mixed forests (Hyypä *et al*., 2000; Tomppo *et al*., 2002; Mäkelä and Pekkarinen, 2004). Studies relating satellite images with wood volume in Mediterranean areas are scarce, although they have been carried out on boreal and tropical forests. In this respect, our study offered the chance of learning about the behaviour of this relation in Mediterranean environments and the results obtained indicated that the relation between fraction images and stand volume confirmed both northern and tropical forests studies (Adams *et al*., 1995; Hall *et al*., 1995; García-Haro *et al*., 1996; Peddle *et al*., 1999; Peddle and Johnson, 2000) and this relation was also verified in Mediterranean environments. Further discussion and deeper insights can be found in Chapter I and Chapter IV.

Concerning to fire severity studies, a few fire severity studies have been performed in the Mediterranean Basin (e.g. de Santis and Chuvieco, 2007; de Santis *et al*., 2009; Díaz-Delgado *et al*., 2003; Veraverbeke *et al*., 2010; Quintano *et al*., 2013). To our knowledge, few studies have been carried out combining SMA and OBIA for fire severity mapping (Quintano *et al*., 2006; Fernández-Manso *et al*., 2009) and fire scars estimation (Quintano and Shimabukuro, 2009). Lippitt *et al*. (2012) investigated the affect of several common remote sensing data transformation (SMA, principal components analysis (PCA), NDVI, and visible atmospherically resistant index (VARI)) on segmentation and final OBIA product accuracy. In our work, the incorporation of fraction image into the classification procedure increased the accuracy for both subpixel- and object-based approaches. The better results obtained by approaches that included OBIA into its process were mainly due to the ability of a context-based classification to reduce the speckle in the classification. Besides, combined-based approach performed better results at individual class level. It dealt satisfactory with the problem of classes confusion using the information contained into the fraction imagery to the object-based classification. In addition, high accuracy values per class reached in this combined-based approach indicated that confusion between problematic classes were minimized and it was helpful for improving separability between classes. Further discussion and deeper insights can be found in Chapter II.

In surface mining, our work showed that the remote sensing techniques applied were useful tools, capable of aiding in the process of monitoring forest cover changes caused by mining activities. Fernández-Manso *et al*. (2012) used these three same types of fraction images (obtained by LSMA) to examine three areas of coal extraction in the world: Spain, United States of America (USA), and Australia. Specifically, the authors found that mining affected areas (dark and light), vegetation (GV) and shade fraction images led to the most accurate estimate of forest areas affected by mining activities. Similarly, Adams and Gillespie (2006) found that the ability to discriminate components depends on the properties of each type of landscapes. There are some studies, however, that used fraction images derived from LSMA to identify mine affected areas. Richter *et al*. (2008) quantified the rehabilitation process in mine tailing areas and Shang *et al*. (2009) characterized mine tailings Lévesque and Staenz (2008) monitored mine tailings re-vegetation using multitemporal hyperspectral images. In their work, total vegetation fraction (high/low photosynthetic), total tailings fraction (fresh/oxidized), and texture of the vegetation fraction were used in a K-mean unsupervised classification, producing an Over All (OA) equal to 78.13% and a κ statistic of 0.74. We obtained a similar values, OA was estimated to be 84.91% and κ statistic was 72.05%. As remote sensing technology advances, its potential role in monitoring surface mining and reclamation will be enhanced. This study provides a basis upon which future research can build and it is an open research line with a great potential for extracting information from multispectral satellite imagery. Further discussion and deeper insights can be found in Chapter III.

CONCLUSIONS

This doctoral thesis includes discussions on practical aspects of integrating image analysis techniques for forestry applications. The emphasis is mainly on using LSMA and/or OBIA when estimating, mapping, assessing and monitoring forest attributes and forest impacts. In *Objectives* we made four questions that we have answered in the four Chapters.

How can the study of forest attributes such as AGB be estimated in a regional scale in a cost-effective way?. How much biomass is stored in a Mediterranean pine forest?.

There is a potential for quantification of Mediterranean pine (*P.pinaster* Ait.) AGB at compartment level using fraction images from LSMA as independent variables in multiple linear regression models using ASTER satellite data. A combination of ASTER bands, red and short wave infrared (B2 and B8) and GV fraction image was the best predictor of AGB. A combination of these three image data yielded an R^2_{adj} value of 0.632 and RMSE of 13.3 Mg ha^{-1} and $RMSE_r$ of 37.7% resulting from cross-validation. GV fraction image from LSMA improved the predictive power of the models analyzed generated for estimating AGB (R^2_{adj}= 0.574, RMSE of 20.32 Mg ha^{-1},when no fraction images were included).

Fraction images (particularly GV) are useful for estimating AGB of Mediterranean pine in Central Spain. Additionally, the spatial distribution of estimated AGB may help in a practical way to guide forest managers' decisions in future studies and in similar forest ecosystems by assisting them in monitoring and managing the forested area. Spatial distribution of AGB reached the estimated mean value of 42.4 Mg ha^{-1} (SD=11.9 Mg ha^{-1}).

How can be estimated fire severity in large forest fires in a cost-effective way?. What would be one of the most adequate ways to estimating fire severity in large Mediterranean fire scars using remote sensing techniques?. Are there any synergies combining LSMA and OBIA as main image analysis techniques?.

Fire severity mapping is an important step by providing operational information for post-fire restoration.

Fraction images generated by unmixing of a Landsat ETM+ post-fire image can be used as input in an object-based classification for mapping fire severity since it improves the result accuracy (due to its ability to produce fractions representative of subpixel components directly related to fire severity).

Among the approaches tested, the accuracy of fire severity categories was better combining LSMA and OBIA. McNemar's test was used to evaluate the statistical significance of the difference between the four methods tested. The difference in accuracy expressed in terms of proportions of correctly allocated pixels was statistically significant at the 0.1% level, which meant that the thematic mapping result using the combined approach (LSMA/OBIA) achieved a much higher accuracy than the rest of

approaches. This shows synergies between LSMA and OBIA and a great potential for estimating fire severity into fire scars.

How can be monitored surface mining activities in large areas at low cost?. Which role does play remote sensing techniques for quantifying forest cover changes caused by mining activities?. Could this approach be considered for monitoring effective reclamation?.

Combining LSMA and OBIA allows the elaboration of forest cover change maps in the current moment in one of the main mining regions of the European Union in the obtaining of non metallic minerals.

The model works optimally for mining impacts largest than 5 ha. The tessellation and complexity of the land uses make that the smallest impacts are of difficult segregation. This apparent problem, in the practice, is resolved since the type of exploitation of more impact, surface mining, generally occupies large surfaces.

The obtained maps have a great utility for the analysis of the regressive changes in the forest since these activities correspond to the main genesis of changes and it can be used for monitoring reclamation processes.

How do remote sensing techniques estimate wood volume in conifer stands?. How do fraction images improve the results?. How much volume is stored in Scots pine forests in Mediterranean areas?.

Quantifying the volume of a stand of *Pinus sylvestris* L. in Mediterranean environments it is possible using fraction images from LSMA of Landsat TM images in regression models.

Using fraction images in regression models improve the results of predicting biophysical variables of different tree species since they are less sensitive to internal (such as canopy geometry, terrain factors, species composition) and external factors (sun elevation angle, zenith view angle, atmospheric conditions) that affect vegetation reflectance values.

Digital volume maps from satellite images can be integrated as a new source of information in the information system of the regional forestry authority. This information can help to plan forestry activities in a rational way and they show the ranges of volume distribution into the study area.

CONCLUSIONES

Esta tesis doctoral incluye discusiones de aspectos prácticos relacionados con la integración de técnicas de análisis de imágenes de satélite para aplicaciones forestales. Se hace énfasis principalmente en el uso del modelo de análisis de mezclas espectrales y/o análisis de imágenes basada en objetos en la estimación, cartografía, valoración y seguimiento de atributos e impactos forestales. En el apartado de *Objetivos* se hicieron cuatro preguntas que se han respondido durante el desarrollo de los cuatro capítulos (publicaciones).

¿Cómo puede el estudio de atributos forestales, tales como la biomasa forestal aérea, ser estimados a escala regional de manera económicamente eficiente?.

Existe un potential en la utilización de imágenes fracción obtenidas a partir del análisis de mezclas espectrales lineal de datos del sensor ASTER como variables independientes dentro de modelos de regresión lineal múltiple para la cuantificación de masas de pino negral (*Pinus pinaster* Ait.). El mejor predictor de la biomasa arbórea forestal fue una combinación de las bandas originales del sensor ASTER (B2, rojo y B8, infrarojo corto) y la imagen fración vegetación verde (GV). Una combinación de estas tres variables produjo como resultados un valor de R^2_{adj} de 0,632 y un RMSE de 13,3 Mg ha^{-1} y $RMSE_r$ of 37,7% (a partir de crosvalidación).

La imagen fracción vegetación verde (GV) mejoró el poder predictivo para la estimación de la biomasa arbórea forestal en relación con los modelos analizados que no incluyeron dicha variable (R^2_{adj}= 0,574, RMSE de 20,32 Mg ha^{-1}, mejor resultado sin utilizar imágenes fracción). Basándonos en los resultados alcanzados en el presente estudio, concluimos que las imágenes fracción (en particular GV) son útiles para la estimación de la biomasa arbórea forestal de masas forestales de pino negral en el centro de España. Adicionalmente, la distribución espacial de la biomasa arbórea forestal estimada puede ayudar de forma práctica en la toma de decisiones de los gestores forestales en futuros estudios dentro de similares ecosistemas en relación al seguimiento y la gestión de las zonas forestales arboladas. La distribución espacial de la biomasa arbórea forestal en la zona de estudio alcanzó un valor medio estimado de 42,4 Mg ha^{-1} (SD=11,9 Mg ha^{-1}).

¿Cómo puede ser estimada la severidad en grandes incendios forestales con un coste eficiente?. ¿Cuál sería una de las más adecuadas maneras de estimar la severidad de incendios forestales en el entorno Mediterráneo dentro de los perímetros del incendio usando técnicas de teledetección?. ¿Existe alguna sinergia entre el modelo de análisis de mezclas espectrales y/o análisis de imágenes basada en objetos en la estimación de severidad de incendios forestales?.

La cartografía de severidad de incendios forestales es de vital importancia ya que aporta información operacional después del incendio para la rehabilitación de la zona afectada.

Las imágenes fracción generadas por descomposición espectral de imágenes Landsat ETM+ (obtenidas de fechas posteriores al incendio forestal), pueden ser empleadas como variables de análisis dentro de clasificaciones basadas en objetos para la generación de cartografía de severidad de incendios forestales, ya que mejora la precisión de los resultados (debido a la posibilidad de obtener fracciones representativas de los componentes dentro de un pixel relacionadas directamente con la severidad de incendios forestales).

De entre los enfoques testados, el método que combina el análisis de mezclas espectrales lineal y análisis de imágenes basado en objetos es el que genera la cartografía de severidad de incendios más precisa (McNemar test) y las categorías de severidad de incendios forestales (alta, media y baja) más precisas. Esto indica sinergias entre ambos métodos y, con gran potencial para la estimación de niveles de severidad en áreas quemadas.

¿Cómo puede ser controladas las actividades de minería a cielo abierto en grandes áreas con un bajo coste económico?. ¿Qué papel juegan las técnicas de teledetección en la cuantificación de cambios en la cobertura forestal causada por actividades mineras?. ¿Podría ser considerado este enfoque en el control efectivo de las tareas de recuperación?.

La combinación de análisis de mezclas espectrales lineal y análisis de imágenes basado en objetos permite elaborar cartografía de cambios de cobertura forestal en una de las principales regiones mineras de la Unión Europea en la explotación de minerales no metálicos.

Este modelo funciona, de una forma óptima, en impactos producidos por minería con un tamaño superior a 5 ha. La segragación de impactos más pequeños es muy dificil debido a la complejidad y teselación de los usos del suelo del área de estudio. Este aparente problema, en la práctica, puede ser resuelto ya que minería a cielo abierto, que es el tipo de explotación con mayor impacto, generalmente ocupa grandes superficies.

Este tipo de mapas son de gran utilidad para el análisis de cambios regresivos de masas forestales ya que estas actividades corresponden con la principal génesis de los cambios y pueden se utilizados para el seguimiento de procesos de rehabilitación.

¿Cómo estiman el volumen maderable de masas forestales las técnicas de teledetección?. ¿Cómo mejoran los resultados el empleo de imágenes fracción?. ¿Cuánto volumen maderable es almacenado en masas forestales de pino silvestre en áreas mediterráneas?.

La cuantificación del volumen de masas forestales de pino silvestre en entornos mediterráneso es posible utilizando imágenes fracción, obtenidas por el análisis de mezclas espectrales lineal de imágenes de satélite Landsat TM, en modelos de regresión.

La utilización de imágenes fracción dentro de los modelos mejora la predicción de variables biofísicas de especies forestales ya que son menos sensibles a factores internos (geometría de la cubierta, factores del terreno, composición de especies) y externos (ángulo de elevación del Sol, ángulo de visión cenital, condiciones atmosféricas) que afectan a los valores de reflectancia de la vegetación.

Es posible integrar mapas digitales de volumen obtenidos de imágenes de satélite como nueva fuente de información en los sistemas de información de la administración forestal regional. Este tipo de información puede ayudar en la planificación de actividades forestales de una forma más racional y muestra los rangos de distribución del volumen dentro del área de estudio (0,55->150 m^3 ha^{-1}).

REFERENCES

Abrams, M., Hook, S., 2002. ASTER User Handbook. Version 2. Jet Propulsion Laboratory. California Institute of Technology. EROS Data Center, Sioux Falls. 135 pp.

Adams, J. B., Gillespie, A. R., 2006. Remote Sensing of Landscapeswith Spectral Images. A PhysicalModeling Approach. New York: Cambridge University Press Ed. 362 pp.

Adams, J.B., Sabol, D.E., Kapos, V., Almeida, R., Roberts, D.A., Smith, M.O., Gillespie, A.R., 1995. Classification of multispectral images based on fractions of endmembers – Application to Land-Cover change in the Brazilian Amazon. *Remote Sensing of Environment*, 52 (2), 137-154.

Adams, J.B., Smith, M.O., Gillispie, A.R., 1993. Imaging spectroscopy: interpretations based on spectral mixture analysis. In: Remote Geochemical Analysis: Elemental and Mineralogical Composition (C. M. Pieters and P. A. Englert, Eds.), Cambridge University Press, Cambridge, UK, 145-166.

Addink, E.A., de Jong, S.M., Pebesma, E.J., 2007. The importance of scale in object-based mapping of vegetation parameters with hyperspectral imagery. *Photogrammetric Engineering & Remote Sensing* 73 (8), 905-912.

AEMET, 2014. Agencia Estatal de Meteorología de España. www.aemet.es (last date accessed: 15 November 2014).

Agresti, A., 1996. An Introduction to Categorical Data Analysis, New York: Wiley.

Anselin, L., 1992. Spatial data analysis with GIS: An introduction to application in the social sciences. Technical Report 92–10. University of California, Santa Barbara: National Center for Geographic Information and Analysis.

Anselin, L., 2003. An introduction to spatial autocorrelation analysis with GeoDa. University of Illinois, Urbana-Champaign: Spatial Analysis Laboratory, Department of Agricultural and Consumer Economics.

Arvidson, T., Goward, S., Gasch, J., Williams, D., 2006. Landsat-7 Long-Term Acquisition Plan: Development and Validation. *Photogrammetric Engineering and Remote Sensing*, 72(10), 1137-1146.

Asner, G.P., Hicke, J.A., Lobell, D.B., 2003. Per-pixel analysis of forest structure. In: Wulder, M.A., Franklin, S.E. (eds.) Remote sensing of forest environments: Concepts and case studies. Kluwer Academic Publishers, Boston, USA.

Avery, T.E., Burkhart, H.E., 1994. Forest measurements, 4th ed. McGraw-Hill, Boston, MA. 408 pp.

Avitabile V, Baccini A, Friedl MA, Schmullius C, 2012. Capabilities and limitations of Landsat and land cover data for aboveground woody biomass estimation of Uganda. *Remote Sensing of Environment* 117, 366-380.

Baatz, M., Benz, U., Dehghani, S., Heynen, M., Höltje, A., Hofmann, P., Lingenfelder, I., Mimler, M., Sohlbach, M., Weber, M., Willhauck, G., 2004, User guide 4. eCognition Professional 4.0. Definiens imaging. Munich, Germany.

Bateson, A., Asner, G.P., Wessman, A., 2000, Endmember bundles: a new approach to incorporating endmember variability into spectral mixture analysis. *IEEE Transactions on Geoscience and Remote Sensing*, 38, 1083–1094.

Benz, U. C., Hofmann, P., Willhauck, G., Lingenfelder, I., Heynen, M., 2004, Multi-resolution, object-oriented fuzzy analysis of remote sensing data for GIS-ready information. *ISPRS Journal of Photogrammetry and Remote Sensing*, 58, 239–258

Bierwirth, P., 1990, Mineral mapping and vegetation removal via data-calibrated pixel unmixing, using multispectral images. *International Journal of Remote Sensing*, 11,1999–2017.

Blaschke, T., 2010. Object Based Image Analysis for Remote Sensing, ISPRS Journal of Photogrammetry and Remote Sensing, 65, 2-16.

Blaschke, T., Hay, G.J., Kelly, M., Lang, S., Hofmann, P., Addink, E., Feitosa, R., Van Der Meer, F., Van Der Werff, H., Van Coillie, F., Tiede, D., 2014. Geographic Object-based Image Analysis: a new

paradigm in Remote Sensing and Geographic Information Science. *ISPRS International Journal of Photogrammetry and Remote Sensing* 87(1), 180-191.

Boardman, J.W., 1993. Automating spectral unmixing of AVIRIS data using convex geometry concepts. In Summaries 4th Annu. JPL Airborne GeoscienceWorkshop, JPL Publication 93–26, 1, 11–14.

Borel, C. C., Gerstl, S. A., 1994. Nonlinear spectral mixing models for vegetative andvsoil surfaces. *Remote Sensing of Environment*, 47, 403−416.

Bossard, M., Feranec, J., Otahel, J., 2000. 'Corine land cover technical guide — Addendum 2000'. Technical report, No 40. Copenhagen (EEA). http://terrestrial. eionet.eu.int

Boyd, D.S., Danson, F.M., 2005. Satellite remote sensing of forest resources: three decades of research development. *Progress in Physical Geography*. 29, 1, 1-26.

Bradley, J. V., 1968. Distribution-free Statistical Tests, New Jersey: Prentice-Hall.

Bravo, F., Río, M., Pando, V., San Martín, R., Montero, G., Ordoñez, C., Cañellas, I., 2002. El diseño de las parcelas del inventario forestal nacional y la estimación de variables dasómetricas. In: El Inventario Forestal Nacional, Elemento Clave para la Gestión Forestal Sostenible; Bravo, F., Rio, M., Peso, C., (eds.). Fundación General de la Universidad de Valladolid: Valladolid, Spain, 19-35.

Bravo, F., Ordóñez, A.C., Del Río, M., 2005. BASIFOR 2.0: Aplicación informática para el manejo de bases de datos del Segundo y del Tercer Inventario Forestal Nacional.

Burnett, C., Blaschke, T., 2003. A multi-scale segmentation/object relationship modelling methodology for landscape analysis. *Ecological Modelling* 168 (3), 233–249.

Caetano, M.S., Mertes, L.A.K., Pereira, J.M.C., 1994. Using spectral mixture analysis for fire severity mapping. In: Proceedings of the 2nd Conference on Forest Fire Research, 11, 667-677.

Caetano, M.S., Mertes, L.A.K., Cadete, L., Pereira, J.M.C., 1996. Assessment of AVHRR data for characterising burned areas and post-fire vegetation recovery, In: EARSEL Advances on Remote Sensing, 4 (4-XI), 124-134.

Calle, A., Casanova, J.-L., González-Alonso, F., 2009. Impact of point spread function of MSG-SEVIRI on active fire detection. *International Journal of Remote Sensing*, 30(17), 4567-4579.

Campbell, J.B., 2002. Introduction to Remote Sensing, 3rd edition. The Guilford Press, New York.

Carpenter, G., Gopal, S., Macomber, S., Martens, S., Woodcock, C., 1999. A neural network method for mixture estimation for vegetation mapping. *Remote Sensing of Environment*, 70, 138– 152.

Chander, G., Markham, B.L., Helder, D.L., 2009. Summary of current radiometric calibration coefficients for Landsat MSS, TM, ETM+, and EO-1 ALI sensors. *Remote Sensing of Environment*, 113, 893-903.

Chang, C., Plaza, A., 2006, A fast iterative algorithm for implementation of pixel purity index. *IEEE Geoscience and Remote Sensing Letters*, 3, 63–67.

Charou, E., Stefouli, M., Dimitrakopoulos, D., Vasiliou, E., Mavrantza, O. D., 2010. Using remote sensing to assess impact of mining activities on land and water resources. *Mine Water Environment*, 29, 45–52.

Chen, Y., Shi, P., Fung, T., Wang, J., Li, Y., 2007. Object-oriented classification for urban land cover mapping with ASTER imagery. International Journal of Remote Sensing 28 (29), 4645-4651.

Chirici, G., Corona, P., 2005. An overview of pass- ive remote sensing for post-fire monitoring. *Forest@* 2 (3), 282-289.

Cho, H., 2002. Untersuchungen über die Erfassung von Walflächen und deren Veränderungen mit Hilfe der Satellitenfernerkundung und segmentbasierter Klassification, Dissertation. Fakultät für Fortwissenschaften und Waldökologie. Georg-August-Universität Göttingen. Germany. pp. 137 (in German).

Chubey, M. S., Franklin, S. E., Wulder, M. A., 2006. Object- based analysis of IKONOS- imagery for extraction of forest inventory parameters, *Photogramm. Eng. Remote Sens*., 72(4), 383–394.

Chuvieco, E., 2002. Teledetección ambiental. Editorial Ariel, S.A. 685 pp. Barcelona. (España).

Chuvieco, E., De Santis, A., Riaño, D., Halligan, K., 2007. Simulation approaches for burn severity estimation using remotely sensed images. *Journal of Fire Ecology*, 3, 129–150.

Chuvieco, E., Pilar Martin, M., Palacios, A., 2002. Assessment of different spectral indices in the red-near-infrared spectral domain for burned land discrimination. *Remote Sens. Environ*. 112, 2381-2396.

Clark, M.L., Roberts, D.A., Ewel, J.J., Clark, D.B., 2011. Estimation of tropical rain for-est aboveground biomass with small-footprint lidar and hyperspectral sensors. *Remote Sens. Environ*. 115, 2931-2942.

Cohen, W.B., Maiersperger, T.K., Spies, T.A., Oetter, D.R., 2001. Modelling forest cover attributes as continuous variables in a regional context with thematic mapper data. *International Journal of Remote Sensing*, 22, 2279-2310.

Colby, J.D., 1991. Topographic normalization in rugged terrain. *Photogrammetric Engineering and Remote Sensing*, 57(5), 531-537.

Coppin, P., Jonckheere, I., Nackaerts, K., Muys, B., 2004. Digital change detection methods in ecosystem monitoring: a review. *International Journal of Remote Sensing*, 25 (9), 1565-1596.

Crist, E. P., Cicone, R. C., 1984. A physically based transformation of Thematic Mapper data- the TM tasseled Cap. *IEEE Transactions on Geoscience and Remote Sensing*, 22, 256-263.

Crist, E. P., 1985. A TM Tasseled Cap equivalent transformation for reflectance factor data. Remote Sensing of Environment, 17, 301-306.

Cunia, T., 1981. A review of the methods of forest inventory. In: Woodpower- New perspectives on forest usage, Talbot and Swanson (eds), Pergamon Press, *International Science and Technology Institute*, 9-20.

Cutler, M.E.J., Boyd, D.S., Foody, G.M., Vetrivel, A., 2012. Estimating tropical forest biomass with a combination of SAR image texture and Landsat TM data: an assessment of predictions between regions. *ISPRS J. Photogramm. Remote Sens*. 70 (1), 66–77.

Demarchi, L., Canters, F., Chan, J., Van De Voorde, T., 2012. Multiple endmember unmixing of CHRIS/Proba imagery for mapping impervious surfaces in urban and suburban environments. *IEEE Trans. Geosci. Remote Sens*. 50 (9), 3409–3424.

de Santis, A., Asner, G. P., Vaughan, P. J., Knapp, D. E., 2010. Mapping burn severity and burning efficiency in California using simulation models and Landsat imagery. *Remote Sensing of Environment*, 114, 1535–1545.

de Santis, A., Chuvieco, E., 2007. Burn severity estimation from remotely sensed data: Performance of simulation versus empirical models, *Remote Sensing of Environment*, 108, 422-435.

de Santis, A., Chuvieco, E., 2009. GeoCBI: A modified version of the Composite Burn Index for the initial assessment of the short-term burn severity from remotely sensed data. *Remote Sensing of Environment,* 113, 554–562.

de Santis, A., Chuvieco, E., Vaughan, P., 2009. Short-term assessment of burn severity using the inversion of PROSPECT and GeoSailmodels. *Remote Sensing of Environment*, 113, 126–136.

da Silva, R. D., Galvão, L. S., dos Santos, J. R., de J. Silva, C. V., de Moura, Y. M., 2014. Spectral/textural attributes from ALI/EO-1 for mapping primary and secondary tropical forests and studying the relationships with biophysical parameters. *GIScience & Remote Sensing*, 51(6), 677-694.

Desclée, B., Bogaert, P., Defourny, P., 2006. Forest change detection by statistical object-based method. *Remote Sensing of Environment* 102 (1-2), 1-11.

Deng, C., Wu, C., 2013. Examining the impacts of urban biophysical compositions on surface urban heat island: a spectral unmixing and thermal mixing approach. *Remote Sensing of Environment* 131, 262–274.

Díaz-Delgado, R., Lloret, F., Pons, X., 2003. Influence of fire severity on plant regeneration by means of remote sensing imagery. *International Journal of Remote Sensing*, 24, 1751-1763.

Díaz-Delgado, R., Pons, X., 1999. Empleo de imágenes de teledetección para el análisis de los niveles de severidad causados por el fuego. *Revista de Teledetección* 12, 63-68.

Díaz-Delgado, R., Pons, X., Lloret, F., 2001. Fire severity effects on vegetation recovery after fire. The Bigues i Riells wildfire case study. In: 3rd International Workshop on Remote Sensing and GIS applications for Forest Fires Management. New methods and sensors, Chuvieco, E. and Martín, M.P. (Eds.), pp. 152-155. Paris: EARSeL.

Di Gregorio, A., 2005. Land Cover Classification System. Classification concepts and user manual. Software version 2. FAO, Environment and Natural Resources Series number 8. Rome, Italy. 190 pp & CD-ROM.

Dong, J., Kaufmann, R.K., Myneni, R.B., Tucker, C.J., Kauppi, P.E., Liski, J., Buermann, W., Alexeyev, V., Hughes, M.K., 2003. Remote sensing estimates of boreal and temperate forest woody biomass: carbon pools, sources and sinks. *Remote Sensing of Environment*, 84, 393-410.

Drake, N.A., Mackin, S., Settle, J.J., 1999. Mapping vegetation, soils, and geology in semiarid shrublands using spectral matching and mixture modelling of SWIR AVIRIS imagery. *Remote Sensing of Environment*, 68, 12–25.

Duveiller, G., Defourny, P., Desclée, B., Mayaux, P., 2008. Deforestation in Central Africa: Estimates at regional, national and landscape levels by advanced processing of systematically-distributed Landsat extracts. *Remote Sensing of Environment* 112 (5), 1969-1981.

EEA-ETC/TE, 2002. Corine land cover update, Image 2000 and CLC2000 project, Technical guidelines, http://terrestrial.eionet.eu.int

Ekstrand, S., 1996. Landsat TM-based forest damage assessment: Correction for topographic effects, *Photogrammetric Engineering & Remote Sensing*, 62(1), 151–161.

ENVI, 2000. ENVI User's Guide. Research Systems Inc., Boulder, Colorado, pp. 930.

Fazakas, Z., Nilsson, M., Olsson, H., 1999. Regional forest biomass and wood volume estimation using satellite data and ancillary data. *Agricultural and Forest Meteorology*, 98-99, 417-425.

Fernández-Manso, O., Fernández-Manso, A., Quintano, C., 2014. Estimation of aboveground biomass in Mediterranean forests by statistical modelling of ASTER fraction images, *International Journal of Applied Earth Observation and Geoinformation,* 31, 45-56.

Fernández-Manso, O., Fernández-Manso, A., Quintano, C., Álvarez, F., 2005a. Mapping forest cover changes caused by mining activities using spectral mixture analysis and object oriented classification. ForestSat 2005 -Scientific workshop in operational tools in forestry using remote sensing techniques. May 31 - June 3, 2005, Borås -Sweden-. In Håkan Olsson (ed.) Proceedings of ForestSat 2005 - Scientific workshop in operational tools in forestry using remote sensing techniques, 8c, 77-81.

Fernández-Manso, O., Quintano, C., Fernández-Manso, A., 2009. Combining spectral mixture analysis and object-based classification for fire severity mapping. *Forest systems*, 18(3), 296-313.

Fernández-Manso, A., Quintano, C., Fernández-Manso, O., dos Santos, J.R., Maldonado, F.D., 2005b. Spectral Mixture Modeling to estimate wood volume in the north of Spain from optical satellite data. *Ambiência*, 1 (2), 213-222.

Fernández-Manso, A., Quintano, C., Roberts, D., 2012. Evaluation of potential of multiple endmember spectral mixture analysis (MESMA) for surface coal mining affected area mapping in different world forest ecosystems. *Remote Sensing of Environment*., 127, 181-193.

Foody, G., Boyd, D., Cutler, M., 2003. Predictive relations of tropical biomass from Landsat TM data and their transferability between regions. *Remote Sensing of Environment*, 85, 463-474.

Franklin, S.E., 2010. Remote Sensing for Biodiversity and Wildlife Management: Synthesis and Applications. McGraw-Hill Companies, Inc., USA.

Gabban, A., San-Miguel-Ayanz, J., Barbosa, P., Libertà, G., 2006. Analysis of NOAA-AVHRR NDVI inter-annual variability for forest fire risk estimation. *International Journal of Remote Sensing*, 27(8), 1725-1732.

Garcia-Haro, F.J., Gilabert, M.A., Melia, J., 1996. Linear spectral mixture modelling to estimate vegetation amount from optical spectral data. *International Journal of Remote Sensing*, 17(17), 3373-3400.

García-Haro, F., Gilabert, M., Meliá, J., 1999. Extraction of endmembers from spectral mixtures. *Remote Sensing of Environment*, 68, 237–253.

Ghasemi, N., Sahebi, M.R., Mohammadzadeh, A., 2013. Biomass estimation of a tem-perate deciduous forest using wavelet analysis. *IEEE Trans. Geosci. Remote Sens*., 51, 765–776.

Gjertsen AK, 2007. Accuracy of forest mapping based on Landsat TM data and a kNN-based method. *Remote Sensing of Environment* 110, 420-430.

Gong, P., Miller, J., Spanner, M., 1994. Forest canopy closure from classification and spectral unmixing of scene components – multisensor evaluation of an open canopy. *IEEE Transactions on Geoscience and Remote Sensing*, 32, 1067–1079.

Gong, P., Xu, B., 2003. Remote sensing of forests over time: change types, methods, and opportunities. In Remote Sensing of Forest Environments: Concepts and Case Studies, Wulder, M.A., S.E. Franklin, S.E. (eds.), (Dordrecht/Boston/London: Kluwer Academic Publishers).

Goovaerts, P., Jazquez, G. M., Marcus, A., 2005. Geostatistical and local cluster analysis of high resolution hyperspectral imagery for detection of anomalies. *Remote Sensing of Environment*, 95, 351-367.

Green, A.A., Berman, M., Switzer, P., Craig, M.D., 1988. A transformation for ordering multispectral data in terms of image quality with implications for noise removal. *IEEE Transactions on Geoscience and Remote Sensing*, 26, 65-74.

Guo, Q.H., Kelly, M., Gong, P., Liu, D.S., 2007. An object-based classification approach in mapping tree mortality us- ing high spatial resolution imagery. *Giscience & Remote Sensing*, 44(1), 24-47.

Hall, O., Hay, G.J., Bouchard, A., Marceau, D.J., 2004. Detecting dominant landscape objects through multiple scales: An integration of object-specific methods and watershed segmentation. *Landscape Ecology*, 19, 59-76.

Hall, F.G., Shimabukuro, Y.E., Huemmrich, K.F., 1995. Remote sensing of forest biophysical structure in boreal stands of picea mariana using mixture decomposition and geometric reflectance models. *Ecological Applications*, 5, 993-1013.

Hall, R.J., Skakun, R.S, Arsenault, E.J., Caser, B.S., 2006. Modeling forest stand structure attributes using Landsat ETM+ data: Application to mapping of aboveground biomass and stand volume. *Forest Ecology and Management*, 225, 378-390.

Hamdan, O., Aziz, H. Khali, Rahman, K. Abd, 2011. Remotely Sensed L-Band SAR Data for Tropical Forest Biomass. *Journal of Tropical Forest Science*, 23 (3), 318.

Hansen, M. J., Franklin, S. E., Woudsmaa, C. G., Peterson, M., 2001. Caribou habitat mapping and fragmentation analysis using Landsat MSS, TM, and GIS data in the North Columbia Mountains, British Columbia, Canada. *Remote Sensing of Environment*, 77, 50-65.

Harris, S., Veraverbeke, S., Hook, S., 2011. Evaluating spectral indices for assessing fire severity in chaparral ecosystems (southern California) using MODIS/ASTER (MASTER) airborne simulator data. *Remote Sensing*, 3, 2403-2419.

Hay, G.J., Castilla, G., Wulder, M.A., Ruiz, J.R., 2005. An automated object-based approach for the multiscale image segmentation of forest scenes. *International Journal of Applied Earth Observation and Geoinformation* 7 (4), 339–359.

Hay, G.J., Blaschke, T., 2010. Forward: special issue on Geographic Object-Based Image Analysis (GEOBIA). *Photogrammetric Engineering and Remote Sensing* 7 (2), 121–122.

Hay, G.J., Castilla, G. C., 2006. Object-Based Image Analysis: Strengths, weaknesses, opportunities and threats (SWOT), Proceedings from Bridging Remote Sensing and GIS: International Symposium on Object-based Image Analysis, 04–05 July, Salzburg, Center for Geoinformatics, URL:(http://www.commission4.isprs.org/obia06/ (last date accessed: 02 December 2009).

Hay, G.J., Castilla, G. C., 2008. Geographic Object-Based Image Analysis (GEOBIA): a new name for a new discipline. In: Blaschke, T., Lang, S., Hay, G. (Eds.), Object-Based Image Analysis. Springer, Heidelberg, Berlin, New York, pp. 75–89.

He, L., Li, Z., 2012. Enhancement of a fire detection algorithm by eliminating solar reflection in the mid-IR band: application to AVHRR data, *Int. J. Remote Sens*., 33, 7047-7059.

Healey, S.P., Yang, Z., Cohen, W.B., Pierce, D.J., 2006. Application of two regression-based methods to estimate the effects of partial harvest on forest structure using Landsat data. *Remote Sensing of Environment,* 101, 115-126.

Helmer, E.H., Brown, S., Cohen, W.B., 2000. Mapping montane tropical successional stage and land use with multi-date Landsat imagery. *International Journal of Remote Sensing*, 21, 2163-2183.

Heymann, Y., Steenmans, C., Croissille, G., Bossard, M., 1994. 'Corine land cover'. Technical guide. EUR 12585, Luxembourg, Office for Official Publications of the European Communities.

Holmgren, J., Joyce, S., Nilsson, M., Olsson, H., 2000. Estimating stem volume and basal area in forest compartments by combining satellite image data with field data. *Scandinavian Journal of Forest Research*, 15, 103-111.

Huang, J., Chen, D., Cosh, M.H., 2009. Sub-pixel reflectance unmixing in estimatingvegetation water content and dry biomass of corn and soybeans cropland usingnormalized difference water index (NDWI) from satellites. *Int. J. Remote Sens*.30, 2075–2104.

Huang, C., Wylie, B., Yang, L., Homer, C., Zylstra, G., 2002. Derivation of a tasseled cap transformation based on Landsat 7 at-satellite reflectance. *International Journal Remote Sensing*, 23, 1741-1748.

Huesca, M., Merino-de-Miguel, S., González-Alonso, F., Martínez, S., Miguel Cuevas, J., Calle, A., 2013. Using AHS hyper-spectral images to study forest vegetation recovery after a fire. *International Journal of Remote Sensing*, 34(11), 4025-4048.

Hudak, A., Morgan, P., Bobbitt, M., Smith, A., Lewis, S., Lentile, L., 2007. The relationship of multispectral satellite imagery to immediate fire effects. *Journal of Fire Ecology*, 3, 64–90.

Hyyppä, J., Hyyppä, H., Inkinen, M., Engdahl, M., Linko, S., Zhu, Y. H., 2000. Accuracy comparison of various remote sensing data sources in the retrieval of forest stand attributes. *Forest Ecology and Management*, 128, 109-120.

Irons, J. R., Masek, J. G., 2006. Requirements for a Landsat Data Continuity Mission. *Photogrammetric Engineering and Remote Sensing*, 72, 1102-1108.

Iwasaki, A., Tonooka, H., 2005. Validation of a crosstalk correction algorithm for ASTER/SWIR, *IEEE Transactions on Geoscience and Remote Sensing*, 43, 2747- 2751.

Iwasaki, A., Fujisada, H., Akao, H. Shindou, O., Akagi, S., 2002. Enhancement of Spectral Separation Performance for ASTER/SWIR, *SPIE Proceedings*, 4486, 42-50.

Jensen, J.R., 2005. Introductory digital image processing. A remote sensing perspective. Third edition. Prentice Hall, NJ, USA.

Ji, L., Wylieb, B.K., Nossovc, D.R., Petersona, B., Waldropd, M.P., McFarlandd, J.W., Roverb, J., Hollingsworth, T.N., 2012. Estimating aboveground biomass in interior Alaskawith Landsat data and field measurements. *International Journal of Applied Earth Observation and Geoinformation* 18, 451-461.

Jiang, H., Feng, M., Zhu, Y., Lu, N., Huang, J., Xiao, T., 2014. An Automated Method for Extracting Rivers and Lakes from Landsat Imagery. *Remote Sens*. 6(6), 5067-5089.

Jin, S., Sader, S.A., 2005. Comparison of time series tasseled cap wetness and the normalized difference moisture index in detecting forest disturbances. *Remote Sensing of Environment*, 94, 364-372.

Johansen, K., Coops, N.C., Gergel, S.E., Stange, J., 2007. Application of high spatial resolution satellite imagery for riparian and forest ecosystem classification. *Remote Sensing of Environment* 110 (1), 29-44.

Kajisa, T., Murakami, T., Mizoue, N., Kitahara, F., Yoshida, S., 2008. Estimation of stand volumes using the k-nearest neighbors method in Kyushu, Japan. *Journal of Forest Research* 13, 249-254.

Kajisa, T., Murakami, T., Mizoue, N., Top, N., Yoshida, S., 2009. Object-based forest biomass estimation using Landsat ETM+ in Kampong Thom Province, Cambodia. *Journal of Forest Research*, 14(4), 203-211.

Kalluri, S.N.V., Huang, C., Mathieu-Marni, S., Townshend, J.R.G., Yang, K., Chellapa, R., 1997. A comparison of mixture modeling algorithms and their applicability to the MODIS data. IEEE International Geoscience and Remote Sensing Symposium (IGARSS) Singapore, 1, 171–173.

Kauth, R.J., Thomas, G.S., 1976. The tasseled cap—a graphic description of the spectral-temporal development of agricultural crops as seen in Landsat, In: Proceedings on the Symposium on Machine

Processing of Remotely Sensed Data, West Lafayette, Indiana, June 29 - July 1, 1976, (West Lafayette, Indiana: LARS, Purdue University), pp. 41-51.

Keshava, N., Mustard, J., 2002. Spectral unmixing. Signal Process- ing Magazine, IEEE 19 (1), 44–57.

Key, C.H., Benson, N.C., 2006. Landscape Assessment: Ground measure of severity, the Composite Burn Index; and Remote sensing of severity, the Normalized Burn Ratio. In D.C. Lutes; R.E. Keane; J.F. Caratti; C.H. Key; N.C. Benson; S. Sutherland; and L.J. Gangi. 2006. FIREMON: Fire Effects Monitoring and Inventory System. USDA Forest Service, Rocky Mountain Research Station, Ogden, UT. Gen. Tech. Rep. RMRS-GTR-164-CD: LA 1-51.

Kruse, F., Lefkoff, A.B., Boardman, J.W., Heidebrecht, K.B., Shapiro, A.T., Barloon, P.J., Goetz, A.F., 1993. The spectral image processing system (SIPS) – interactive visualization and analysis of imaging spectrometer data. *Remote Sensing of Environment*, 44, 145–163.

Labrecque, S., Fournier, R.A., Luther, J.E., Piercey, D., 2006. A comparison of four methods to map biomass from Landsat-TM and inventory data in western Newfoundland. *Forest Ecology and Management*, 226, 129-144.

Lackner, M., Conway, T.M., 2008. Determining land-use information from land cover through an object-oriented classification of IKONOS imagery. *Canadian Journal of Remote Sensing* 34 (2), 77-92.

Lang, S., 2005. Image-objects and landscape objects interpretation, hierarchical representation and significance. Academic dissertation, Salzburg.

Lang, S., Langanke, T., 2006. Object-based mapping and object-relationship modeling for land use classes and habitats. Photogrammetrie, Fernerkundung, *Geoinformation* 10 (1), 5-18.

Lasaponara, R., Lanorte, A., 2006. Multispectral fuel type characterization based on remote sensing data and Prometheus model. *Forest Ecology and Management*, 234, S226.

Latifovic, R., Fytas, K., Chen, J., Paraszczak, J., 2005. Assessing land cover change resulting from large surface mining development. *International Journal of Applied Earth Observation and Geoinformation*, 7, 29–48.

Lauer, D.T., Morain, S.A., Salomonson, V.V., 1997. The Landsat program: its origins, evolution and impacts. *Photogrammetric Engineering and Remote Sensing*, 63 (7), 831-838.

Lea, R., Blodgett, C., Diamond, D., Schanta, M., 2004. Using the tasseled cap transformation to identify change in the missouri ozark forests, In: Proceedings of the ASPRS Fall Conference: Images to Decisions: Remote Sensing Foundations for GIS Applications.

Lee, J.B., Woodyatt, A.S., and Berman, M., 1990. Enhancement of High Spectral Resolution Remote Sensing Data by a Noise-Adjusted Principal Components Transform, *IEEE Transactions on Geoscience and Remote Sensing*, 28, (3), 295-304.

Lefsky, M.A., Harding, D.J., Keller, M., Cohen, W.B., Carabajal, C.C., Del Bom Espirito-Santo, F., Hunter, M.O. de Oliveira, R., 2005. Estimates of forest canopy height and aboveground biomass using ICESat. *Geophysical Research Letters* 32.

Lentile, L., Holden, Z., Smith, A., Falkowski, M., Hudak, A., Morgan, P., 2006. Remote sensing techniques to assess active fire characteristics and post-fire effects. *International Journal of Wildland Fire*, 15, 319–345.

Lentile, L. B., Smith, A. M. S., Hudak, A. T., Morgan, P., Bobbitt, M. J., Lewis, S. A., 2009. Remote sensing for prediction of 1-year post-fire ecosystem condition. *International Journal of Wildland Fire*, 18, 594–608.

Lévesque, J., Staenz, K., 2008. A method for monitoring mine tailings re-vegetation using hyperspectral remote sensing. Proceedings of 2004 IEEE International Geoscience and Remote Sensing Symposium (IGARSS 2004), 20–24 September 2004, Anchorage, AK (pp. 575–587).

Lippitt, C.D., Coulter, Ll. L., Freeman, M., Lamantiabishop, J., Pang, W., Stow, D. A., 2012. The effect of input data transformations on object-based image analysis. *Remote Sens Lett*. 3(1), 21–29.

Liu W., Song C., Schroeder T.A., Cohen W.B., 2008. Predicting forest successional stages using multitemporal Landsat imagery with forest inventory and analysis data. *International Journal of Remote Sensing* 29, 3855-3872.

Liu, D., Xia, F., 2010. Assessing object-based classification: Advantages and limitations. *Remote Sensing Letters*, 1(4), 187-194.

Loveland, T.R., Dwyer, J.L., 2012. Landsat: building a strong future. *Remote Sensing of Environment*, 122, 22-29.

Lu, D., 2006. The potential and challenge of remote sensing-based biomass estimation. *International Journal of Remote Sensing*, 27, 1297-1328.

Lu, D., Chen, Q., Wang, G., Liu, L., Li, G., Moran, E., 2014. A survey of remote sensing-based aboveground biomass estimation methods in forest ecosystems. *International Journal of Digital Earth*, 1-43.

Lu, D., Mausel, P., Brondizio, E., Moran, E., 2004. Relationships between forest stands parameters and Landsat TM spectral responses in the Brazilian Amazon Basin. *Forest Ecology and Management*, 198, 149-167.

Lu, D., Moran, E., Batistella, M., 2003. Linear mixture model applied to Amazonian vegetation classification. *Remote Sensing of Environment*, 87(4), 456-469.

Lu, D., Batistella, M., Moran, E., 2005. Satellite estimation of aboveground biomassand impacts of forest stand structure. *Photogramm. Eng. Remote Sens*. 71, 967–974.

Luther, J.E., Fournier, R.A., Piercey, D.E., Guindon, L., Hall, R.J., 2006. Biomass mapping using forest type and structure derived from Landsat TM imagery. *International Journal of Applied Earth Observation and Geoinformation* 8, 173-187.

Magnusson, M., Fransson, J.E.S., 2005. Estimation of forest stem volume using multispectral optical satellite and tree height data in combination. *Scandinavian Journal of Forest Research* 20, 431-440.

Mäkelä, H., Pekkarinen, A., 2004. Estimation of forest stand volumes by Landsat TM imagery and stand-level field-inventory data. *Forest Ecology and Management*, 196(2-3), 245-255.

Manna, S., Nandy, S., Chanda, A., Akhand, A., Hazra, S., Dadhwal, V., 2014. Estimating aboveground biomass in avicennia marina plantation in indian sundarbans using high-resolution satellite data. J. *Appl. Remote Sens.* 8(1), 083638.

Manolakis, D.G., Ingle, V.K., Kogon, S.M., 2000. Statistical and Adaptive Signal Processing (New York: McGraw-Hill).

Manzo-Delgado, L., Sánchez-Colón, S., Álvarez, R., 2009. Assessment of seasonal forest fire risk using NOAA-AVHRR: a case study in central Mexico. *International Journal of Remote Sensing*, 30(19), 4991-5013.

Mallinis, G., Koutsias, N., Tsakiri-Strati, M., Karteris, M., 2008. Object-based classification using Quickbird imagery for delineating forest vegetation polygons in a Mediterranean test site. *ISPRS Journal of Photogrammetry and Remote Sensing*, 63, 237-250.

Martínez-Millán, J., 1997. Country report from Spain. In: European Commission (1997): Study of European forestry information and communication system- Reports on forestry inventory and survey systems, Luxemburg, pp. 905-954.

Maselli, F., Chiesi, M., Montaghi, A., Pranzini, E., 2011. Use of ETM+ images to extend stem volume estimates obtained from LiDAR data. *International Journal of Remote Sensing*, 66(5), 662-671.

Matthew, M.W., Adler-Golden, S.M., Berk, A., Richtsmeier, S.C., Levine, R.Y., Bern-stein, L.S., Acharya, P.K., Anderson, G.P., Felde, G.W., Hoke, M.P., Ratkowski, A.,Burke, H., Kaiser, R.D., Miller, D.P., 2000. Status of atmospheric correction usinga MODTRAN4-based algorithm. In: SPIE Proceedings, Algorithms for Multispec-tral, Hyperspectral, and Ultraspectral Imagery VI, 4049, 199–207.

McRoberts, R.E., 2009. A two-step nearest neighbors algorithm using satellite imagery for predicting forest structure within species composition classes. *Remote Sensing of Environment*, 113(3), 532-545.

McRoberts R.E., 2012. Estimating forest attribute parameters for small areas using nearest neighbors techniques. *Forest Ecology and Management* 272, 3-12.

Metternitch, G.I., Fermont, A., 1998. Estimating erosion surface features by linear mixture modeling. *Remote Sensing of Environment*, 64, 254–265.

Meyers, S.D., Kelly, B.G., O'Brien, J.J., 1993. An introduction to wavelet analysis in oceanography and meteorology: with application to the dispersion of Yanai waves. *American Meteorological Society*, 121, 2858-2866.

Michishita, R., Gong, P., Xu, B., 2012. Spectral mixture analysis for bi-sensor wetland mapping using Landsat TM and Terra MODIS data. *International Journal of Remote Sensing*, 33(11), 3373–3401.

Miettinen, J., Hyer, E., Chia, A. S., Kwoh, L. K., Liew, S. C., 2013. Detection of vegetation fires and burnt areas by remote sensing in insular Southeast Asian conditions: current status of knowledge and future challenges. *International Journal of Remote Sensing*, 34(12), 4344-4366.

Minnaert, N., 1941. The Reciprocity Principle in Lunar Photometry. *Astrophysical Journal*, 93, 403-410.

Mitri, G.H., Gitas, I.Z., 2004. A semi-automated object-oriented model for burned area mapping in the Mediterranean region using Landsat-TM imagery. *International Journal of Wildland Fire*, 13, 367-376.

Mitri, G.H., Gitas, I.Z., 2008. Mapping the severity of fire using object-based classification of IKONOS imagery. *International Journal of Wildland Fire*, 17, 431-442.

Moeur, M., Stage, A.R., 1995. Most similar neighbor: An improved sampling inference procedure for natural resource planning. *Forest Science* 41. 337-359.

Möller, M., Lymburner, L., Volk, M., 2007. The comparison index: a tool for assessing the accuracy of image segmentation. *International Journal of Applied Earth Observation and Geoinformation*, 9, 311–321.

Moran, P.A.P., 1948. The interpretation of statistical maps. *Journal of the Royal Statistical Society*, Series B 37(2): 243–251.

Morel, A. C., Fisher, J. B., Malhi, Y., 2012. Evaluating the potential to monitor aboveground biomass in forest and oil palm in Sabah, Malaysia, for 2000-2008 with Landsat ETM+ and ALOS-PALSAR. *International Journal of Remote Sensing*, 11, 3614-3639.

Muukkonen, P., Heiskanen, J., 2005. Estimating biomass for boreal forests using ASTER satellite data combined with standwise forest inventory data. *Remote Sensing of Environment*, 99, 434-447.

Navon, D., 1977. Forest before trees: The precedence of global features in visual perception. *Cognitive Psychology*, 9, 353-383.

Neubert, M., Herold, H., Meinel, G., 2008. Assessing image segmentation quality.Concepts, methods and application. In: Blaschke, T., Lang, S., Hay, G.J. (Eds.), Object Based Image Analysis. Springer, Heidelberg, Berlin, New York, pp. 760-784.

Palandjian, D., Gitas, I. Z., Wright, R., 2009. Burned area mapping and post-fire impact assessment in the Kassandra peninsula (Greece) using Landsat TM and Quickbird data. *Geocarto International*, 24(3), 193-205.

Parks, N. F., Peterson, G. W., Baumer, G. M., 1987. High resolution remote sensing of spatially and spectrally complex coal surface mines of Central Pennsylvania: A comparison between SPOT, MSS and Landsat-TM, *Photogrammetric Engineering and Remote Sensing*, 53, 415- 420.

Pascual, C., García-Abril, A., García-Montero, L.G., Martín-Fernández, S., Cohen, W.B., 2008. Object-based semi-automatic approach for forest structure characterization using lidar data in heterogeneous Pinus sylvestris stands. *Forest Ecology and Management* 255 (11), 3677-3685.

Patterson, M.W., Yool S.R., 1998. Mapping fire-induced vegetation mortality using Landsat Thematic Mapper data: a comparison of linear transformation techniques. *Remote Sensing of Environment*, 65, 132-142.

Peddle, D.R., Brunke, S.P., Hall, F.G., 2001. A comparison of spectral mixture analysis and ten vegetation indices for estimating Boreal forest biophysical informationfrom airborne data. *Can. J. Remote Sens*. 27, 627–635.

Peddle, D.R., Hall, F.G., Ledrew, F.G., 1999. Spectral mixture analysis and geometric-optical reflectance modeling of boreal forest biophysical structure. *Remote Sensing of Environment*, 67, 288 297.

Peddle, D.R., Johnson, R.L., 2000, Spectral mixture analysis of airbone remote sensing imagery for improved prediction of Leaf Area Index in mountainous terrain, Kananoskis Alberta. *Canadian Journal of Remote Sensing*, 26, 177-188.

Peddle, D.R., Teillet, Ph.M., Wulder, M.A., 2003. Radiometric processing. In: Remote Sensing of Forest Environments: Concepts and Case Studies, Wulder, M.A., Franklin, S.E. (eds.), (Dordrecht/Boston/London: Kluwer Academic Publishers).

Peterson, U., Nilson, T. 1993. Successional reflectance trajectories in northern temperate forests. *International Journal Remote Sensing*, 14, 609-613

Peterson, S.H., Stow, D.A., 2003. Using multiple image endmember spectral mixture analysis to study chaparral regrowth in southern California. *International Journal of Remote Sensing*, 24, 4481–4504.

Piao, S.L., Fang, J.Y., Liu, H.Y., Zhu, B., 2005. NDVI-indicated decline in desertification in China in the past two decades. *Geophys. Res. Lett*. 32.

Poulain, M., Peña, M., Schmidt, A., Schmidt, H., Schulte, A., 2012. Abovegroundbiomass estimation in intervened and non-intervened Nothofagus pumilioforests using remotely sensed data. *Int. J. Remote Sens.* 33, 3816–3833.

Powell, S.L., Cohen, W.B., Healey, S.P., Kennedy, R.E., Moisen, G.G., Pierce, K.B., Ohmann, J.L., 2010. Quantification of live aboveground forest biomass dynamics with Landsat time-series and field inventory data: A comparison of empirical modeling approaches. *Remote Sensing of Environment* 114, 1053-1068.

Quintano, C., Fernández-Manso, A., Fernández-Manso, O., Shimabukuro, Y., 2006. Mapping burned areas in Mediterranean countries using Spectral Mixture Analysis from a unitemporal perspective. *International Journal of Remote Sensing*, 27(4), 645–662.

Quintano, C., Fernández-Manso, A., Roberts, D.A., 2013. Multiple Endmember Spectral Mixture Analysis (MESMA) to map burn severity levels from Landsat images in Mediterranean countries *Remote Sensing of Environment*, 136, 76-88.

Quintano, C., Shimabukuro, Y.E., 2009. Estimación de superficie quemada mediante la aplicación sinérgica de OBIA y SMA a imágenes WFI CBERS. Anais do XIV Simpósio Brasileiro de Sensoramiento Remoto - SBSR, Natal-RN, 25-30 de abril de 2009, pp. 2119-2126

Rathore, C.S., Wright, R. 1993. Monitoring environmental impacts of surface coal mining. *International Journal of Remote Sensing.* 14, 1021-1042.

Ray, T.W., Murray, B.C., 1996. Nonlinear spectral mixing in dessert vegetation. *Remote Sensing of Environment*, 55, 59-64.

Reese, H., Nilsson, M., Sandström, P., Olsson, H., 2002. Applications using estimates of forest parameters derived from satellite and forest inventory data. *Computers and Electronics in Agriculture* 37, 37-55.

Riaño, D., Chuvieco, E., Salas, J., Aguado, I., 2003. Assessment of different topographic corrections in Landsat-TM data for mapping vegetation types. *IEEE Transactions on Geoscience and remote sensing,* 41(5), 1056-1061.

Richter, N., Staenz, K., Kaufmann, H., 2008. Spectral unmixing of airborne hyperspectral data for baseline mapping of mine tailings areas. *International Journal of Remote Sensing*, 29, 3937–3956.

Roberts, D.A., Adams, J.B. and Smith, M.O., 1993. Discriminating green vegetation, non-photosynthetic vegetation and soils in AVIRIS data. *Remote Sensing of Environment*, 44, pp. 255-269.

Roberts, D.A., Batista, G.T., Pereira, J.L.G., Waller, E.K., and Nelson, B.W., 1998. Change identification using multitemporal spectral mixture analysis: Applications is eastern Amazonia, Remote Sensing Change Detection: Environmental Monitoring Methods and Applications (R. S. Lunetta and C. D. Elvidge, editors). Ann Arbor Press, Ann Arbor, Mich., pp. 137-161.

Roberts, D.A., Green, R.O., Adams, J.B., 1997. Temporal and spatial patterns in vegetation and atmospheric properties from AVIRIS: *Remote Sensing of Environment*, 62, 223-240.

Roder, A., Kuemmerle, T., Hill, J., 2005. Extension of retrospective datasets using multiple sensors. An approach to radiometric intercalibration of Landsat TM and MSS data. *Remote Sensing of Environment*, 95, 195-210.

Rogan, J., Franklin, J., 2001. Mapping burn severity in Southern California using spectral mixture analysis. In: Proceedings of the International Geoscience and Remote Sensing Symposium (IGARRS 01), Sydney, Australia, 9-13 July.

Rosenqvist, A., Milne, A., Lucas, R., Imhoff, M., Dobson, C., 2003. A review of remote sensing technology in support of the Kyoto Protocol. *Environmental Science and Policy*, 6, 441–455.

Rouse, J.W., Haas R.H., Schell J.A., Deering D.W., 1973. Monitoring vegetation systems in the Great Plains with ERTS. In: Fraden S.C., Marcanti E.P., Becker M.A. (eds.). Third ERTS-1 Symposium, 10–14 Dec. 1973, NASA SP-351, Washington D.C. NASA, pp. 309–317.

Roy, P.S., Ravan, S.A., 1996. Biomass estimation using satellite remote sensing data—An investigation on possible approaches for natural forest. *Journal of Biosciences*, 21(4), 535-561.

Sayn-Wittgenstein, L., 1986. Forest information requirements. *Remote Sensing Reviews* 2, 7-26.

Scarascia-Mugnozza, G., Oswald, H., Piussi, P., Radoglou, K., 2000. Forests of the Mediterranean region: Gaps in knowledge and research needs. *Forest Ecology and Management* 132, 97-109.

Schmidt, H., Glaesser, C., 1998. Multitemporal analysis of satellite data and their use in the monitoring of the environmental impacts of open cast lignite mining areas in Eastern Germany. *International Journal of Remote Sensing*. 12, 2245-2260.

Schmid, T., Koch, M., Gumuzzio, J., Mather, P.M., 2004. A spectral library for a semiarid wetland and its application to studies of wetland degradation using hyperspectral and multispectral data. *International Journal of Remote Sensing*, 25, 2485–2496.

Schroeter, L. E., 2011. Analyses and monitoring of lignite mining lakes in Eastern Germany with spectral signatures of Landsat TM satellite data. *International Journal of Coal Geology*, 86, 27–39.

Settle, J., Campbell, N., 1998. On the errors of two estimators of sub-pixel fractional cove when mixing is linear. *IEEE Geoscience and Remote Sensing*, 36, 163-170.

Settle, J.J., Drake, N.A., 1993. Linear mixing and the estimation of ground cover proportions. *International Journal of Remote Sensing*, 14, 1159-1177.

Shang, J., Morris, B., Howarth, P., Lévesque, J., Staenz, K., Neville, B., 2009. Mapping mine tailing surface mineralogy using hyperspectral remote sensing. *Canadian Journal of Remote Sensing/Journal canadien de Télédétection*, 3, S126–S141.

Shendryk, I., M. Hellström, L. Klemedtsson, N. Kljun, 2014. Low-density LiDAR and optical imagery for biomass estimation over boreal forest in Sweden, *Forests*, 5, 992-1010.

Shimabukuro, Y.E., 1987. Shade images derived from linear mixing models of multispectral measurements of forested areas. In Dissertation Degree of Doctor of Philosophy (Fort Collins, CO : Colorado State University).

Shimabukuro, Y.E., Batista, G.T., Mello, E.M., Moreira, J.C., Duarte, V., 1998. Using shade fraction image segmentation to evaluate deforestation in Landsat Thematic Mapper images of the Amazon Region. *International Journal of Remote Sensing*, 19, 535–541.

Shimabukuro, Y.E., Smith, J., 1991. The least-squares mixing models to generate fraction images derived from remote sensing multispectral data. *IEEE Transactions on Geoscience and Remote Sensing*, 29, 16-21.

Small, C., 2001. Estimation of urban vegetation abundance by spectral mixture analysis. *International Journal of Remote Sensing*, 22, 1305– 1334.

Small, C., 2004. The Landsat ETM+ spectral mixing space. *Remote Sensing of Environment*, 93, 1-17.

Smith, M.O., Johnson, P.E., Adams, J.B., 1985. Quantitative determinatión of mineral types and abundances from reflectance spectra using principal components analysis. *Journal of Geophysical Research*, 90, 797–804.

Smith, A. M. S., Lentile, L. B., Hudak, A. T., Morgan, P., 2007. Evaluation of linear spectral unmixing and ΔNBR for predicting post-fire recovery in a North American ponderosa pine forest. *International Journal of Remote Sensing*, 28, 5159–5166.

Smith, A.M.S., Wooster M.J., Drake, N.A., Dipotso, F.M., Falkowski, M.J., Hudak, A.T., 2005. Testing the potential of multi-spectral remote sensing for retrospectively estimating fire severity in African savanna environments. *Remote Sensing of Environment*, 97 (1), 92-115.

Smith, M.O., Ustin, S.L., Adams, J.B., and Gillespie, A.R., 1990. Vegetation in deserts: I. A regional measure of abundance from multispectral images. *Remote Sensing of Environment*, 31, 1-26.

Soenen, S.A., Peddle, D.R., Hall, R.J., Coburn, C.A., Hall, F.G., 2010. Estimating aboveground forest biomass from canopy reflectance model inversion in mountainous terrain. *Remote Sensing of Environment*, 114 (7), 1325–1337.

Sohn, Y., McCoy, R. M., 1997. Mapping desert shrub rangeland using spectral unmixing and modeling spectral mixtures with TM data. *Photogrammetric Engineering and Remote Sensing* 63(5), 707-716.

Song, M., Civco, D.L., Hurd, J.D., 2005. A competitive pixel-object approach for land cover classification. *International Journal of Remote Sensing*, 26, 4981–4997

Song, X.-P., Huang, C., Feng, M., Sexton, J.O., Channan, S., Townshend, J.R., 2014. Integrating global land cover products for improved forest cover characterization: an application in North America. *International Journal of Digital Earth*. DOI: 10.1080/17538947.2013.856959

Soverel, N. O., Perrakis, D. D. B., Coops, N. C., 2010. Estimating burn severity from Landsat dNBR and RdNBR indices across western Canada. *Remote Sensing of Environment*, 114, 1896–1909.

Tan, B., J. Masek, R. Wolfe, F. Gao, C. Huang, E. Vermote, J.O. Sexton, G. Ederer., 2013. Improved forest change detection with terrain illumination-corrected images. *Remote Sensing of Environment*, 136, 469–483.

Teillet, P.M., Guindon, B., Goodenough, D.G., 1982. On the slope-aspect correction of multispectral scanner data. *Can. J. Remote Sens*. 8, 84-106.

Tompkins, S., Mustard, J.F., Pieters, C.M., Forsyth, D.W., 1997. Optimization of endmembers for spectral mixture analysis. *Remote Sensing of Environment*, 59, 472–489.

Tomppo, E., Nilsson, M., Rosengren, M., Aalto, P., Kennedy, P., 2002. Simultaneous use of Landsat-TM and IRS-1c WiFs data in estimating large area tree stem volume and aboveground biomass. *Remote Sensing of Environment*, 82, 156-171.

Tonooka, H., Iwasaki, A., 2003. Improvement of ASTER/SWIR Crosstalk Correction, SPIE Proceedings, 5234, 168-179.

Townsend, P.A., Helmers, D.P., Kingdon, C.C., McNeil, B.E., de Beurs, K.M., Eshleman, K.N., 2009. Changes in the extent of surface mining and reclamation in the Central Appalachians detected using a 1976–2006 Landsat time series. *Remote sensing of environment*. 113, 62-72.

Townshend, J.R., Masek, J.G., Huang, C., Vermote, E.F., Gao, F., Channan, S., Sexton, J.O., Feng, M.R., Narasimhan, D.-H. Kim, K. Song, D. Song, X. Song, P. Noojipady, B. Tan, M.C. Hansen, M. Li, R. Wolfe. 2012. Global characterization and monitoring of forest cover using Landsat data: opportunities and challenges. *International Journal of Digital Earth*,.5, 373-397.

Trigg, S., Flasse, S., 2001. An evaluation of different bi-spectral spaces for discriminating burned shrub-savanna. *Int. J. Remote Sens*., 22, 2641-2647.

Trotter CM, Dymond JR, Goulding CJ, 1997. Estimation of timber volume in a coniferous plantation forest using Landsat TM. *International Journal of Remote Sensing* 18: 2209-2223.

Tso, B., Mather, P.M., 2001. Classification methods for remotely sensed data. Taylor and Francis, Inc.

Turner, M.G., Tinker, D.B., Romme, W.H., Kashian, D.M., Litton, C.M., 2004. Landscape patterns of sapling density, leaf area, and aboveground net primary production in postfire lodgepole pine forests, Yellowstone National Park (USA). *Ecosystems* 7, 751–775.

Van der Meer, F., 1995. Spectral unmixing of Landsat Thematic Mapper data. *International Journal of Remote Sensing*, 16, 3189–3194.

Van der Meer, F., De Jong, S.M., 2000. Improving the results of spectral unmixing of LANDSAT TMimagery by enhancing the orthogonality of end-members. *International Journal of Remote Sensing*, 21, 2781–2797.

Van der Werff, H.M.A., van der Meer, F.D., 2008. Shape-based classification of spectrally identical objects. *ISPRS Journal of Photogrammetry and Remote Sensing* 63 (2), 251-258.

Van Wagtendonk, J. W., Root, R. R., 2003. The use of multi-temporal Landsat Normalized Difference Vegetation Index (NDVI) data for mapping fuel models in Yosemite National Park, USA. *International Journal of Remote Sensing*, 24(8), 1639-1651.

Veraverbeke, S., Lhermitte, S., Verstraeten, W. W., Goossens, R., 2011. Evaluation of pre/post-fire differenced spectral indices for assessing burn severity in a Mediterranean environment with Landsat Thematic Mapper. *International Journal of Remote Sensing*, 32(12), 3521–3537.

Veraverbeke, S., Verstraeten, W.W., Lhermitte, S., Goossens, R., 2010. Evaluating Landsat Thematic Mapper spectral indices for estimating burn severity of the 2007 Peloponnese wildfires in Greece. *Int. J. Wildland Fire*, 19, 558-569.

Viana, H., Aranha, J., Lopes, D., Cohen, W.B., 2012. Estimation of crown biomass of Pinus pinaster stands and shrubland above-ground biomass using forest inventory data, remotely sensed imagery and spatial prediction models. *Ecological Modelling* 226, 22-35.

Wuest, B., Zhang, Y., 2009. Region based segmentation of QuickBird multispectral imagery through band ratios and fuzzy comparison. *ISPRS Journal of Photogrammetry and Remote Sensing* 64 (1), 55-64.

Wulder, M. A., Masek, J. G., Cohen, W. B., Loveland, T. R., Woodcock, C. E., 2012. Opening the archive: How free data has enabled the science and monitoring promise of Landsat. *Remote Sensing of Environment*, 122, 2-10.

Wulder, M.A., White, J.C., Fournier, R.A., Luther, J.E., Magnussen, S., 2008. Spatially explicit large area biomass estimation: Three approaches using forest inventory and remotely sensed imagery in a GIS. *Sensors* 8, 529-560.

Wulder, M. A., White, J. C., Bentz, C., Alvarez, M. F., Coops, N. 2006. Estimating the probability of mountain pine beetle red attack damage. *Remote Sensing of Environment*, 101(2), 150-166.

Xie, Y., Sha, Z., Yu, M., Bai, Y., and Zhang, L., 2009. A comparison of two models with Landsat data for estimating above ground grassland biomass in Inner Mongolia, China. *Ecological Modelling*, 220(15), 1810-1818.

Yan, G., 2003. Pixel based and object oriented image analysis for coal fire research. MasterThesis, ITC, Netherlands.

Zheng, G., Chen, J.M., Tian, Q.J., Ju, W.M., Xia, X.Q., 2007. Combining remote sensing imagery and forest age inventory for biomass mapping. *Journal of Environmental Management* 85, 616-623.

Zheng, D., Rademacher, J., Chen, J., Crow, T., Bresee, M., Lemoine, J., Ryu, S.R., 2004. Estimating aboveground biomass using Landsat 7 ETM+ data across a managed landscape in northern Wisconsin, USA. *Remote Sensing of Environment*, 93(3), 402-411.

Zolkos, S.G., Goetz, S.J., Dubayah, R., 2013. A meta-analysis of terrestrial above-ground biomass estimation using lidar remote sensing. *Remote Sens. Environ.*128, 289–298.

PUBLICATIONS

PUBLICATIONS

Chapter I

O. Fernández-Manso, A. Fernández-Manso, C. Quintano, 2014. **Estimation of aboveground biomass in Mediterranean forests by statistical modelling of ASTER fraction images**. *International Journal of Applied Earth Observation and Geoinformation*, 31, 45-56

Resumen

Estimación de biomasa aérea en bosques mediterráneos mediante modelización estadística de imágenes fracción extraídas del sensor ASTER

La estimación de biomasa aérea forestal a través de imágenes ópticas de satélite está basada normalmente en modelos de regresión utilizando las bandas originales de satélite o bandas sintéticas. En este trabajo se propone la utilización de las imágenes fracción obtenidas a partir de un análisis lineal de mezclas espectrales con el fin de mejorar la pobre relación que existe entre la biomasa aérea forestal y las bandas espectrales de sensores de resolución espacial media. Este estudio se localiza en el centro de España, dentro de un pinar de pino negral (*Pinus pinaster* Ait.) ordenado. Un total de 1033 parcelas de muestreo circulares fueron empleadas para la estimación de la biomasa aérea forestal a partir de datos del sensor ASTER. Para identificar las variables predictoras más adecuadas del conjunto de variables (bandas originales, imágenes fracción, índice de vegetación diferencial normalizado (NDVI) y componentes de la transformación Tasselled Cap) se utilizaron el coeficiente de correlación de Pearson y el método de regresión lineal múltiple paso a paso. Fueron analizados cuatro modelos lineales y un modelo no lineal. El modelo que mejor predijo la biomasa aérea forestal (R^2_{adj}= 0,632, el RMSE de la biomasa aérea forestal estimada fue 13,3 Mg ha^{-1} (o 37,7%), como resultado de crosvalidación) fue el que utilizó como variables predictoras las bandas 2 (roja, 0,630-0,690 μm) y 8 (infrarrojo medio o de onda corta 5, 2,295-2,365 μm) del sensor ASTER y la imagen fracción vegetación (obtenida a partir del modelo de mezclas espectrales lineal). Los resultados indicaron que el empleo de imágenes fracción del sensor ASTER dentro de modelos de regresión mejora la estimación de la biomasa aérea forestal de pinares de pino negral. La distribución espacial de la biomasa aérea forestal obtenida a partir de modelos lineales de regresión multiple pueden ser usados como información de base por los gestores forestales en futuros estudios, tales como la cuantificación del balance de carbono a nivel regional, acumulación de combustible forestal o el seguimiento de prácticas de gestión forestal.

Palabras clave: ASTER, estimación de biomasa, análisis de mezclas espectrales, regresión lineal múltiple, inventario forestal, pino negral

International Journal of Applied Earth Observation and Geoinformation 31 (2014) 45–56

Contents lists available at ScienceDirect

International Journal of Applied Earth Observation and Geoinformation

journal homepage: www.elsevier.com/locate/jag

Estimation of aboveground biomass in Mediterranean forests by statistical modelling of ASTER fraction images

O. Fernández-Manso[a,b,*], A. Fernández-Manso[b], C. Quintano[c,d]

[a] Civil Protection Agency, Castilla y León Government, Valladolid, Spain
[b] Agrarian Engineering and Sciences Department, University of León, Campus of Ponferrada, León, Spain
[c] Electronic Technology Department, University of Valladolid, Spain
[d] Sustainable Forest Management Research Institute, University of Valladolid-INIA, Spain

ARTICLE INFO

Article history:
Received 10 December 2013
Accepted 10 March 2014

Keywords:
ASTER
Biomass estimation
Spectral mixture analysis
Multiple linear regression
Forest inventory
Mediterranean pine

ABSTRACT

Aboveground biomass (AGB) estimation from optical satellite data is usually based on regression models of original or synthetic bands. To overcome the poor relation between AGB and spectral bands due to mixed-pixels when a medium spatial resolution sensor is considered, we propose to base the AGB estimation on fraction images from Linear Spectral Mixture Analysis (LSMA). Our study area is a managed Mediterranean pine woodland (*Pinus pinaster* Ait.) in central Spain. A total of 1033 circular field plots were used to estimate AGB from Advanced Spaceborne Thermal Emission and Reflection Radiometer (ASTER) optical data. We applied Pearson correlation statistics and stepwise multiple regression to identify suitable predictors from the set of variables of original bands, fraction imagery, Normalized Difference Vegetation Index and Tasselled Cap components. Four linear models and one nonlinear model were tested. A linear combination of ASTER band 2 (red, 0.630–0.690 μm), band 8 (short wave infrared 5, 2.295–2.365 μm) and green vegetation fraction (from LSMA) was the best AGB predictor ($R^2_{adj} = 0.632$, the root-mean-squared error of estimated AGB was 13.3 Mg ha^{-1} (or 37.7%), resulting from cross-validation), rather than other combinations of the above cited independent variables. Results indicated that using ASTER fraction images in regression models improves the AGB estimation in Mediterranean pine forests. The spatial distribution of the estimated AGB, based on a multiple linear regression model, may be used as baseline information for forest managers in future studies, such as quantifying the regional carbon budget, fuel accumulation or monitoring of management practices.

1. Introduction

Information about aboveground biomass (AGB) has in recent years become a goal for inclusion in forest management, given the increasing interest of industrial, energy and environmental sectors. The potential of forests as a biomass source for yielding clean energy and as carbon sinks makes it a frequent issue in regional and county level studies (Zheng et al., 2004; Gallaun et al., 2010). Accurate estimation of biomass is fundamental for assessing the role of forests in the global carbon cycle, particularly when defining their contribution towards sequestering carbon (Popescu, 2007; Zolkos et al., 2013).

Forest inventory data often provide the base data required to enable large area mapping of biomass over a range of scales, whereby measurements of tree size and stand structure, along with statistical models, are used in estimating tree and stand biomass (Fazakas et al., 1999). According to the International Panel on Climate Change Good Practice Guidance (IPCC CPG, 2003), remote sensing techniques are useful for verifying Land Use and Land cover (LULC) and LULC changes, carbon estimation and, especially, forest AGB in the Kyoto protocol context. Specifically, remote sensing has been considered a relatively fast, reliable and cost-effective approach in forest inventory and mapping by means of the correlation of parameters such as tree density, basal area, volume, biomass, and so forth, with the reflectance values recorded in satellite images (Kwak et al., 2007; Blackard et al., 2008).

AGB is usually estimated from remote sensed data via a direct relationship between the spectral response (original or transformed sensor bands) and AGB. In this sense, the Normalized Difference Vegetation Index (NDVI) is the most commonly used vegetation index (e.g. Zheng et al., 2004; Soenen et al., 2010; Ji et al., 2012; Poulain et al., 2012). Linear transformation of multiple bands, such as Tasselled Cap (TC) transform, has been also utilized as

* Corresponding author at: Civil Protection Agency, Castilla y León Government, Valladolid, Spain. Tel.: +34 983 216418; fax: +34 983 410092.
E-mail address: out-fermanos@jcyl.es (O. Fernández-Manso).

http://dx.doi.org/10.1016/j.jag.2014.03.005
0303-2434/

variable in regression models for estimating forest parameters (e.g. Phua and Saito, 2003; Lu et al., 2004; Hall et al., 2006). Some authors have focused on multiple regression analysis techniques (e.g. Dong et al., 2003; Ji et al., 2012; Ghasemi et al., 2013); some, on non-parametric *k*-nearest neighbour techniques (*k*-NN) (e.g. Labrecque et al., 2006; Fuchs et al., 2009) or on artificial neural networks (ANN) (e.g. Foody et al., 2001). Other works used indirect relationships whereby attributes estimated from canopy parameters, such as crown diameter, are first derived from remotely sensed data using multiple regression analysis of different canopy reflectance models (e.g. Phua and Saito, 2003; Soenen et al., 2010). Previous literature, however, has indicated that multiple regression analysis may be the most common approach for development of AGB estimation models, especially when medium spatial resolution data are used (Lu, 2006).

Remote sensing studies (e.g. Elmore et al., 2000; Ji et al., 2012; Tian et al., 2012; Gao et al., 2013; Main-Knorn et al., 2013; Barbosa et al., 2014;) have estimated AGB using both active and passive sensors in a broad range of scales (global, regional and local), although optical satellite data (particularly data from Landsat sensors) is often used. The limitation in spatial, spectral and radiometric resolution inherent in the optical remotely sensed data is an important factor affecting the AGB estimation performance (Lu, 2006). A problem typically observed in forests when using a coarse or medium resolution sensor like Landsat ETM+ (30-m spatial resolution) is the 'mixed pixel' condition (Asner, 1998). The combined reflectance observed is not only due to the amount of vegetation present, but also to other factors such as soil or shadow (Davidson and Csillag, 2001). The relation between AGB and vegetation indices or spectral bands may be poor because of this effect.

Spectral mixture analysis (SMA) is a frequently used subpixel-method to reduce the mixed-pixel problem (e.g. Lewis et al., 2012; Kuusinena et al., 2013). It unmixes a multispectral image into fraction images that represent the areal proportion of each endmember (e.g. vegetation abundance, soil and other spectrally distinct materials that basically contribute to the spectral signal of mixed pixels) in a pixel (Lu, 2006; Quintano et al., 2012). In remote sensing data applications, SMA has been used extensively in past studies for determining urban vegetation abundance (e.g. Demarchi et al., 2012; Michishita et al., 2012; Deng and Wu, 2013), estimating biophysical parameters such as leaf area index, biomass and net primary productivity (e.g. Zheng et al., 2004; Wang and Qi, 2008; Huang et al., 2009), mapping burned areas (Quintano et al., 2006, 2013; Fernández-Manso et al., 2009) or mapping surface coal affected areas (Fernández-Manso et al., 2012). Regarding AGB, previous studies (e.g. Peddle et al., 2001; Soenen et al., 2010; Morel et al., 2012) showed the superiority of fraction images derived from SMA compared to original bands or vegetation indices to estimate biomass from medium spatial resolution imagery.

Most AGB studies have been carried out in uniform boreal forests of coniferous plantations (Häme et al., 1997; Muukkonen and Heiskanen, 2005) and temperate and tropical forests (Phua and Saito, 2003; Cutler et al., 2012). There is a lack of experience for estimating AGB in Mediterranean environments (Salvador and Pons, 1998). However, the study of Sevillano-Marco et al. (2013) can be mentioned. They estimated AGB from the Chinese-Brazilian Earth Resources Satellite (CBERS) and Advanced Spaceborne Thermal Emission and Reflection Radiometer (ASTER) data in *Pinus radiata* D. Don in Spain.

In this sense, our study is innovative. It estimates AGB in Mediterranean ecosystems where Mallinis et al., 2004 found that Landsat TM spatial resolution did not seem to be adequate, given the patchy and fragmented spatial pattern of forest resources. To overcome such limitations, we use ASTER data whose three first bands (VNIR) have a higher spatial resolution than Landsat data (15 m vs. 30 m) and let us artificially extend such spatial resolution to the rest of short wave infrared (SWIR) bands by means of a spectral sharpening algorithm (Welch and Ahlers, 1987). In addition, to minimize the mixed-pixel problem (which still occurs at 15 m spatial resolution), we propose to use fraction images from LSMA to improve the AGB estimation. The study will determine which ASTER spectral band, fraction imagery, NDVI and/or TC component show a good statistical relation with AGB. Multiple regression analysis will help us to develop AGB estimation models. The spatial distribution of the estimated AGB from spectral data may help forest managers and the not, as yet, established biomass market that could be an alternative to the decline being suffered by traditional productive uses (timber and resin tapping).

2. Materials and methods

2.1. Study area

The study site is located in the area known as 'Tierra de Pinares Segoviana', in the Southeast of Castilla y León, province of Segovia (Fig. 1). It lies on sandy materials composed mainly of quartz grains over Miocenic materials. The terrain is a peneplain with low relief and a general, gentle slope from the southeast to northeast with a range of elevations 750–900 m above sea level. Mediterranean pine (*Pinus pinaster* Ait.) is the only vegetation type in our study area, that is the centre of a surface of approximately 20 000 ha of a monospecific pine forest. Currently, floristic composition and vegetation structure is a consequence of an anthropic management of over a hundred years.

Specifically, the study area corresponds to a public forest in the province of Segovia, 6850 ha in extent. The forest performs an important role against erosion and, no less important, in mitigating climate change. In recent years, it has gained importance for the use of biomass from both shelterwood cuttings and waste produced from silvicultural treatments. It has been managed by a Forest Management Plan since 1912 with the main goals of yielding resin and timber, generating the landscape, biodiversity and recreational areas. The forest was delineated to management compartments (photointerpretation and field work) by the Regional Forest Board. The forest compartment is the smallest unit for which decision-supporting information is collected and stored and it consists of a homogeneous forest in terms of tree species and age classes. Compartment size was in the range of 13.3–61.8 ha (mean = 33.2 ha, standard deviation = 10.6 ha). The borderlines of the compartments can be seen in Fig. 1.

2.2. Materials

Field data was acquired from an intensively sampled local test area with 1 033 circular sample plots (r = 16 m), which were allocated in a 200 m-quadratic grid. A field survey was conducted between May and July, 2001. Field measurements included the diameter at breast height (DBH) of each tree with a DBH over 10 cm, which was measured to the nearest 0.1 cm with digital callipers. Total height was measured to the nearest 0.1 m with a digital hypsometer (Vertex III) in two trees of each plot (closest trees to the plot centre oriented to the north and south).

We used an ASTER level L1B image (radiometric calibrated and co-registered data on all image channels), recorded on 6 June 2001 to estimate the AGB.

2.3. Methods

Fig. 2 shows the steps followed to estimate AGB from ASTER optical data. First, we calculated the AGB within each plot from the DBH measured in the field. Second, the ASTER data was pre-processed and then NDVI and TC components were calculated.

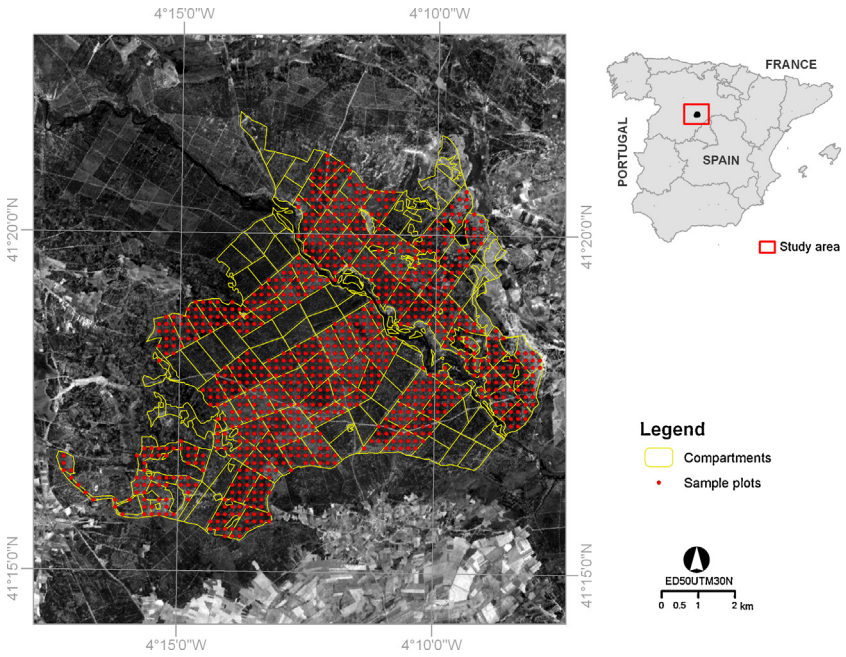

Fig. 1. Study area location.

Third, LSMA was applied to the ASTER pre-processed data and three fraction images were obtained: green vegetation, soil and shade. Fourth, we created a work database integrating both AGB measured in the field and satellite data (original bands and fraction images). Finally, statistical analysis of the work database searched for the regression model that best fitted the data.

2.3.1. Aboveground biomass calculation from field data

Calculation of the biomass of individual trees is commonly based on species, DBH and, in some cases, height as the main information sources (Parresol, 1999). In our study, forest AGB was calculated from the allometric equation established for Mediterranean pine based on destructive techniques by Montero et al. (2005): see Eqs.

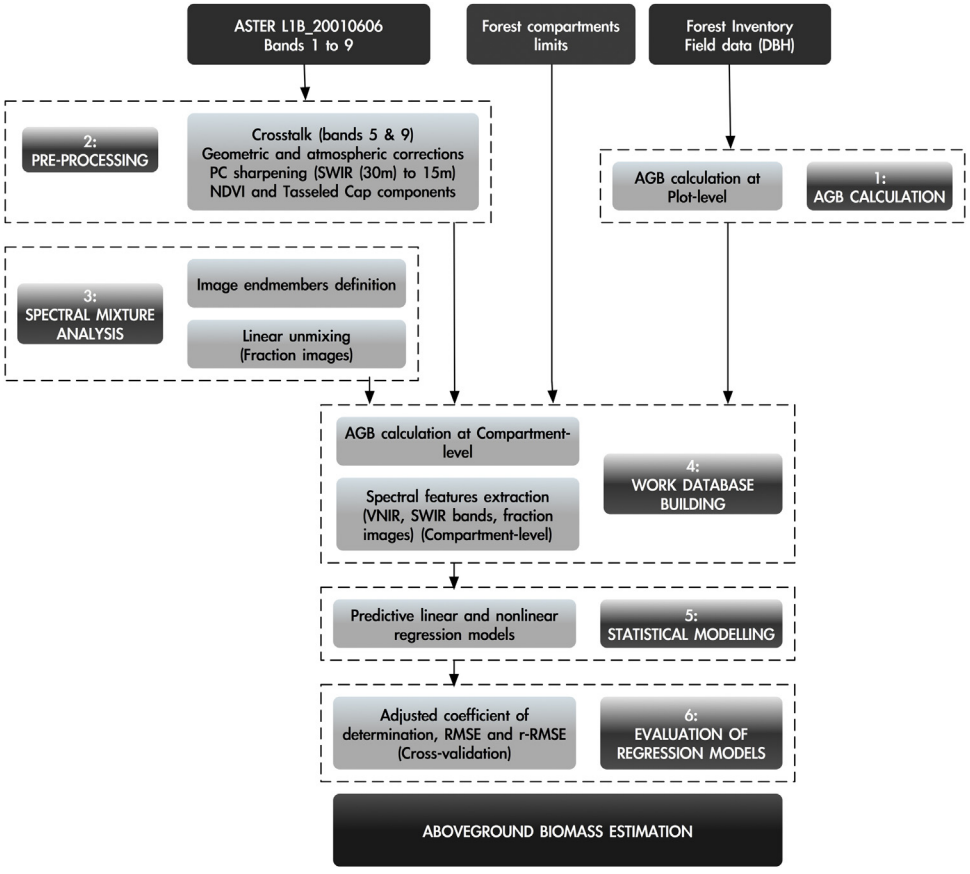

Fig. 2. Methodology flowchart.

(1) and (2) where W is the aboveground biomass (Mg) of individual trees, a, b are the regression parameters, DBH is the diameter at breast height (cm), SEE is the standard error of estimation and CF is the correction factor which allowed us to calculate W in all plots retained for the analysis. Unbiased estimates were obtained by multiplying the predicted values by CF expressed in Eq. (2).

$$W = [\exp^{a}\mathrm{DBH}^{b}]\mathrm{CF} \quad (1)$$

$$\mathrm{CF} = \exp^{(\mathrm{SEE}^2/2)} \quad (2)$$

W was then summed for each plot and divided by the plot area to give total biomass (Mg) and total aboveground biomass (Mg ha^{-1}) within the plot (Aldred and Alemdag, 1988).

2.3.2. Preprocessing of optical remote sensing data

Although the study area presents features such as confined places, a flat nature and an excellent atmospheric visibility of about 150 km at the time of image acquisition, an atmospheric radiation transfer model was used to produce an estimate of the true surface reflectance (Lu, 2006). To accurately compensate for atmospheric effects, the atmospheric correction model applied was the MODTRAN-based Fast line-of-sight Atmospheric Analysis of Spectral Hypercubes (FLAASH) (Matthew et al., 2000). Thermal infrared data were not used. The units of the output image were proportional to the apparent surface reflectances. Bands 5 and 9 were corrected from the crosstalk phenomenon (Iwasaki and Tonooka, 2005). The satellite image dataset were rectified to the local and accurate spatial reference system (EPSG: 25830) using a set of 21 ground control points (GCPs). A first-order polynomial warp function was applied and a nearest-neighbour resampling protocol was used. The total root mean square error (RMSE) for the transformation was 0.26. As our study area is flat, it was not necessary to compensate the image for different solar illuminations due to the irregular shape of the terrain by a topographic normalization.

Finally, the six short wave infrared (SWIR) bands (30 m spatial resolution) of the ASTER image were resampled to 15 m spatial resolution of the three visible-near infrared (VNIR) bands by a principal components (PC) based spectral sharpening algorithm (PC Spectral Sharpening) (Welch and Ahlers, 1987). A nearest neighbour resampling method was used to preserve the original values of the pixels.

NDVI was derived from ASTER band 3 (near-infrared, NIR) and ASTER band 2 (red). To compute TC components, we used the approximation of the TC transform for ASTER based on Gramm–Schmidt method elaborated by Wang and Sun (2005). Although coefficients are available for nine transformation components, we focused in the first three Kauth–Thomas components (brightness, greenness, and wetness) since they typically explain 97–99% of the variability in the data.

2.3.3. Spectral mixture analysis

A linear spectral mixture model was used which is based on the assumption that the image spectra are formed by a linear combination of n pure spectra, called endmembers. Eq. (3) describes mathematically the spectral unmixing process.

$$\rho_b = \sum_{i=1}^{n} f_i \rho_{i,b} + \varepsilon_b \quad (3)$$

where for each pixel, ρ_b is the reflectance in band b, $\rho_{i,b}$ is the reflectance for endmember i, in band b, f_i the fraction of endmember i, and ε_b is the residual error for band b (see Keshava, 2003; Plaza et al., 2011; Quintano et al., 2012; for more detail).

Endmember selection is a key step in LSMA. It determines how accurately the mixture model can represent the spectra. The definition of appropriate spectral endmembers may be done either by using reference endmembers from spectral libraries or from the image itself (image endmembers) (Keshava, 2003). As appropriate reference endmembers were not available for the study site, we used image endmembers. For most LSMA applications, image endmembers are utilized because they can be easily obtained and can represent spectra measured at the same scale as the image data (Roberts et al., 1998).

Before extracting endmembers, we applied a Minimum Noise Fraction (MNF) transformation to the original bands to determine the inherent dimensionality of image data (ASTER preprocessed-image), to segregate noise in the data and to reduce the computational requirements for subsequent processing (Boardman and Kruse, 1994). This transformation when applied with the same rotation statistics to the image and endmember set would reduce multi-collinearity (Van der Meer and Jia, 2012). Collinearity and multi-collinearity (that occur when endmembers are highly correlated) have an adverse effect (instability) on the inversion process that solves the linear system of equations of unknown fractions (Van der Meer and De Jong, 2000; Chen et al., 2010).

The new MNF transformed bands were then analyzed to find the most 'spectrally pure' pixels or extreme pixels in the image using a Pixel Purity Index (PPI) algorithm (Boardman et al., 1995). The PPI is calculated by repeatedly projecting n-dimensional scatter plots onto a random unit vector. Pixels which are marked as extreme in each projection are recorded and the sum of the times a pixel is marked extreme is recorded as well. Once this step has been completed, a PPI image is created where pixel values correspond to the number of times a pixel was recorded as extreme (Mustard and Sunshine, 1999).

Although likely PPI will return a set of n pure endmembers best characterizing the spectral variation in the image, the endmembers may not necessary represent materials of interest to the user (Van der Meer and Jia, 2012). In our study, clusters of extreme pixels in the image were selected by means of n-D visualizer (scatter plot of points representing spectra where n is the number of bands) using ground-based local knowledge. Three endmembers were selected to characterize the variance in the imagery: GV, soil and shade (defined using pixels representing a river). As previous studies (e.g. Goodwin et al., 2005; Fernández-Manso et al., 2009), the definitive endmembers were determined by means of an iterative process that involved examining the spatial mapping of the endmembers and comparing with local knowledge. Specifically, after the purer pixels were identified in the n-dimensional scatter plot, an inverse-MNF transform was applied to obtain the endmembers spectra, and their spectral response was visually verified using local knowledge. GV signature was defined using pine pixels. As pine is the only vegetation type in our study area, we did not try adding different vegetation endmembers to the analyses. Shade was defined using the reflectance values of water body (river) pixels as some studies suggested (e.g. Weng and Lu, 2008; Zanotta et al., 2012).

Once the endmembers were selected, the image fractions were computed, based on a model with a low RMSE average using a least-squares solution (Shimabukuro and Smith, 1991) as a method for solving the linear mixture model due to its simplicity and ease of implementation. RMSE was used to assess the fit of the model (Roberts et al., 1998) as shown in Eq. (4), where m is the number of bands. A partially constrained least-square solution was used to unmix the mixture model (only the sum-to-unity constraint was included in the linear mixing algorithm).

$$\mathrm{RMSE} = \sqrt{\sum\nolimits_{b=1}^{m} \varepsilon_b^2 / m} \quad (4)$$

2.3.4. Work database building

Before integrating the information from field and satellite data, the 1033 field plots were grouped into compartments. The reason

Table 1
Tested regression models.

Model #	Model equation	# Independent variables	References
1	$y = a\exp^{bx}$	1	Heiskanen (2006)
2	$y = a + bx$	1	Freitas et al. (2005) and Heiskanen (2006)
3	$y = a + bx + cx^2$	1	Labrecque et al. (2006)
4	$y = a + bx_1 + cx_2$	2	Freitas et al. (2005) and Labrecque et al. (2006)
5	$y = a + bx_1 + cx_2 + dx_3$	3	Labrecque et al. (2006)

a, b, c, d: regression coefficients; x, $x_{i\,i=1,2,3}$: independent variables (ASTER spectral bands, fraction images, NDVI or Tasselled Cap components); and y: dependent variable (AGB). $n = 162$.

for working at compartment level is two-fold. First, forest management planning in Spanish forests is usually based on information collected by forest compartments and they constitute the primary mapping and description unit used for forestry planning. Second, a compartment-level approach has been reported to improve the estimation accuracies (Poso et al., 1999; Koivuniemi and Korhonen, 2006; Mozgeris, 2008).

Thus, a work database with information at compartment-level was developed combining the AGB information obtained from field measurements with satellite data. From the W obtained by applying Eqs. (1) and (2) (see Section 2.3.1), we calculated AGB (Mg ha^{-1}) at compartment level by summing all AGB (plot-level) in each compartment and dividing by the number of plots in each compartment. Summarized AGB data corresponding to the compartments used for model development ($n = 162$) are: mean value is 35.3 Mg ha^{-1}; minimum value is 3.6 Mg ha^{-1}; maximum value is 88.3 Mg ha^{-1} and standard deviation (SD) is 21.1 Mg ha^{-1}. A total of 162 forest compartments were used to estimate AGB in a research area of 6850 ha.

Accuracy of the compartment reference data is determined by the errors in compartment level data and biomass allometric conversion factors (Muukkonen and Heiskanen, 2005, 2007). In our case, the standard error of the reference data at compartment level was 18%, lower that the 30% defined as maximum by the Spanish Forest Law and the Regional Forest Law (JCyL, 1999).

With regard to the satellite information, the mean values of original ASTER bands (VNIR and SWIR) and of fraction images were extracted for each forest compartment. The pixels located on the borders of the compartments are mixed pixels since they have received responses from two or several compartments. To avoid this, we used only those pixels located in the core areas of the forest compartments (Kilpeläinen and Tokola, 1999; Mäkelä and Pekkarinen, 2004). This resulted in a wide area on the border of the forest compartment which was left unused to compensate for the rectification errors in the remote sensing data and forest field survey dataset.

2.3.5. Statistical modelling for AGB estimation

The work database was tested for spatial autocorrelation using Moran's I test before applying non-spatial statistical analysis. This test evaluates whether the pattern expressed is clustered, dispersed or random by calculating the Z-score and p-value which is based on the randomization null hypothesis computation and indicates whether the null hypothesis can be rejected (Tiefelsdorf and Boots, 1995).

Estimation of forest AGB at compartment level was carried out using statistical modelling. Regression analysis has been successfully employed in the estimation of forest attributes using remote sensing data (Ardö, 1992; Häme et al., 1997; Hyyppä et al., 2000; Muukkonen and Heiskanen, 2005; Ghasemi et al., 2013). Predictive linear and nonlinear regression models successfully used in other similar studies (see Table 1) where tested for estimation trials, quantifying the relationships between AGB (dependent variable) and ASTER spectral bands, fraction imagery, NDVI and TC components (independent variables). Specifically, we utilized a nonlinear model (Table 1, model #1) as recommended by Heiskanen (2006), and four linear polynomial models (Table 1; models #2–#5): model #2, first order, one independent variable, as proposed by Freitas et al. (2005) and Heiskanen (2006); model #3, a second order, one independent variable, proposed by Labrecque et al. (2006); model #4, first order, two independent variables, recommended by Freitas et al. (2005) and Labrecque et al. (2006); and model #5, first order, three independent variables, as suggested by Labrecque et al. (2006). Models #1–#3 have just one independent variable, whereas models #4 and #5 have 2 and 3 independent variables, respectively.

Pearson's correlation coefficient (r) was used to analyze relationships between AGB and image data, including ASTER spectral bands, fraction data, NDVI and TC components. Because the correlation coefficient measures the strength of linear relationships between two variables (Runyon et al., 2000), analysis of correlation coefficients provides a way of finding potential variables for developing AGB estimation models. Selection of suitable variables is a critical step for developing an AGB estimation model. If the variables are weakly related to AGB, incorporation of such variables may reduce the AGB estimation performance (Lu, 2006). In our study, a stepwise multiple regression technique was used to identify the suitable variables and to assess their individual significance to develop AGB estimation models in Mediterranean pine forests on sandy soils (independent variable probability of α-to-enter = 0.05, independent variable probability of α-to-remove = 0.05).

2.3.6. Evaluation of regression models

Evaluation of tested regression models (Table 1) was based on the adjusted coefficient of determination (R^2_{adj}), a statistical measure that is independent of the number of explanatory variables and sample size, and on a visual analysis of residuals. The increment in the number of independent variables will always increase the coefficient of determination (R^2), while the R^2_{adj} may decrease if the additional variables present low explanatory power and/or if the degrees of freedom become too small (Hair et al., 1998).

Model performance was assessed based on the agreements between modelled and observed values. The agreements were quantified using RMSE (Eq. (5)) and RMSE$_r$ (relative-RMSE, Eq. (6)) as indicators (Mäkelä and Pekkarinen, 2004). RMSE indicates the accuracy of our models and RMSE$_r$ let us compare the accuracy of our results with other biomass estimation studies. In general, a high R^2 or a low RMSE value often indicates a good fit between the model developed and the sample data (Lu, 2006).

$$\mathrm{RMSE} = \sqrt{\sum_{i=1}^{n} (y_i - y_{i,\mathrm{est}})^2 / n} \tag{5}$$

$$\mathrm{RMSE_r} = \frac{\mathrm{RMSE}}{y_{\mathrm{mean}}} 100 \tag{6}$$

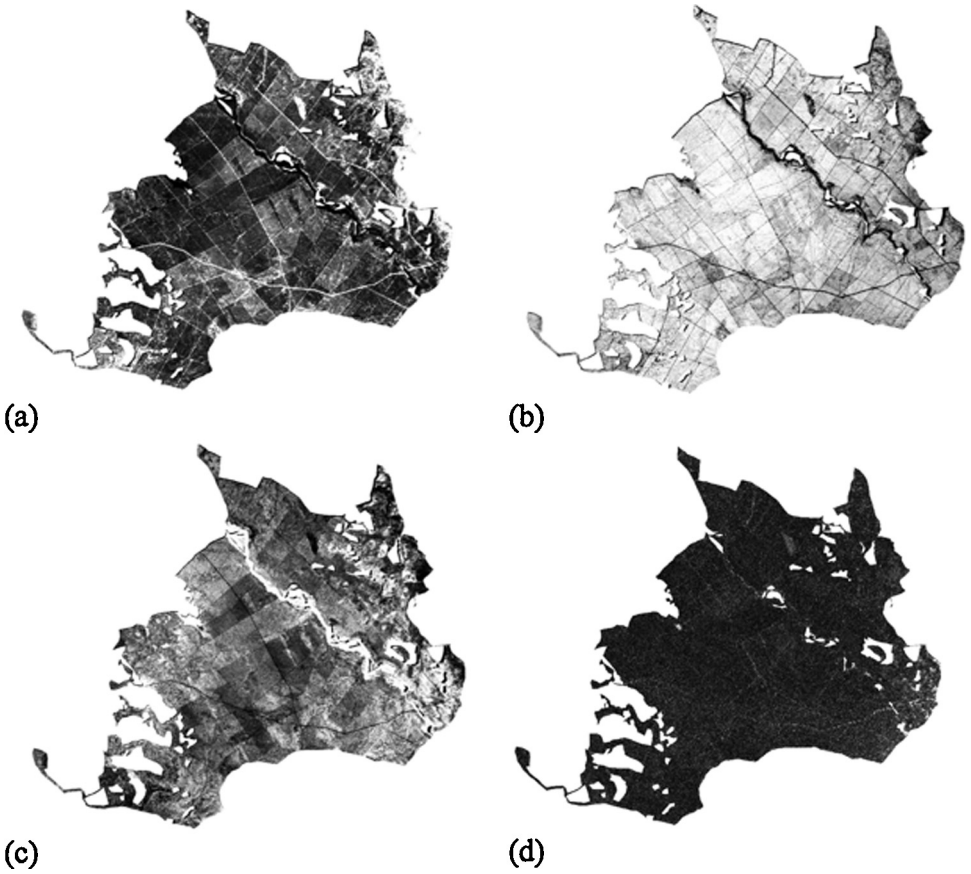

Fig. 3. ASTER fraction images from linear spectral mixture analysis. (a) Soil fraction image, (b) vegetation fraction image, (c) shade fraction image, and (d) root mean square error (RMSE).

where $y_{i,est}$ is the estimated value for AGB, y_i is the observed values of AGB, y_{mean} is the mean of the observed values and n is the number of observations.

The work database was not split into a training and evaluation subset. Rather, the accuracy of the AGB estimates at compartment scale was evaluated directly from the training dataset by what is known as cross-validation or 'leave-one-out method'. This validation strategy was followed by other authors such as Köhl et al. (2006) and Van der Heijden et al. (2007). As the name suggests, the leave-one-out cross-validation involves using a single observation from the original sample as the validation data, and the remaining observations as the training data. This is repeated so that each AGB observation in the work database is used once as the validation data. Specifically, in our study, of the 162 compartments, 161 were used as training data to test a regression model and one was retained as validation data. This process was repeated 162 times, with each of the 162 AGB observations at compartment level used exactly once as the validation data. This method is a mathematically sound approach to error estimation and gives a realistic and reliable picture of the true error.

3. Results

The original ASTER image contains statistical noise and important spectral feature information. The MNF transform has been helpful for isolating noise from the image and selecting a few meaningful MNF components based on the screen plot approach. The fraction images showed differentiation in abundances between GV, shade and exposed soil. Shade was well predicted over the scene and high shade fractional values were most evident along the river and well distributed throughout the forest stands. The soil fractional endmember showed localized areas of high soil abundance, particularly in the continental sand-dune areas. GV endmember was extracted from a canopy of pine stands. The three computed fraction images (shade, soil and GV) together with the RMSE image are shown in Fig. 3.

Moran's I test, used to check whether our work database had any spatial autocorrelation, evidenced that feature values are randomly distributed across the study area. The Z-score was −2.15, p-value was 0.05, showing statistical significance and Moran's I index was −0.53, indicating a tendency towards dispersion.

Table 2 provides the Pearson correlation coefficients between AGB and ASTER spectral bands, fraction imagery, NDVI and TC components. GV fraction is strongly positively correlated with AGB (0.729), but shade fraction is weakly negatively correlated (−0.033). The GV relationship with AGB is slightly stronger than the relationship between ASTER original bands and AGB (the highest coefficient between AGB and band B6 (SWIR3) is −0.655), or with NDVI or TC wetness component that are 0.612 and −0.593, respectively. The GV fraction image also has a stronger relationship with AGB than shade or soil fraction images. The SWIR spectral range (B4–B9) showed higher correlations with AGB than the NIR (B3) band but similar to the visible spectral range (B1–B2). The correlations with band 2 (red) and band 6 (SWIR3) are the strongest.

To test the five models showed in Table 1, firstly, we used only a type of independent variable: ASTER spectral bands, fraction images, NDVI or TC components. Thus, Table 3 displays the parameters of the regression models that had the highest R^2_{adj}, grouped by each type independent variable. From Table 3, we observed the same trend in the four cases considered. When we used ASTER spectral bands as only independent variables, R^2_{adj} value was increasing from model #1 (one variable, exponential) (0.425) to model #5

Table 2
Pearson correlation coefficient between ASTER data (spectral bands, fraction images, NDVI and Tasselled Cap components) and aboveground biomass.

ASTER spectral bands (B1–B9)								
B1	B2	B3	B4	B5	B6	B7	B8	B9
−0.613	−0.659	−0.296	−0.597	−0.599	−0.655	−0.612	−0.619	−0.569

Fraction images, NDVI and Tasselled Cap components						
SH	SO	GV	NDVI	TC-B	TC-G	TC-W
−0.033	−0.429	0.729	0.612	−0.591	−0.563	−0.593

AGB: aboveground biomass; B_i: band i of ASTER bands (B1–B3 corresponds to visible-nearinfrared and B4–B9 to short wave infrared); SH: shade fraction; SO: soil fraction; GV: green vegetation fraction; NDVI: Normalized Difference Vegetation Index; TC-B: Tasselled Cap Brightness; TC-G: Tasselled Cap Greenness; TC-W: Tasselled Cap Wetness. Correlation is significant at the 0.01 level. $n = 162$.

Table 3
Comparison of regression models that better performed using ASTER spectral bands, fraction images, NDVI and Tasselled Cap components.

Model #	Variables	a	b	c	d	R^2	R^2_{adj}	RMSE	$RMSE_{xval}$
Independent variables: only spectral bands									
1	B2	6905	−0.088	–	–	0.429	0.425	18.34	20.32
2	B2	185.84	−2.4	–	–	0.435	0.430	15.44	17.52
3	B2	555	−14	0.09	–	0.475	0.468	14.60	16.11
4	B2/B3	−23.9	−4.3	4.68	–	0.564	0.557	13.71	15.35
5	**B1/B2/B8**	**−108.71**	**14.46**	**−8.95**	**−8.45**	**0.581**	**0.574**	**13.82**	**14.42**
Independent variables: only fraction images									
1	GV	8.8	10.89	–	–	0.499	0.495	15.6	17.30
2	GV	3.28	304.74	–	–	0.532	0.529	14.5	16.50
3	GV	5.22	258.4	216.1	–	0.533	0.526	14.57	16.10
4	GV/SO	15.21	276.62	−32.33	–	0.583	0.577	16.68	18.37
5	**GV/SH/SO**	**142.86**	**75.15**	**−101.64**	**−183.87**	**0.587**	**0.578**	**13.71**	**14.17**
Independent variables: only NDVI									
1	NDVI	0.33	16.2	–	–	0.482	0.477	16.42	18.23
2	NDVI	−87.32	449.45	–	–	0.502	0.486	15.97	18.87
3	**NDVI**	**26.34**	**−400.8**	**1562**	**–**	**0.514**	**0.506**	**13.75**	**5.18**
Independent variables: only Tasselled Cap components									
1	TC-W	26,903	−0.0147	–	–	0.356	0.351	19.40	20.71
2	TC-W	221.9	−0.398	–	–	0.352	0.348	17.10	19.21
3	TC-B	902.2	−0.2545	0.000018	–	0.417	0.409	16.27	17.62
4	TC-G/TC-W	−218.49	7.434	−4.40	–	0.485	0.477	15.30	16.98
5	**TC-B/TC-G/TC-W**	**−272.98**	**0.0976**	**9.149**	**−6.675**	**0.515**	**0.504**	**14.90**	**15.54**

a, b, c, d: regression coefficients; B2: ASTER band 2, VNIR2; B3: ASTER band 3, VNIR3; B8: ASTER band 8, SWIR5; GV: green vegetation fraction image; SO: soil fraction image; SH: shade fraction image; NDVI: Normalized Difference Vegetation Index; TC-B: Tasselled Cap Brightness; TC-G: Tasselled Cap Greenness; TC-W: Tasselled Cap Wetness; R^2: coefficient of determination; and R^2_{adj}: adjusted coefficient of determination; RMSE: root mean square error; $RMSE_{xval}$: root mean square error cross-validation; $n = 162$; bold: maximum R^2_{adj} value.

Table 4
Comparison of regression models that better performed using combination of ASTER spectral bands, fraction images, NDVI and Tasselled Cap components.

Model #	Variables	a	b	c	d	R^2	R^2_{adj}	RMSE	$RMSE_{xval}$
4	**B2/GV**	**88.10**	**−1**	**218.00**	**–**	**0.598**	**0.592**	**13.51**	**14.9**
	B2/NDVI	−156.49	0.67	548	–	0.589	0.583	13.62	15.23
	B2/TC-G	42.75	−5.38	1.06	–	0.489	0.482	15.23	17.02
	GV/NDVI	−63.43	102.44	322.41	–	0.588	0.583	13.78	15.43
	GV/TC-W	85	244.10	−0.1605	–	0.564	0.558	14.07	16.12
	NDVI/TC-B	−267.83	667.30	0.0201	–	0.573	0.564	14.24	16.89
5	**B2/B8/GV**	**56.4**	**−5.94**	**5.75**	**216**	**0.639**	**0.632**	**12.84**	**13.3**
	B2/B8/NDVI	−173.83	−3.61	5.1	529.92	0.624	0.616	13.12	13.65
	B2/B8/TC-G	60.85	−7.43	3.44	0.78	0.511	0.489	15.13	15.54
	B2/GV/NDVI	3.5	−0.54	149.86	184.1	0.601	0.591	13.53	14.17
	B2/GV/TC-R	34.32	−3.99	216.90	0.0379	0.625	0.617	13.20	13.71
	B2/NDVI/TC-R	−243.08	−2.56	580.36	0.0466	0.619	0.611	13.32	13.91
	GV/SO/B2	131	193.62	41.19	−2.03	0.61	0.601	13.37	14.01
	GV/SO/NDVI	−138.49	−25.3	50.22	595.6	0.614	0.606	13.29	13.83
	GV/SO/TC-W	85.13	244.05	0.09	−0.161	0.565	0.55	14.11	14.61
	NDVI/TC-R/B2	−243.08	580.36	0.0466	−2.564	0.61	0.593	13.90	14.36
	NDVI/TC-R/GV	−370.89	883	0.0291	−95.29	0.619	0.611	13.20	13.74

a, b, c, d: regression coefficients; B2: ASTER band 2, VNIR2; B8: ASTER band 8, SWIR5; GV: green vegetation fraction image; SO: soil fraction image; SH: shade fraction image; NDVI: Normalized Difference Vegetation Index; TC-B: Tasselled Cap Brightness; TC-G: Tasselled Cap Greenness; TC-W: Tasselled Cap Wetness; R^2: coefficient of determination; and R^2_{adj}: adjusted coefficient of determination; RMSE: root mean square error; $RMSE_{xval}$: root mean square error cross-validation; $n = 162$; bold: maximum R^2_{adj} value.

Table 5
Accuracy statistics and their relative counterparts (best results for each type of model) for cross-validation.

Model #	Variable/s	RMSE	$RMSE_r$	$RMSE_{xval}$	$(RMSE_{xval})_r$
1	GV	15.60	44.2	17.30	49.0
2	GV	14.50	41.1	16.50	46.7
3	GV	14.57	41.3	16.10	45.6
4	B2/GV	13.51	38.2	14.90	42.2
5	**B2/B8/GV**	**12.84**	**36.3**	**13.30**	**37.7**

RMSE: total root mean square error (Mg ha^{-1}); $RMSE_{xval}$: RMSE for cross-validation; and $RMSE_r$: relative RMSE (%); $(RMSE_{xval})_r$: RMSE relative for cross-validation (%); bold: maximum R^2_{adj} value.

(three variables, first order polynomial) (0.574). When fraction images were used as independent variables, again, model #1 had the lowest R^2_{adj} value (0.495) and model #5 had the highest R^2_{adj} value (0.578). The R^2_{adj} values obtained with these two types of independent variables were quite similar, though a bit higher when using fraction images. In the third case, only NDVI was used as independent variable and we could not test models #4 and #5. Model #1 had the lowest R^2_{adj} value (0.477) and model #3, the highest R^2_{adj} value (0.506). These R^2_{adj} values were comprised between the R^2_{adj} values obtained using only ASTER spectral bands, and the R^2_{adj} values obtained using only fraction images. Finally, when we utilized the TC components as only independent variables, model #1 presented again the lowest R^2_{adj} value (0.351) and model #5 displayed the highest one (0.504). The R^2_{adj} values obtained using only TC components were the lowest of the four considered cases.

Next, we tested the models using as independent variables all the variables computed (ASTER spectral bands, fraction images, NDVI and TC components) without grouping by type of variable. Table 4 displays the obtained results. In this case, only models #4 and #5 were used because models #1–#3 have only an independent variable. The stepwise regression analysis indicated that, when using model #4 (two independent variables, first order polynomial), the combination of GV fraction image and ASTER spectral band 2 (red, 0.630–0.690 μm), increased the R^2_{adj} value (0.592) versus using the same model with just one type of independent variable. Regarding model #5 (three independent variables, first order polynomial) (Labrecque et al., 2006), the combination of GV fraction image, ASTER spectral band 2 and ASTER spectral band 8 (SWIR 5, 2.295–2.365 μm) improved also the regression performance (R^2_{adj} value = 0.632) compared to the performance using just a type of independent variable.

Table 5 displays the statistical accuracy and their relative counterparts for each tested regression model (both cases: just a type of independent variable and combining them). As observed from Tables 3 and 4, model #5 showed the lowest RMSE (12.84 Mg ha^{-1} and 13.3 Mg ha^{-1} from cross-validation) ($RMSE_r$ = 36.3% and 37.7%, resulting from cross-validation) with ASTER bands 2 and 8, and GV fraction as independent variables.

The goodness of fit of the selected model was examined with analysis of scatter diagram and residual graph (see Fig. 4, right and left, respectively). The residual graph shows a well-known phenomenon for forestry and biological response variables that affects analyses involving variances (precision, confidence intervals). In the present case, logarithmic transformation of dependent and independent variables did not stabilize the variances but only increased the standard error of residuals (Fig. 4, left), and over- or under-estimates AGB near extreme values.

Finally, a spatial distribution of the AGB (Fig. 5) was produced based on the multiple linear regression model #5, generating the estimated mean value of 42.4 Mg ha^{-1} (SD is 11.9 Mg ha^{-1}). Areas in dark green correspond to logging roads, firebreaks, and continental dunes. The green and yellow colours are areas where cuttings were recently done. Blue areas represent a water body (river). Finally, the orange and red colours are places with a high density of trees and the oldest forest stands (tree density from 130 to 229 stems ha^{-1}, average of 159 stems ha^{-1}, SD = 24.7 stems ha^{-1}).

4. Discussion

The relationship between AGB and ASTER data was analyzed to retrieve a biomass regression model. As other authors (e.g. Ardö, 1992; Häme et al., 1997; Muukkonen and Heiskanen, 2005), we found a negative relationship between AGB and all ASTER spectral bands, which is typical for coniferous stands. GV fraction was strongly positively correlated with AGB (r = 0.729). This strong relationship implies that GV fraction is suitable for AGB estimation. This result agrees with the findings of other authors as Lu et al. (2005) in successional forest biomass estimation. As expected, NDVI was positively correlated with AGB (r = 0.612). However, NDVI had only limited success of predicting the actual biomass (Calvao and Palmeirim, 2004; Mutanga and Skidmore, 2004). Finally, TC components (brightness, greenness and wetness) were negatively correlated with AGB. Though greenness index was also correlated significantly with biomass (r = −0.563), its correlation remains lower than that of brightness and wetness index (−0.591 and −0.593, respectively). Other studies showed the same results: Hall et al. (2006) found that correlation coefficients generated from Landsat ETM+ image bands were higher than those generated from TC brightness, greenness, and wetness (−0.52, −0.53, 0.45, $p < 0.05$); and Roy and Ravan (1996) observed that TC transformation

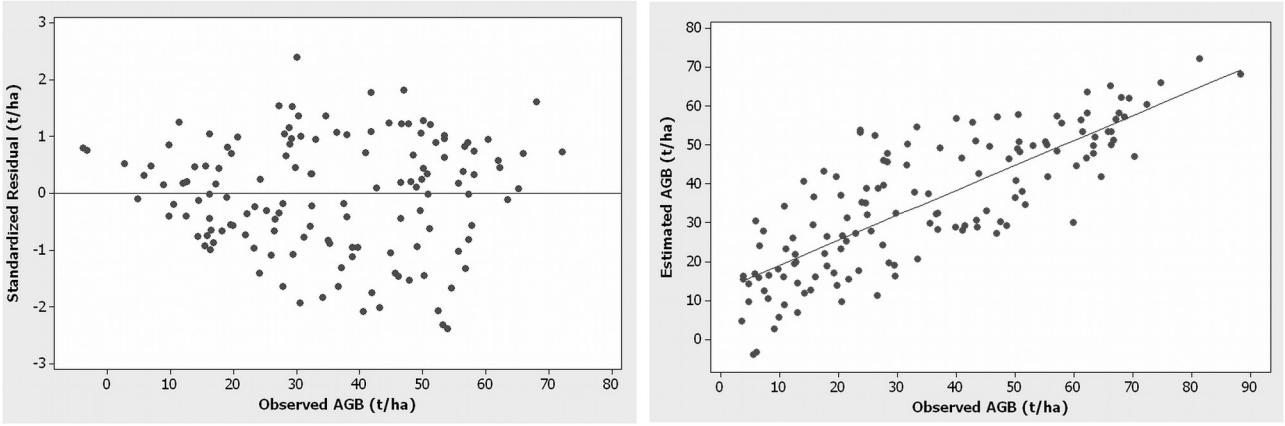

Fig. 4. Regression model #5. Left: residuals versus observed AGB; right: estimated versus observed AGB.

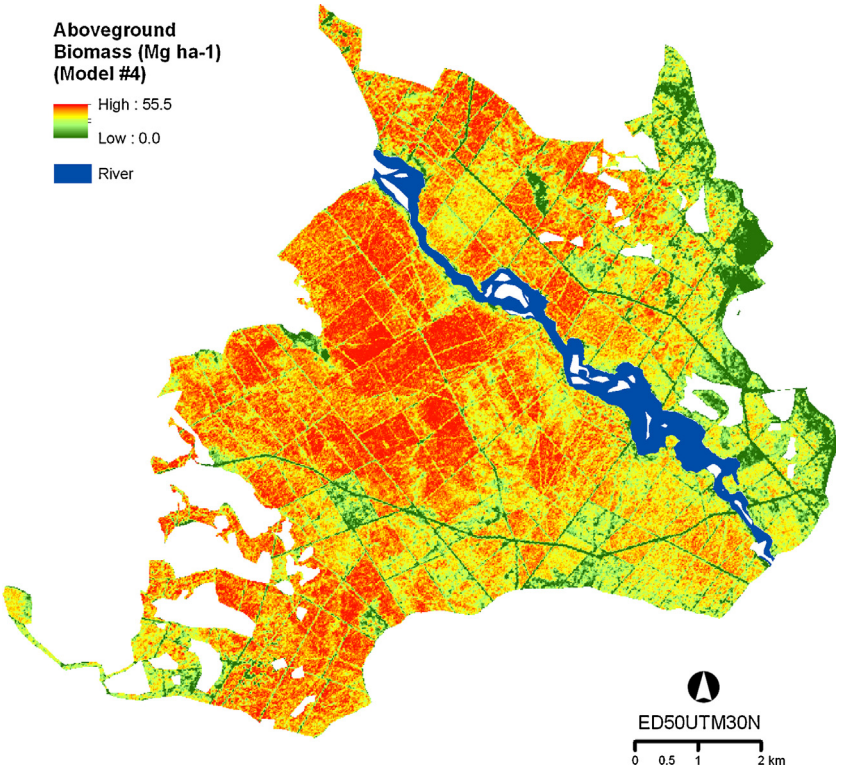

Fig. 5. Spatial distribution of the estimated aboveground biomass applying regression model #5.

brightness and wetness indices (0.688, 0.638, respectively) were better correlated with biomass than greenness (0.589).

Our work shows that the inclusion of fraction images as independent variables improved the statistical modelling of AGB as a function of ASTER data in Mediterranean ecosystems. The best predictor of AGB was model #5 (three independent variables, first order polynomial) (Labrecque et al., 2006), using ASTER original bands 2 and 8 and GV fraction as independent variables. The suitability of GV fraction image to AGB estimation has been shown in different ecosystems, mainly boreal and tropical biomes. For example, Lu et al. (2005) reported that the regression model using GV fraction image slightly improves the estimation performance for successional forests; and Poulain et al. (2012) found that the most accurate regression model for estimating AGB in *Nothofagus pumilio* forest stands located in Southern Chile, used GV fraction image as an independent variable.

Regarding the selected model (model #5, Labrecque et al., 2006), the comparison of predicted versus observed values of AGB (Fig. 4, right) reveals an overestimation of lower values (AGB < 10 Mg ha^{-1}) and underestimation of higher values (AGB > 60 Mg ha^{-1}). Inside of this interval, the residuals showed an appropriate behaviour, distributed around a mean value of zero. The mean and total are preserved well, which corresponds to the findings of Labrecque et al. (2006). Muukkonen and Heiskanen (2005) also found that the two models they tested (non-linear multiple regression and neural networks) resulted in over-estimation of low biomass levels and under-estimation of the high biomass levels. And Fuchs et al. (2009) reported that linear regression estimation performs worse with respect to extreme observations. In our study area, this is not a problem since mostly of our data are inside of the interval.

The accuracy test levels of our research are comparable to vegetation studies of other biomes. For example, Muukkonen and Heiskanen (2005) reported that RMSE of the total AGB of forest stands in their study of biomass for boreal forests using regression and neural network models with ASTER satellite were 48.2 Mg ha^{-1} (RMSE$_r$ of 39.5%) and 44.7 Mg ha^{-1} (RMSE$_r$ of 36.7%). Xie et al. (2009) developed two models: artificial neural network (ANN) and multiple linear regression (MLR), to estimate typical grassland aboveground dry biomass using Landsat ETM+. The ANN model provided a more accurate estimation (RMSE of 59.60 Mg ha^{-1}, RMSE$_r$ = 39.88% for the training set and RMSE of 63.20 Mg ha^{-1}, RMSE$_r$ = 42.36% for the testing set) than MLR (RMSE of 78.36 Mg ha^{-1}, RMSE$_r$ = 49.51% for the training, and RMSE of 79.36 Mg ha^{-1}, RMSE$_r$ = 53.20% for the testing). In our study, the lowest RMSE was 12.8 Mg ha^{-1}, RMSE$_r$ = 36.3% in model #5 (RMSE of 13.3 Mg ha^{-1}, RMSE$_r$ = 37.7% resulting from cross-validation), reporting better results than other studies carried out in boreal coniferous and mixed forests (Hyyppä et al., 2000; Tomppo et al., 2002; Mäkelä and Pekkarinen, 2004).

The regression modelling of AGB can be affected by potentially influential factors that are not directly considered in the regression models (Lu, 2006). The reflectance of forests is typically highly anisotropic and determined by the optical properties of canopy components, canopy, landscape level structural characteristics and topography (Asner, 1998). In addition, compartment reflectance is also affected by background and understory characteristics, particularly in sparse and open regions (Spanner et al., 1990; Rautiainen et al., 2007). The uncertainty in co-registration of field and satellite data is another source of unexplained variation. Additionally, inaccuracies in calibration and validation data can also reduce model fit and accuracy statistics. The forest compartment level field data is assumed to be less sensitive to the co-registration errors than plot-level data (Mäkelä and Pekkarinen, 2004).

The spatial distribution of AGB (Fig. 5) based on the model #5, may be used as starting information for forest managers in future studies such as quantifying the regional carbon budget, accumulation fuel or monitoring management practices. Further, it could be updated (to year 2013) using the estimated mean annual increment of AGB (Mg ha-year^{-1}) for Mediterranean pine (*P. pinaster* Ait.) forests in the Segovia province (MITYC, 2010), based on allometric

equations (Montero et al., 2005) and the 3rd National Forest Inventory (MMA, 2006), reaching an average value of 73 Mg ha^{-1}.

Since spectral information on optical remote sensing data lacks sensitivity to forest attributes at the moderate and high biomass levels (Lu, 2006), alternative imaging technology such as high spatial resolution imagery (Quickbird, Ikonos, WorldView-2, etc.) could be used to better capture the fine spatial distribution of trees in the forest stand (e.g. Leboeuf et al., 2007; Sarker and Nichol, 2011; Mutanga et al., 2012). Another type of sensor that can be used to capture the textural characteristic of the forest stand is Synthetic Aperture Radar (SAR). Several authors (e.g. Kuplich et al., 2005; Cutler et al., 2012; Gao et al., 2013) demonstrated that the use of backscatter (a measure of canopy texture) improves AGB estimation accuracy. However, one limitation is that backscatter tends to saturate as AGB becomes large (above 60 Mg ha^{-1}) (Lucas et al., 2006; Englhart et al., 2011). As found in our study, AGB in 'Tierra de Pinares Segoviana' is below this value so backscatter does not start to saturate and could be successfully used for AGB estimation. Light Detection and Ranging (LiDAR) technology to estimate forest biomass has accelerated rapidly in recent years and has recently been proven to be effective in extracting AGB information (Swatantran et al., 2011; Clark et al., 2011; Zolkos et al., 2013). Therefore, more accurate results would be expected if these data sources were used in future studies in the research area.

5. Conclusion

There is a potential for quantification of Mediterranean pine (*P. pinaster* Ait.) AGB at compartment level using fraction images from LSMA as independent variables in multiple linear regression models using ASTER satellite data. A combination of ASTER bands, red and short wave infrared (B2 and B8) and GV fraction image was the best predictor of AGB. A combination of these three image data yielded an R^2_{adj} value of 0.632 and RMSE of 13.3 Mg ha^{-1} and $RMSE_r$ of 37.7% resulting from cross-validation. GV fraction image from LSMA improved the predictive power of the models analyzed generated for estimating AGB ($R^2_{adj} = 0.574$, RMSE of 20.32 Mg ha^{-1}, when no fraction images were included).

Based on the results from this study we conclude that fraction images (particularly GV) are useful for estimating AGB of Mediterranean pine in Central Spain. Additionally, the spatial distribution of estimated AGB may help in a practical way to guide forest managers' decisions in future studies and in similar forest ecosystems by assisting them in monitoring and managing the forested area.

Acknowledgments

All the authors would like to thank the Ministry of Environment of the Castilla y León regional government for its collaboration in this work. Finally, the authors wish to thank two anonymous reviewers who significantly improved the quality of the manuscript.

References

Aldred, A.H., Alemdag, I.S., 1988. Guidelines for Forest Biomass Inventory. Inf. Report. PI-X-77. Canadian Forest Service, Petawawa National Forest Institute.

Ardö, J., 1992. Volume quantification of coniferous forest compartments using spectral radiance recorded by Landsat Thematic Mapper. Int. J. Remote Sens. 3 (9), 1779–1786.

Asner, G.P., 1998. Biophysical and biochemical sources of variability in canopy reflectance. Remote Sens. Environ. 64 (3), 234–253.

Barbosa, J.M., Melendez-Pastor, I., Navarro-Pedreño, J., Bitencourt, M.D., 2014. Remotely sensed biomass over steep slopes: an evaluation among successional stands of the Atlantic forest, Brazil. ISPRS J. Photogramm. Remote Sens. 88, 91–100.

Blackard, J.A., Finco, M.V., Helmer, E.H., Holden, G.R., Hoppus, M.L., Jacobs, D.M., Lister, A.J., Moisen, G.G., Nelson, M.D., Riemann, R., Ruefenacht, B., Salajanu, D., Weyermann, D.L., Winterberger, k.C., Brandeis, T.J., Czaplewski, R.L., McRoberts, R.E., Patterson, P.L., Tymcio, R.P., 2008. Mapping U.S. forest biomass using nationwide forest inventory data and moderate resolution information. Remote Sens. Environ. 112, 1658–1677.

Boardman, J.W., Kruse, F.A.,1994. Automated spectral analysis: a geologic example using AVIRIS data, north Grapevine Mountains, Nevada. In: Proceedings of Tenth Thematic Conference on Geologic Remote Sensing. Environmental Research Institute of Michigan, Ann Arbor, MI, pp. I-407–I-418.

Boardman, J.M., Kruse, F.A., Green, R.O.,1995. Mapping target signature via partial unmixing of AVIRIS data. In: Summaries of the Fifth JPL Airbone Earth Science Workshop, vol. 95, no. 1. JPL Publication, pp. 23–26.

Calvao, T., Palmeirim, J.M., 2004. Mapping Mediterranean scrub with satellite imagery: biomass estimation and spectral behavior. Int. J. Remote Sens. 25, 3113–3126.

Chen, X., Chen, J., Jia, X., Wu, J., 2010. Impact of collinearity on linear and nonlinear spectral mixture analysis. In: Benediktsson, J.A. (Ed.), 2nd Workshop on Hyperspectral Image and Signal Processing (WHISPERS): Evolution in Remote Sensing. IEEE, Reykjavik, Iceland.

Clark, M.L., Roberts, D.A., Ewel, J.J., Clark, D.B., 2011. Estimation of tropical rain forest aboveground biomass with small-footprint lidar and hyperspectral sensors. Remote Sens. Environ. 115, 2931–2942.

Cutler, M.E.J., Boyd, D.S., Foody, G.M., Vetrivel, A., 2012. Estimating tropical forest biomass with a combination of SAR image texture and Landsat TM data: an assessment of predictions between regions. ISPRS J. Photogramm. Remote Sens. 70, 66–77.

Davidson, A., Csillag, F., 2001. The influence of vegetation index and spatial resolution on a two-date remote sensing-derived relation to C4 species coverage. Remote Sens. Environ. 75, 138–151.

Demarchi, L., Canters, F., Chan, J.C.-W., van de Voorde, T., 2012. Multiple endmember unmixing of CHRIS/proba imagery for mapping impervious surfaces in urban and suburban environments. IEEE Trans. Geosci. Remote Sens. 50, 3409–3424.

Deng, C., Wu, C., 2013. Examining the impacts of urban biophysical compositions on surface urban heat island: a spectral unmixing and thermal mixing approach. Remote Sens. Environ. 131, 262–274.

Dong, J., Kaufmann, R.K., Myneni, R.B., Tucker, C.J., Kauppi, P.E., Liski, J., Buermann, W., Alexeyev, V., Hughes, M.K., 2003. Remote sensing estimates of boreal and temperate forest woody biomass: carbon pools, sources and sinks. Remote Sens. Environ. 84, 393–410.

Elmore, A.J., Mustard, J.F., Manning, S.J., Lobell, D.B., 2000. Quantifying vegetation change in semiarid environments: precision and accuracy of spectral mixture analysis and the Normalized Difference Vegetation Index. Remote Sens. Environ. 73, 87–102.

Englhart, S., Keuck, V., Siegert, F., 2011. Aboveground biomass retrieval in tropical forests – the potential of combined X- and L-band SAR data use. Remote Sens. Environ. 115, 1260–1271.

Fazakas, Z., Nilsson, M., Olsson, H., 1999. Regional forest biomass and wood volume estimation using satellite data and ancillary data. Agric. For. Meteorol. 98-99, 417–425.

Fernández-Manso, O., Quintano, C., Fernández-Manso, A., 2009. Combining spectral mixture analysis and object-based classification for fire severity mapping. Invest. Agrar. Sist. Recur. For. (For. Syst.) 18, 296–313.

Fernández-Manso, A., Quintano, C., Roberts, D.A., 2012. Evaluation of potential of multiple endmember spectral mixture analysis (MESMA) for global surface coal mining affected area mapping. Remote Sens. Environ. 127, 181–193.

Foody, G.M., Cutler, M.E., Mcmorrow, J., Pelz, D., Tangki, H., Boyd, D.S., Douglas, I., 2001. Mapping the biomass of Bornean tropical rain forest from remotely sensed data. Global Ecol. Biogeogr. 10, 379–387.

Freitas, S.R., Mello, M.C.S., Cruz, C.B.M., 2005. Relationships between forest structure and vegetation indices in Atlantic rainforest. For. Ecol. Manage. 218, 353–362.

Fuchs, H., Magdon, P., Kleinn, C., Flessa, H., 2009. Estimating aboveground carbon in a catchment of the Siberian forest tundra: combining satellite imagery and field inventory. Remote Sens. Environ. 113, 518–531.

Gallaun, H., Zanchi, G., Nabuurs, G.J., Hengeveld, G., Schardt, M., Verkerk, P.J., 2010. EU-wide maps of growing stock and above-ground biomass in forests based on remote sensing and field measurements. For. Ecol. Manage. 260, 252–261.

Gao, S., Niu, Z., Huang, N., Hou, X., 2013. Estimating the leaf area index, height and biomass of maize using HJ-1 and RADARSAT-2. Int. J. Appl. Earth Obs. Geoinf. 24, 1–8.

Ghasemi, N., Sahebi, M.R., Mohammadzadeh, A., 2013. Biomass estimation of a temperate deciduous forest using wavelet analysis. IEEE Trans. Geosci. Remote Sens. 51, 765–776.

Goodwin, N., Coops, N.C., Stone, C., 2005. Assessing plantation canopy condition from airborne imagery using spectral mixture analysis and fractional abundances. Int. J. Appl. Earth Obs. Geoinf. 7, 11–28.

Hair, J.F., Anderson, R.E., Tatham, R.L., Black, W.C. (Eds.), 1998. Multivariate Data Analysis. Prentice Hall, Upper Saddle River, NJ, p. 730.

Hall, R.J., Skakun, R.S., Arsenault, E., Case, B.S., 2006. Modeling forest stand structure attributes using LANDSAT ETM+ data: application to mapping of aboveground biomass and stand volume. For. Ecol. Manage. 225, 378–390.

Häme, T., Salli, A., Andersson, K., Lohi, A., 1997. A new methodology for the estimation of biomass of conifer-dominated boreal forest using NOAA AVHRR data. Int. J. Remote Sens. 18, 3211–3243.

Heiskanen, J., 2006. Estimating aboveground tree biomass and leaf area index in a mountain birch forest using ASTER satellite data. Int. J. Remote Sens. 27, 1135–1158.

Huang, J., Chen, D., Cosh, M.H., 2009. Sub-pixel reflectance unmixing in estimating vegetation water content and dry biomass of corn and soybeans cropland using normalized difference water index (NDWI) from satellites. Int. J. Remote Sens. 30, 2075–2104.
Hyyppä, J., Hyyppä, H., Inkinen, M., Engdahl, M., Linko, S., Zhu, Y.H., 2000. Accuracy comparison of various remote sensing data sources in the retrieval of forest stand attributes. For. Ecol. Manage. 128, 109–120.
IPCC CPG (Ed.), 2003. Good Practice Guidance for Land Use. Land-Use Change and Forestry. IPCC National Greenhouse Gas Inventories Programme, Hayama, Japan, p. 295.
Iwasaki, A., Tonooka, H., 2005. Validation of a crosstalk correction algorithm for ASTER/SWIR. IEEE Trans. Geosci. Remote Sens. 43, 2747–2751.
Ji, L., Wylie, B.K., Nossov, D.R., Peterson, B., Waldrop, M.P., McFarland, J.W., Rover, J., Hollingsworth, T.N., 2012. Estimating aboveground biomass in interior Alaska with Landsat data and field measurements. Int. J. Appl. Earth Obs. Geoinf. 18, 451–461.
JCyL (Junta de Castilla León) (Ed.), 1999. Catálogo de los Montes de Utilidad Pública de la provincia de Segovia. Consejería de Medio Ambiente, Zamora, p. 275.
Keshava, N., 2003. A survey of spectral unmixing algorithms. Linc. Lab. J. 14, 55–78.
Kilpeläinen, P., Tokola, T., 1999. Gain to be achieved from stand delineation in Landsat TM image-based estimates of stand volume. For. Ecol. Manage. 124, 105–111.
Köhl, M., Magnussen, S., Marchetti, M., 2006. Sampling Methods, Remote Sensing and GIS Multiresource Forest Inventory. Springer-Verlag Press, New York.
Koivuniemi, J., Korhonen, K.T., 2006. Inventory by compartments. In: Kangas, A., Maltamo, M. (Eds.), Forest Inventory. Methodology and applications. Managing Forest Ecosystems, vol. 10. Springer, Dordrecht, pp. 271–278.
Kuplich, T.M., Curran, P.J., Atkinson, P.M., 2005. Relating SAR image texture to the biomass of regenerating tropical forest. Int. J. Remote Sens. 26, 4829–4854.
Kuusinena, N., Tomppo, E., Berningera, F., 2013. Linear unmixing of MODIS albedo composites to infer subpixel land cover type albedos. Int. J. Appl. Earth Obs. Geoinf. 23, 324–333.
Kwak, D.A., Lee, W.K., Lee, J.H., Biging, G.S., Gong, P., 2007. Detection of individual trees and estimation of tree height using LiDAR data. J. For. Res. 12, 425–434.
Labrecque, S., Fournier, R.A., Luther, J.E., Piercey, D., 2006. A comparison of four methods to map biomass from Landsat-TM and inventory data in western Newfoundland. For. Ecol. Manage. 226, 129–144.
Leboeuf, A., Beaudoin, A., Fournier, L., Guindon, L., Luther, J.E., Lambert, M.C., 2007. A shadow fraction method for mapping biomass of northern boreal black spruce forests using QuickBird imagery. Remote Sens. Environ. 110, 488–500.
Lewis, S.A., Robichaud, P.R., Hudak, A.T., Austin, B., Liebermann, R.J., 2012. Utility of remotely sensed imagery for assessing the impact of salvage logging after forest fires. Remote Sens. 4, 2112–2132.
Lu, D., Mausel, P., Brondízio, E., Moran, E., 2004. Relationships between forest stand parameters and Landsat TM spectral responses in the Brazilian Amazon Basin. For. Ecol. Manage. 198 (1–3), 149–167.
Lu, D., 2006. The potential and challenge of remote sensing-based biomass estimation. Int. J. Remote Sens. 27, 1297–1328.
Lu, D., Batistella, M., Moran, E., 2005. Satellite estimation of aboveground biomass and impacts of forest stand structure. Photogramm. Eng. Remote Sens. 71, 967–974.
Lucas, R.M., Cronin, N., Moghaddam, M., Lee, A., Armston, J., Bunting, P., Witte, C., 2006. Integration of radar and Landsat-derived foliage projected cover for woody regrowth mapping, Queensland, Australia. Remote Sens. Environ. 100, 388–406.
Mäkelä, H., Pekkarinen, A., 2004. Estimation of forest stand volumes by Landsat TM imagery and stand-level field-inventory data. For. Ecol. Manage. 196, 245–255.
Main-Knorn, M., Cohen, W.B., Kennedy, R.E., Grodzki, W., Pflugmacher, D., Griffiths, P., Hostert, P., 2013. Monitoring coniferous forest biomass change using a Landsat trajectory-based approach. Remote Sens. Environ. 139, 277–290.
Mallinis, G., Koutsias, N., Makras, A., Karteris, M., 2004. Forest parameters estimation in a European Mediterranean landscape using remotely sensed data. For. Sci. 50, 450–460.
Matthew, M.W., Adler-Golden, S.M., Berk, A., Richtsmeier, S.C., Levine, R.Y., Bernstein, L.S., Acharya, P.K., Anderson, G.P., Felde, G.W., Hoke, M.P., Ratkowski, A., Burke, H., Kaiser, R.D., Miller, D.P., 2000. Status of atmospheric correction using a MODTRAN4-based algorithm. In: SPIE Proceedings, Algorithms for Multispectral, Hyperspectral, and Ultraspectral Imagery VI, vol. 4049, pp. 199–207.
MMA (Ed.), 2006. Criterios e indicadores de gestión forestal sostenible en los bosques españoles. Ministerio de Medio Ambiente, Dirección General para la Biodiversidad, Madrid, p. 155.
Michishita, R., Jiang, Z., Xu, B., 2012. Monitoring two decades of urbanization in the Poyang Lake area, China through spectral unmixing. Remote Sens. Environ. 117, 3–18.
MITYC (Ed.), 2010. Estimación de la biomasa forestal potencialmente aprovechable en la provincia de Segovia (Castilla y León). Observatorio industrial de la madera, Ministerio de Industria, Turismo y Comercio, Gobierno de España, p. 57.
Montero, G., Ruiz-Peinado, R., Muñoz, M. (Eds.), 2005. Producción de biomasa y fijación de CO_2 por los bosques españoles. Monografías INIA, Serie Forestal, Madrid, p. 270.
Morel, A.C., Fisher, J.B., Malhi, Y., 2012. Evaluating the potential to monitor aboveground biomass in forest and oil palm in Sabah Malaysia, for 2000–2008 with Landsat ETM+ and ALOS-PALSAR. Int. J. Remote Sens. 33, 3614–3639.
Mozgeris, G., 2008. Estimation and use of continuous surfaces of forest parameters: options for Lithuanian forest inventory. Baltic For. 14, 176–184.
Mutanga, O., Adam, E., Cho, M.A., 2012. High density biomass estimation for wetland vegetation using WorldView-2 imagery and random forest regression algorithm. Int. J. Appl. Earth Obs. Geoinf. 18, 399–406.
Mutanga, O., Skidmore, A.K., 2004. Narrowband vegetation indices overcome the saturation problem in biomass estimation. Int. J. Remote Sens. 25, 3999–4014.
Mustard, J.F., Sunshine, J.M., 1999. Spectral analysis for earth science: investigations using remote sensing data. In: Rencz, A.N. (Ed.), Remote Sensing for the Earth Sciences: Manual of Remote Sensing, vol. 3, 3rd ed. Wiley, New York, pp. 251–307.
Muukkonen, P., Heiskanen, J., 2005. Estimating biomass for boreal forests using ASTER satellite data combined with standwise forest inventory data. Remote Sens. Environ. 99, 434–447.
Muukkonen, P., Heiskanen, J., 2007. Biomass estimation over a large area based on standwise forest inventory data and ASTER and MODIS satellite data: a possibility to verify carbon inventories. Remote Sens. Environ. 107, 617–624.
Parresol, B.R., 1999. Assessing tree and stand biomass: a review with examples and critical comparisons. For. Sci. 45, 573–593.
Peddle, D.R., Brunke, S.P., Hall, F.G., 2001. A comparison of spectral mixture analysis and ten vegetation indices for estimating Boreal forest biophysical information from airborne data. Can. J. Remote Sens. 27, 627–635.
Phua, M., Saito, H., 2003. Estimation of biomass of a mountainous tropical forest using Landsat TM data. Can. J. Remote Sens. 29, 429–440.
Plaza, A., Du, Q., Bioucas-Dias, J.M., Jia, X., Kruse, F.A., 2011. Foreword to the special issue on spectral unmixing of remotely sensed data. IEEE Trans. Geosci. Remote Sens. 49, 4103–4110.
Popescu, S.C., 2007. Estimating biomass of individual pine trees using airborne LiDAR. Biomass Bioenergy 31, 646–655.
Poso, S., Wang, G., Tuominen, S., 1999. Weighting alternative estimates when using multi-source auxiliary data for forest inventory. Silva Fenn. 33, 41–50.
Poulain, M., Peña, M., Schmidt, A., Schmidt, H., Schulte, A., 2012. Aboveground biomass estimation in intervened and non-intervened *Nothofagus pumilio* forests using remotely sensed data. Int. J. Remote Sens. 33, 3816–3833.
Quintano, C., Fernández-Manso, A., Fernández-Manso, O., Shimabukuro, Y., 2006. Mapping burned areas in Mediterranean countries using Spectral Mixture Analysis from a unitemporal perspective. Int. J. Remote Sens. 27, 645–662.
Quintano, C., Fernández-Manso, A., Shimabukuro, Y.E., Pereira, G., 2012. Spectral unmixing. Int. J. Remote Sens. 33, 5307–5340.
Quintano, C., Fernández-Manso, A., Roberts, D.A., 2013. Multiple Endmember Spectral Mixture Analysis (MESMA) to map fire severity levels from Landsat images in Mediterranean countries. Remote Sens. Environ. 136, 76–88.
Rautiainen, M., Suomalainen, J., Mõttus, M., Stenberg, P., Voipio, P., Peltoniemi, J., Manninen, T., 2007. Coupling forest canopy and understory reflectance in the Arctic latitudes of Finland. Remote Sens. Environ. 110, 332–343.
Roberts, D.A., Batista, G.T., Pereira, J.L.G., Waller, E.K., Nelson, B.W., 1998. Change identification using multitemporal spectral mixture analysis: applications is eastern Amazonia. In: Lunetta, R.S., Elvidge, C.D. (Eds.), Remote Sensing Change Detection: Environmental Monitoring Methods and Applications. Ann Arbor Press, Ann Arbor, MI, pp. 137–161.
Roy, P.S., Ravan, S.A., 1996. Biomass estimation using satellite remote sensing data—an investigation on possible approaches for natural forest. J. Biosci. 21, 535–561.
Runyon, R.P., Coleman, S.A., Pettenger, D.J. (Eds.), 2000. Fundamentals of Behavioral Statistics. McGraw-Hill Higher Education, Boston, MA, p. 656.
Salvador, R., Pons, X., 1998. On the applicability of Landsat-TM images to Mediterranean forest inventories. For. Ecol. Manage. 104, 193–208.
Sarker, M.L.R., Nichol, J.E., 2011. Improved forest biomass estimates using ALOS AVNIR-2 texture indices. Remote Sens. Environ. 115, 968–977.
Sevillano-Marco, E., Fernández-Manso, A., Quintano, C., Poulain, M., 2013. CCD CBERS and ASTER data in dasometric characterization of *Pinus radiata* D. Don (Northwestern Spain). Cerne 19, 103–110.
Shimabukuro, Y.E., Smith, J., 1991. The least-squares mixing models to generate fraction images derived from remote sensing multispectral data. IEEE Trans. Geosci. Remote Sens. 29, 16–21.
Soenen, S.A., Peddle, D.R., Hall, R.J., Coburn, C.A., Hall, F.G., 2010. Estimating aboveground forest biomass from canopy reflectance model inversion in mountainous terrain. Remote Sens. Environ. 114, 1325–1337.
Spanner, M.A., Pierce, L.L., Peterson, D.L., Running, S.W., 1990. Remote sensing of temperate coniferous forest leaf area index. The influence of canopy closure, understory vegetation and background reflectance. Int. J. Remote Sens. 11, 95–111.
Swatantran, A., Dubayah, R., Roberts, D., Hofton, M., Blair, J.B., 2011. Mapping biomass and stress in the Sierra Nevada using lidar and hyperspectral data fusion. Remote Sens. Environ. 115, 2917–2930.
Tian, X., Su, Z., Chen, E., Li, Z., van der Tol, C., Guo, J., He, Q., 2012. Reprint of: estimation of forest above-ground biomass using multi-parameter remote sensing data over a cold and arid area. Int. J. Appl. Earth Obs. Geoinf. 17, 102–110.
Tiefelsdorf, M., Boots, B., 1995. The exact distribution of Moran's I. Environ. Plann. A 27, 985–999.
Tomppo, E., Nilsson, M., Rosengren, M., Aalto, P., Kennedy, P., 2002. Simultaneous use of Landsat-TM and IRS-1c WiFs data in estimating large area tree stem volume and aboveground biomass. Remote Sens. Environ. 82, 156–171.
Van der Heijden, G.W.A.M., Clevers, J.G.P.W., Schut, A.G.T., 2007. Combining close-range and remote sensing for local assessment of biophysical characteristics of arable land. Int. J. Remote Sens. 28, 5485–5502.
Van der Meer, F.D., De Jong, S.M., 2000. Improving the results of spectral unmixing of LANDSAT TM imagery by enhancing the orthogonality of end-members. Int. J. Remote Sens. 21, 2781–2797.

Van der Meer, F.D., Jia, X., 2012. Collinearity and orthogonality of endmembers in linear spectral unmixing. Int. J. Appl. Earth Obs. Geoinf. 18, 491–503.
Wang, C., Qi, J., 2008. Biophysical estimation in tropical forests using JERS-1 VNIR imagery. I: leaf area index. Int. J. Remote Sens. 29, 6811–6826.
Wang, Y., Sun, D., 2005. The ASTER tasseled cap interactive transformation using Gramm–Schmidt method. In: Zhang, L., Zhang, J., Liao, M. (Eds.), Proceedings of the SPIE, vol. 6043. , pp. 184–195.
Welch, R., Ahlers, W., 1987. Merging multiresolution SPOT HRV and Landsat TM data. Photogramm. Eng. Remote Sens. 53, 301–303.
Weng, Q., Lu, D., 2008. A sub-pixel analysis of urbanization effect on land surface temperature and its interplay with impervious surface and vegetation coverage in Indianapolis, United States. Int. J. Appl. Earth Obs. Geoinf. 10, 68–83.
Xie, Y., Sha, Z., Yu, M., Bai, Y., Zhang, L., 2009. A comparison of two models with Landsat data for estimating above ground grassland biomass in Inner Mongolia, China. Ecol. Modell. 220, 1810–1818.
Zanotta, D.C., Haertel, V., Shimabukuro, Y.E., Rennó, C.D., 2012. Residual information to estimate uncertainty and improve the Spectral Linear Mixing Model solution. In: International Geoscience and Remote Sensing Symposium (IGARSS), pp. 3471–3473.
Zheng, D., Rademacher, J., Chen, J., Crow, T., Bresee, M., Lemoine, J., Ryu, S.R., 2004. Estimating aboveground biomass using Landsat 7 ETM+ data across a managed landscape in northern Wisconsin, USA. Remote Sens. Environ. 93, 402–411.
Zolkos, S.G., Goetz, S.J., Dubayah, R., 2013. A meta-analysis of terrestrial aboveground biomass estimation using lidar remote sensing. Remote Sens. Environ. 128, 289–298.

Chapter II

O. Fernández-Manso, C. Quintano, A. Fernández-Manso, 2009. **Combining spectral mixture analysis and object-based classification for fire severity mapping**. *Forest systems*, 18 (3), 296-313

Resumen

Cartografía de severidad de incendios forestales a partir de la combinación del modelo de mezclas espectrales y la clasificación basada en objetos

Este estudio presenta una metodología rápida y precisa para la evaluación de los niveles de severidad que afectan a grandes incendios forestales. El trabajo combina un modelo de mezclas espectrales y un análisis de imágenes basado en objetos con el objetivo de cartografiar distintos niveles de severidad (alto, moderado y bajo) empleando una imagen multiespectral Landsat Enhanced Thematic Mapper (ETM+). Este modelo fue testado en un gran incendio forestal ocurrido en el noroeste de España. Las imágenes fracción obtenidas tras aplicar el modelo de mezclas a la imagen Landsat fueron utilizadas como datos de entrada en el análisis basado en objetos. En este se llevó a cabo una segmentación multinivel y una posterior clasificación usando funciones de pertenencia. Esta metodología fue comparada con otras más simples con el fin de evaluar su conveniencia a la hora de distinguir entre los tres niveles de severidad anteriormente mencionados. El test de McNemar fue empleado para evaluar la significancia estadística de la diferencia entre los métodos testados en el estudio. El método combinado alcanzó la más alta precisión con un 97,32% y un índice Kappa del 95,96%, además de mejorar la precisión de los niveles individualmente.

Palabras clave: incendios forestales, LSMA, OBIA, Landsat ETM+

Instituto Nacional de Investigación y Tecnología Agraria y Alimentaria (INIA)
Disponible on line en www.inia.es/srf

Investigación Agraria: Sistemas y Recursos Forestales 2009 18(3), 296-313
ISSN: 1131-7965

Combining spectral mixture analysis and object-based classification for fire severity mapping

Ó. Fernández-Manso[1*], C. Quintano[2] and A. Fernández-Manso[3]

[1] Junta de Castilla y León. Agencia de Protección Civil y Consumo. C/ García Morato, 24. 47007 Valladolid (Spain).
[2] Universidad de Valladolid. Departamento de Ingeniería Electrónica. 47014 Valladolid. Spain.
[3] Universidad de León. Departamento de Ingeniería Agraria. Campus de Ponferrada. 24400 Ponferrada, León. Spain.

Abstract

This study shows an accurate and fast methodology in order to evaluate fire severity classes of large forest fires. A single Landsat Enhanced Thematic Mapper multispectral image was utilized with the aim of mapping fire severity classes (high, moderate and low) using a combined-approach based in a spectral mixing model and object-based image analysis. A large wildfire in the Northwest of Spain was used to test the model. Fraction images obtained by Landsat unmixing were used as input data in the object-based image analysis. A multilevel segmentation and a classification were carried out by using membership functions. This method was compared with other simpler in order to evaluate the suitability to distinguish between the three fire severity classes above mentioned. McNemar's test was used to evaluate the statistical significance of the difference between approaches tested in this study. The combined approach achieved the highest accuracy reaching 97.32% and kappa index of agreement of 95.96% and improving accuracy of individual classes.

Key words: wildfire, SMA, OBIA, Landsat ETM+.

Resumen

Cartografía de severidad de incendios forestales a partir de la combinación del modelo de mezclas espectrales y la clasificación basada en objetos

Este estudio presenta una metodología rápida y precisa para la evaluación de los niveles de severidad que afectan a grandes incendios forestales. El trabajo combina un modelo de mezclas espectrales y un análisis de imágenes basado en objetos con el objetivo de cartografiar distintos niveles de severidad (alto, moderado y bajo) empleando una imagen multiespectral Landsat Enhanced Thematic Mapper. Este modelo fue testado en un gran incendio forestal ocurrido en el noroeste de España. Las imágenes fracción obtenidas tras aplicar el modelo de mezclas a la imagen Landsat fueron utilizadas como datos de entrada en el análisis basado en objetos. En este se llevó a cabo una segmentación multinivel y una posterior clasificación usando funciones de pertenencia. Esta metodología fue comparada con otras más simples con el fin de evaluar su conveniencia a la hora de distinguir entre los tres niveles de severidad anteriormente mencionados. El test de McNemar fue empleado para evaluar la significancia estadística de la diferencia entre los métodos testados en el estudio. El método combinado alcanzó la más alta precisión con un 97,32% y un índice Kappa del 95,96%, además de mejorar la precisión de los niveles individualmente.

Palabras clave: incendios forestales, SMA, OBIA, Landsat ETM+

Introduction

Large forest fires are becoming more frequent in Mediterranean areas due to climatic factors and changes in lifestyles and economic conditions. They are one of the most important causes of environmental alteration and land degradation in the Mediterranean Basin, because of the post-fire exposure of bare soil to rainfall (Leone and Lovreglio, 2005). The main consequences of fire on vegetation depend largely on fire severity. In

* Corresponding author: out-fermanos@jcyl.es
Received: 21-11-08. Accepted: 29-10-09.

this study, the term fire severity is defined as the conditions resulting from fire, which can be described by the degree of mortality in above ground vegetation (Ryan and Noste, 1985; Patterson and Yool, 1998; Morgan *et al*., 2001; Rogan and Franklin, 2001; Key and Benson, 2002; Miller and Yool, 2002; Van Wagtendonk *et al*., 2004; Doerr *et al*., 2006). Fire severity maps may complement ecosystem management, providing foresters with baseline data on fire severity and extent required for fire management. Data from these maps may be used to identify areas that have experienced differing fire severity, to plan and monitor restoration and recovery activities, to provide a method for updating current vegetation maps and information for future pre-fire planning (Patterson and Yool, 1998; Brewer *et al*., 2005). It is important therefore, to dispose of techniques to efficiently evaluate fire effects in burned areas.

Considering the extremely broad spatial expansion and often limited access to areas affected by fires, satellite remote sensing provides an important means of gathering information about a burned area in a timely and consistent manner (Rogan and Yool, 2001). Optical satellite imagery from Landsat Enhanced Thematic Mapper (ETM+) has been chosen for this work because the mid-infrared reflectance of vegetation is strongly related to important vegetation canopy characteristics relative to fire effects. It was decided to employ only one post-fire image as it is considered of great interest to find quick and affordable methodology for obtaining fire severity maps avoiding the use of pre-fire images. In doing this, money and time would be saved in terms of obtaining, correcting and normalising images. Landsat missions such as Multi Spectral Scanner (MSS), Thematic Mapper (TM) and ETM+ have been widely used for mapping fire severity (Ryan and Noste, 1985; Milne, 1986; Chuvieco and Congalton, 1988; White *et al*., 1996; Key and Benson, 1999; Key *et al*., 2002; Key and Benson, 2004; Roldán-Zamarrón *et al*., 2006; De Santis and Chuvieco, 2007; González-Alonso *et al*., 2007; Miller and Thode, 2007; Wimberly and Reilly, 2007; Hoy *et al*., 2008; Verbyla *et al*., 2008; Norton *et al*., 2009).

A lack of spectral contrast is partly responsible for the classical errors related to post-fire classifications of burned areas (Koutsias *et al*., 1999): confusion of burned areas with dark land covers (water, dark forests), confusion between slightly burned and sparsely unburned vegetation (problem of the mixed pixels), difficulties in discriminating severity of burning, and confusion between burned vegetation and non-vegetated categories, such as urban areas. To minimize these problems, it has usually been necessary to combine diverse remote sensing systems and a variety of image processing techniques (Justice *et al*., 1993). The range of methods dealing with level-of-damage mapping using post-fire satellite data includes, among others: (1) vegetation indices (White *et al*., 1996; Key and Benson, 1999; Key *et al*., 2002; Díaz-Delgado *et al*., 2003; Chafer *et al*., 2004; Van Wagtendonk *et al*., 2004; Epting *et al*., 2005), (2) linear transformation techniques such as principal components (PC) analysis and Kauth-Thomas transform (KT) (Patterson and Yool, 1998), (3) spectral unmixing (Roldán-Zamarrón *et al*., 2006), etc.

Among the large number of techniques applied for the characterization of burned areas, only a few have quantitatively compared their accuracies (Chuvieco and Congalton, 1988; Koutsias *et al*., 1999), offering little information about the potential and limitations of each technique. To address this issue, this study focuses on a quantitative comparison of four approaches for mapping fire severity using a case of study of a large fire that burned in Northwest Spain, in 1998. We are particularly interested in finding synergies combining both a subpixel-based approach such as Spectral Mixture Analysis (SMA) and an Object-based Analysis Image (OBIA). SMA approach has been widely used due to its ability to cope better with the problem of the mixed pixel and minimize the effects of topography on satellite data (Caetano *et al*., 1994; Caetano, 1995; Caetano *et al*., 1996; Cochrane and Souza, 1998; Rogan and Franklin, 2001; Rogan *et al*., 2002). SMA has the potential of producing results that are directly related to post-fire land management (Caetano *et al*., 1994; Cochrane and Souza, 1998; Roldán-Zamarrón *et al*., 2006). In the case of post-fire assessment, the potential of spectral unmixing relies on the sub-pixel analysis of the materials of a burned area and it has been considered advantageous over vegetation index-based methods, due to its improved capability to distinguish burns from other bare or sparsely vegetated areas (Caetano *et al*., 1996; Díaz-Delgado *et al*., 2001). Despite Object-based classifications are increasingly being used to. In comparison with pixels, image objects carry much more useful information and, therefore, can be characterised by far more properties, such as form, texture, neighbourhood or context, than pure spectral or spectral-derivative information (Baatz and Shäpe, 1999). Object-based classification models have been developed and applied on Landsat TM (Mitri and Gitas, 2002; Mitri and Gitas, 2004a; Mitri and Gitas, 2004b), NOAA-AVHRR images (Gitas *et al*., 2004), and IKONOS images (Mitri and Gitas, 2006; Mitri and Gitas, 2008)

resulting in the accurate mapping of burned areas in the Mediterranean areas.

The main objective of our research is to demonstrate the superior accuracy obtained using a combined approach (SMA plus OBIA) for fire severity mapping with medium-resolution remote sensing image than the obtained by a more traditional approaches.

Materials and methods

Study site description

The study site, 'Tabuyo del Monte', is located in the Sierra del Teleno, in Northern Spain (figure 1). It is a small mountain chain in the South-East (SE) of León province (Spain) with SE aspect, a maximum slope of 11% and elevation ranges from sea level between 850 to 2,100 m.

The climate is Mediterranean with an average annual rainfall between 650 and 900 mm and two or three months of dryness in the summer time. Soil in this area is very sandy and acidic (pH=5.5) (Calvo *et al*., 1998). Currently vegetation is a large natural *Pinus pinaster* Ait. community covering 11,500 ha. Spanish Vegetation Map shows that into the fire scar roughly the 78% was covered by pineland, 18% by shrubs and 4% by Pyrenean oak. Fires have occurred frequently in this community, generally affecting small areas and mostly caused by dry spring-summer storms. However, in September 1998 there was a large fire presumably caused by a military manoeuvre, which burned more than 3,000 ha during four days (between September 13 and 17). This fire is the object of this study.

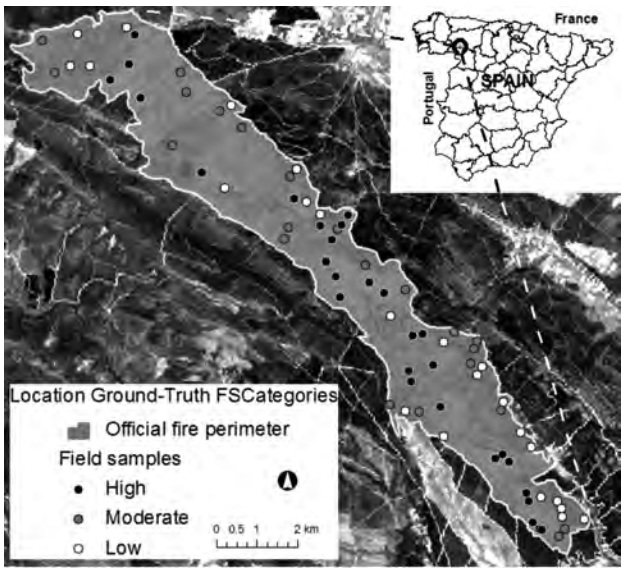

Figure 1. Location of study area in Spain; and location of field samples in the fire scar.

Remotely sensed data

No Landsat cloud-free scenes close to the wildfire date were found so the first scene available corresponded on September, 16 1999. Van Wagtendonk *et al*. (2004) used also one year after the fire occurred post-fire Landsat ETM+ for fire detection. Key (2005) pointed out that extended assessment (EA), (it occurs during the first growing season after fire) may provide more complete representation of actual fire effects. It captures first-order effects that include survivorship and delayed mortality of vegetation present before fire. The former is detected by regrowth from roots and stems of vegetation that burns but remains viable (McCarron and Knapp, 2003; Safford, 2004). Most other first-order effects, such as char, scorch and fuel consumption, are expected to persist until the next growing season, with two exceptions. Areas prone to surface erosion from wind or precipitation may show a decrease in ash cover and an increase of newly exposed mineral soil. Also, canopy foliage that is heat scorched or dies from girdling may drop to ground litter over the interval before EA. Since such effects are more or less complementary in regards to severity assessment, these delayed responses are not expected to significantly alter the remotely sensed magnitude of change detected between initial and extended assessment. In addition, is complete, so the extent of perimeters and distribution of severity represents final conditions.

Preprocessing of remotely sensed images is a preparatory phase that, in principle, improves image quality for further analyses. In this study only a geometric correction was performed. Atmospheric correction was not necessary since only one post-fire image was used to map the fire severity into the fire scar and it was cloud free. In addition, there is a likelihood that uneven implementation of corrections would not necessarily provide a better representation of the mixing space of the SMA model (Elmore *et al*., 2000).

For the geometric correction a set of 22 Ground Control Points (GCP's), selected using the National Topographic Map (Instituto Geográfico Nacional, IGN) at 1:50,000 (UTM 30 T European 1950 mean), and a 25

m-grid size digital elevation model (DEM) were used. A first-order polynomial warp function was applied and a nearest neighbour resampling protocol was then used to preserve original pixel values (Jensen, 1996; Lillesand and Kiefer, 2000). The root mean square error (RMSE) for the transformation was less than 1 pixel. In general, road intersections were used as GCP's since it was possible to locate them in the image. An illumination correction was performed with the C-correction (Teillet *et al*., 1982). This lessens the effects of shadows that may occur due to elevation variations in the landscape.

Field data

In addition to the optical satellite image data, field data were collected in the autumn of 1999 from 72 random plots for fire severity in the Tabuyo burned area (figure 1). Two different datasets were used: one for training and developing the classification rules, and another one for assessing the accuracy of the classification. Separate and independent data were used for training and for accuracy assessment. Despite this time lag, sufficient material remained in the field (scorched leaves on branches and the ground, char on the tree trunks, etc.) for an adequate, qualitative estimate of the degree of severity. Resprouting green leaves did not interfere with these observations.

The field survey plots were sized, with an average area of 0.78 hectare (100 m diameter). Random sampling plots location was correlated with the ETM+ location using a global positioning system. The plots were randoming located within pre-selected large areas with homogenous fire severity levels and low slope gradients by interpreting a 0.7 m-pixel post-fire colour aerial photograph in order to locate in the fire scar representative fire severity categories (scale 1:25,000, digital images orthorectified, mosaicked and examined on-screen in a GIS, captured on October 1998).

Classification of each field plot was determined by visual inspection, based on the observed majority fire severity class within each plot. Three possible fire severity categories were defined according to the degree of scorching vegetation (figure 2). We considered a high-severity, moderate-severity and low-severity as the used by other researchers (e.g., Jakubauskas *et al*., 1990; Turner *et al*., 1994; DeBano *et al*., 1998; Patterson and Yool, 1998; Brown and Smith, 2000; Rogan and Yool, 2001; Arno and Fiedler, 2005). The different fire severity classes were defined as follows:

(1) low: areas where shrubs to 2 m burned and no or partial canopy scorched.
(2) moderate: areas where shrubs incinerated and canopy scorched.
(3) high: areas where shrubs incinerated and canopy completely burned and apparently dead, even though some plants may still be able to sprout.

Data analysis

The development of the main proposed methodology involved two cascaded image analysis techniques: linear spectral mixture (SMA) and object-based image analysis (OBIA).

Image objects were extracted from the fraction images (obtained from SMA algorithm) in the segmentation procedure prior to classification (4th approach). In order to emphasize the benefits achievable using the adopted approach they were provided quantitative evaluations and comparisons with other approaches (1st, 2nd and 3rd) (figure 2).

(1) *First approach: data analysis for Pixel-Based Method (ETM+ISODATA)*

The first approach is a pixel-based image unsupervised classification by Iterative Self-Organizing Data Analysis Technique (ISODATA) (Sunar and Özkan, 2001; Miller and Yool, 2002) to ETM+ image. ISODATA is clustering algorithm that compares the radiometric value of each pixel with predefined number of cluster attractors and shifts the cluster mean values in a way that the majority of the pixels belongs to a cluster. In this case, we interacted with the procedure at the beginning indicating the number of the predefined cluster to be created and the iterations to be carried out and at the end, where it decides which class represents which surface objects and merges or rejects the classes with non-realistic representatives. We masked the satellite image with the official fire perimeter polygon in order to estimate the fire severity categories in the fire scar.

(2) *Second approach: data analysis for Subpixel-Based Method (SMA+ISODATA)*

Because the spatial resolution of Landsat ETM+ imagery is 30 by 30 m, the materials in a given picture element (pixel) are rarely represented by a single physical component. Therefore, in the first stage of this approach (figure 3), a linear spectral model was used which is based on the assumption that the image spectra

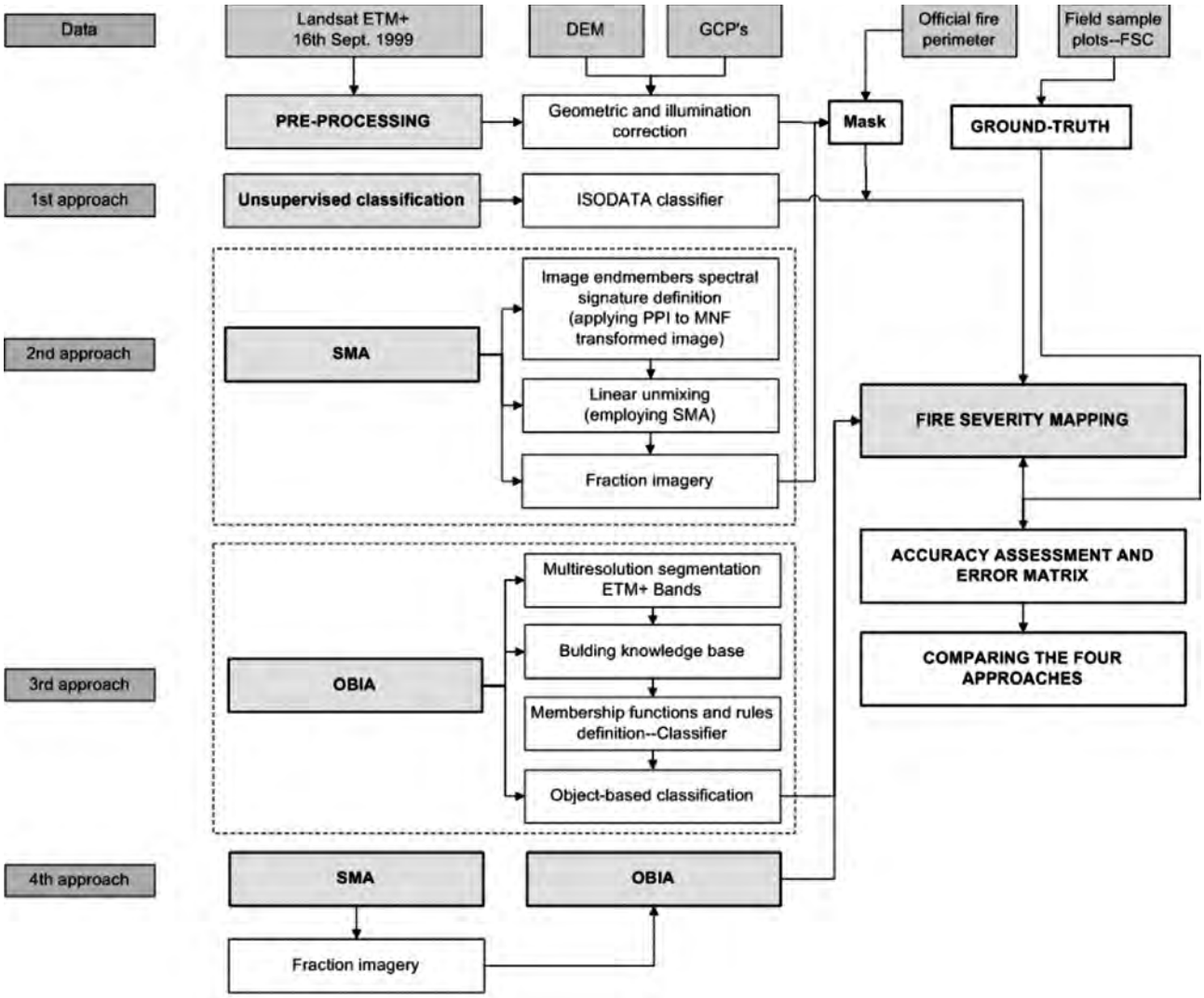

Figure 2. Flowchart of the methodology.

are formed by a linear combination of *n* pure spectra, such that:

$$DN_b = \sum_{i=1}^{n} F_i\ (DN)_{i,b} + \varepsilon_b \qquad [1]$$

where DN_b is the digital number in band *b*, $DN_{i,b}$ is the digital number for endmember *i*, in band *b*, F_i the fraction of endmember *i*, and ε_b is the residual error for each band.

The most common approach is to assume linear unmixing (Shimabukuro *et al*., 1991), although non-linear mixing can occur (Adams *et al*., 1993; Roberts *et al*., 1993). Smith *et al*. (2005) tested the most appropriate mixing model to use (linear or non-linear) in fire severity estimation. Whether the optical mixing was linear or non-linear was largely controlled by the size of the particles present in the ash.

Endmember selection is the most important step in SMA. It determines how accurately the mixture model can represent the spectra. The endmember selection must accommodate the dimensionality of the mixing space. It involves determination of the number of endmembers and the methods to select these endmembers. Possible endmembers, however, are restricted to the number of bands the image data plus one (Hill, 1993; Small, 2004). The Landsat ETM+ sensor has sufficiently low noise that the inherent dimensionality of spectrally diverse images is generally equal to the full six dimensions. We limited this analysis to bands 3, 4, 5, and 7 as White *et al*. (1996) did when they tried to map

fire severity. The definition of appropriate spectral endmembers may be either done using reference endmember from spectral libraries or from the image itself (image endmember). As appropriate reference endmembers were not available for the study site, an approach to extract pure pixels from the image was applied to retrieve image endmembers. For most SMA applications, image endmembers are utilized because they can be easily obtained and can represent spectra measured at the same scale as the image data (Roberts *et al*., 1998a). A minimum noise fraction (MNF) technique (essentially two cascaded principal components transformations) was used to determine the inherent dimensionality of image data, to segregate noise in the data, and to reduce the computational requirements for subsequent processing (Boardman and Kruse, 1994). The data space could be divided into two parts: one part associated with large eigenvalues and coherent eigenimages, and a complementary part with near-unity eigenvalues and noise-dominated images. By using only the coherent portions, the noise was separated from the data, thus improving spectral processing results (ENVI, 2000). It was possible to run an inverse MNF transform using a spectral subset to include only the good bands, or smoothing the noisy bands before the inverse. Separating purer from more mixed pixels reduced the number of pixels to be analyzed for endmember determination and made separation and identification of endmembers easier.

Four new MNF transformed bands were then analysed to find the most spectrally pure (extreme) pixels in the image using a pixel purity index (PPI) classifier. The PPI image was the result of several thousand iterations of the PPI algorithm. The higher values indicated pixels that were nearer to the corners of the n-dimensional data cloud, and were thus relatively purer than pixels with lower values. After the purer pixels were identified in the n-dimensional scatter plot, an inverse-MNF transform was applied to obtain the endmembers spectra, and their spectral response was visually verified using local knowledge (Goodwin *et al*., 2005).

Usually shade could be included either implicitly (fractions sum to 1 or less) or explicitly as an endmember (fractions sum to 1). In our case it was included implicitly (the following equation, $\Sigma Fi = 1.0$, was not included into the equation system of the unmixing model; unconstrained solution).

The least-squares solution is the method most often used for solving the linear mixture model (Smith *et al*., 1990; Shimabukuro and Smith, 1991; García-Haro *et al*., 1996) due to its simplicity and ease of implementation. As the results from the unconstrained solution do not reflect the true abundance fractions of endmembers then the root-mean-square error (RMSE) was used to assess the fit of the model (Adams *et al*., 1993; Roberts *et al*., 1998a) and it is shown in equation (2), where *m* is the number of bands.

$$RMSE = \sqrt{\left(\sum_{b=1}^{m} \varepsilon_b^2\right)/m} \qquad [2]$$

The ISODATA classifier was used to classify fraction image into fire severity categories: high, moderate and low (Sunar and Özkan, 2001; Miller and Yool, 2002; Roldán-Zamarrón *et al*., 2006). Fraction image was masked by fire perimeter polygon before performing unsupervised classification.

(3) *Third approach: data analysis for Object-Based Method (ETM+OBIA)*

Object-based Image Analysis (OBIA) involved two steps: segmentation and classification.

(a) *Image segmentation*

Segmentation is a prerequisite to object-based classification which is the subdivision of an image into separated regions or objects by gathering together many pixels in

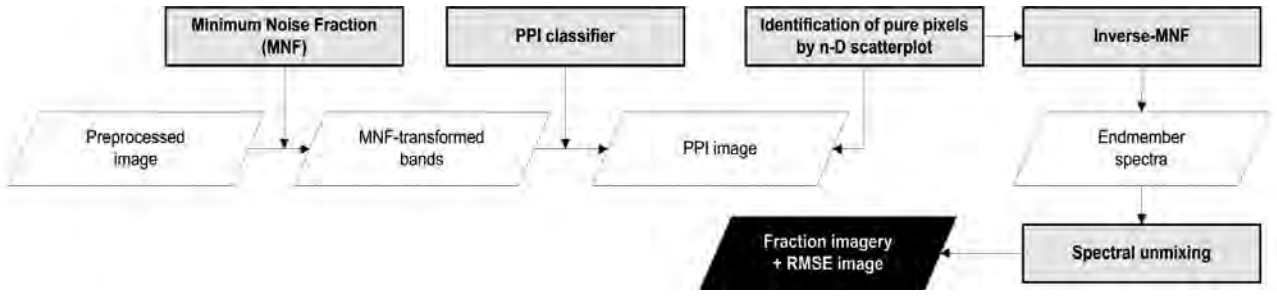

Figure 3. Spectral mixture analysis model.

certain way. In comparison to pixels, image objects carry much more useful information and, therefore, can be characterized by far more properties (such as form, texture, neighbourhood or context) than pure spectral or spectral-derivative information (Baatz and Schäpe, 1999).

The segmentation used in this study was a bottom up region-merging process, starting with one-pixel objects. Throughout the segmentation procedure, the whole image was segmented and image objects were generated based upon several criteria of homogeneity in colour and shape (compactness and smoothness). In a subsequent step smaller image objects (Level 1 or fine scale to define fire severity categories in the fire scar) were merged into bigger ones (Level 2 or coarse scale to define the object boundaries of fire scar). The scale parameter was set to 5 and 20 at level 1 and 2, respectively. The composition of homogeneity criterion was set as follows: colour 0.8 and shape 0.2. For the shape criterion, smoothness was 0.1 and compactness was 0.9.

This process is called multiresolution segmentation, which was used to construct a hierarchical network of image object that simultaneously represented image information in different spatial resolutions (level 1 and 2).

(b) *Object-based classification*

The classification of the image objects was performed by using membership functions based on fuzzy theory combined with user-defined rules. A membership function ranges from 0 to 1 for each object's feature values with regard to the object's assigned class (Navulur, 2007). Spectral, shape, and statistical characteristics as well as relationships between linked levels of the image objects can be used in the rule base to combine objects into meaningful classes (Benz *et al*., 2004). The fuzzy sets were defined by membership functions that identify those values of a feature that are regarded as typical, less typical, or not typical of a class.

(4) *Fourth approach: data analysis for Combined-Based Method (SMA+OBIA)*

After developing fraction images, several methods are commonly used classifying fraction images into different land-cover types, fire severity classes, burned areas, etc. Decision-tree classifiers (DTC) are widely used (e.g., Roberts *et al*., 1998b; Rogan and Franklin, 2001; Rogan *et al*., 2002; Souza *et al*., 2003), as are unsupervised grouping algorithm (ISOSEG) (Quintano *et al*., 2005), and supervised Maximum Likelihood (ML) (Rogan *et al*., 2002; Lu and Weng, 2004).

In our combined approach, an object-based image classification was performed using fraction images obtained in the second approach of this study as input of the model.

Burned vegetation fraction image performed better result in order to fit the image objects on both first and second segmentation levels. The scale parameter was set to 1 and 5 at level 1 and 2, respectively. The composition of homogeneity criterion was set as follows: colour 0.9 and shape 0.1. For the shape criterion, smoothness was 0.2 and compactness was 0.8. As it was done at the third approach, a fuzzy set was defined by membership functions that identified those values of a feature that were regarded as typical, less typical, or not typical of a class.

Classification accuracy was evaluated using ground referenced data. To ensure independence, no training data were used for the validation. Ground referenced data in this context means having been derived from a presumably more accurate data source than the thematic map, in this case from ground visits. The same set of ground data was used in the assessment of the accuracy of the thematic maps obtained by different classifiers in order to compare their suitability in fire severity mapping.

The accuracy assessment was based on confusion matrices, Overall Accuracy (OA), Producer's Accuracy (PA), User's Accuracy (UA) and Kappa Index of Agreement (KIA) statistic (Congalton, 1991). Error matrices were formed with data from thematic map and ground data (Congalton and Green, 1999). McNemar's test was selected to determine significant differences among classifications. Foody (2004) stated that for dependent samples, the statistical significance of the difference between two proportions might be evaluated using McNemar's test. It is a non-parametric test that is based upon confusion matrixes that are 2 by 2 in dimension. The attention is focused on the binary distinction between correct and incorrect class allocations. The McNemar test is based on the standardized normal test statistic (3)

$$Z = \frac{f_{12} - f_{21}}{\sqrt{f_{12} + f_{12}}} \qquad [3]$$

in which f_{ij} indicates the frequency of ground data lying in confusion matrix element i, j. f_{12} and f_{21} are the number of pixels that with one method were correctly classified, while with the other one were incorrectly classified.

Results

General results by approach

The different image processing methods employed and the classification techniques applied with either ISODATA or OBIA yielded varied results (figure 4).

When the unsupervised classification (ISODATA) was applied directly over the satellite image (first approach), the best results for mapping fire severity were reached using bands 3-5 and band 7, 5 iterations and forcing to 3 clusters. This approach could be considered as the best cost-effective method since no image processing technique was applied to the digital number data but it carried out the worst results among the tested approaches.

Regarding second approach, it was obtained a finally four endmembers dataset formed by: soil, two kinds of vegetation (veg1 and veg2) and burned vegetation endmember. The final vegetation 1 (veg 1) endmember was extracted from canopy of pine stands (*Pinus pinaster* Ait.), the vegetation 2 (veg 2) was mainly derived from canopy of *Quercus pyrenaica* Willd., while the soil endmember was located on agricultural areas and the burned vegetation endmember was extracted from the fire scar (figure 5).

Figure 4. Final classified images obtained by means of ISODATA (approaches 1 and 2) and Object-based classification (approaches 3 and 4). Colours corresponding to each class are indicated in the legend.

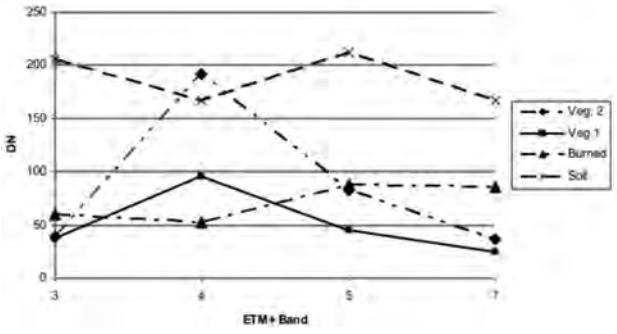

Figure 5. Image endmembers used in the spectral mixing model, expressed in image radiance (DN) for the 3, 4, 5 and 7 reflective ETM+ bands.

Spectral unmixing was performed using the four endmembers derived from the image data leading to 4-fraction images and a root-mean-square error (RMSE) image. The RMSE was calculated for all image pixels. Therefore, the error image was used to assess whether the endmembers were properly selected and whether the number of selected endmembers was sufficient. The value of the RMSE must be lower than the level of noise in the system, in order to guarantee the viability of the results. Landsat ETM+ signal-to-noise value is approximately 2 DN. The unmixing model results were evaluated as proposed by Adams *et al*., 1995. First, we evaluated the RMSE image. Our final model showed low RMSE (<2 DN values). Typically, a reasonable mixing model results in an overall RMS-threshold-error of 2.5 DN values for an image (Roberts *et al*., 1998a). Next, fraction images were evaluated and interpreted in terms of field context and spatial distribution. In this study, final fractions were allowed to be negative or superpositive (Román-Cuesta *et al*., 2005).

Fraction images derived from different combinations of image endmembers were evaluated with visual interpretation and the error extent and distribution in the error fraction image. The criteria used to identify the best suitable fraction images were based on: (1) high-quality fraction images in the fire scar, and (2) relatively low errors in the fire scar. The best results of the spectral mixture analysis for the Tabuyo fire scar are shown in figure 6.

Bright values in these images indicated areas of high fractional abundance for the endmember in question. Bright values on the RMS error image indicated areas that were poorly modelled by the least squares algorithm (values were greater than the 2.5 threshold). A cross-check with the Spanish vegetation map (1:50,000) revealed that these areas with a high RMS error were represented by crops at the time of image acquisition.

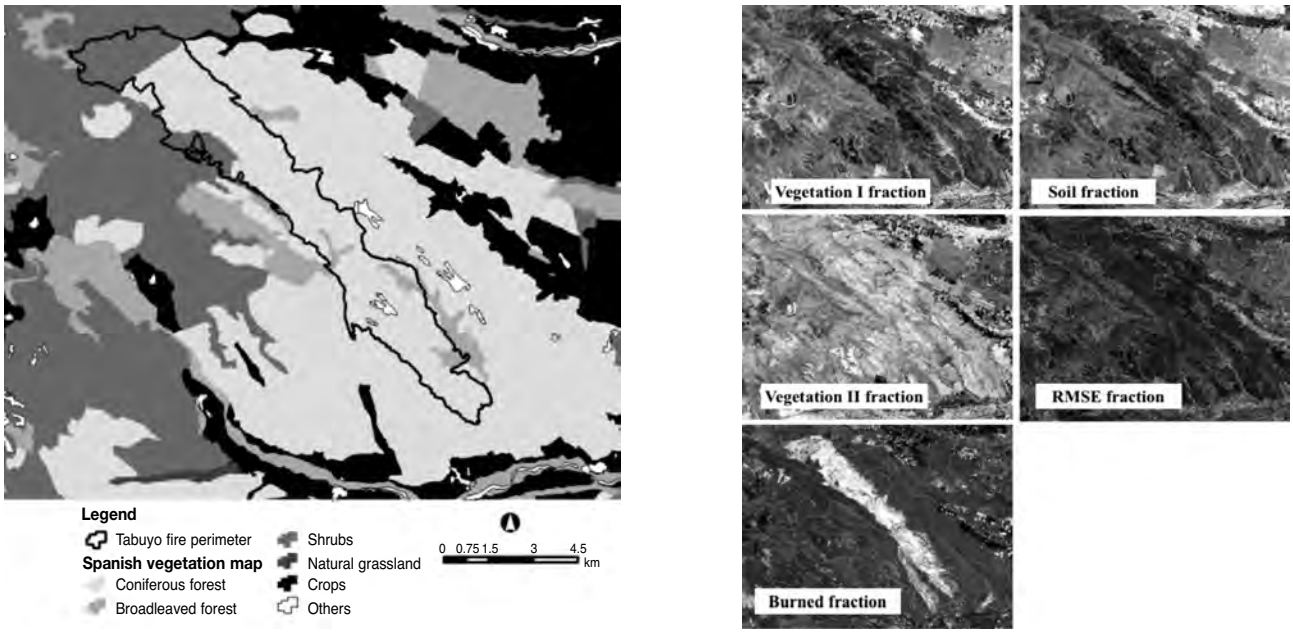

Figure 6. Spanish vegetation map with Tabuyo fire perimeter (left) and spectral unmixing of ETM+ image in fraction imagery (vegetation 1, vegetation 2, burned vegetation, soil and RMSE) (right).

The rest of the image presented a random error distribution. Given the fact that these areas fell outside of the fire scar, we assumed that the endmembers chosen had produced robust and representative image fractions of burned areas, soil and two kinds of vegetation. In this method, fire severity map was carried out by means of applying the ISODATA classifier to burned vegetation fraction image (figure 4).

For the third approach, an object-based analysis was carried out to the ETM+ image. Visual interpretation of different image segmentation results showed that it was extremely beneficial to use band 4 (NIR) and band 7 (SWIR) since they are related with wildfire reflectance values. Official fire perimeter polygon was used as thematic layer in the segmentation in order to a better delineation of fire scar boundaries (figure 7).

Two different levels of image objects representing different scales were created: a fine scale to capture fire severity categories and a coarser scale to define the burned area. Classification at level 2 included the following classes: not burned and possibly burned. This level provided a context to detect the burned area in the image and it was used as super-object information for level 1. Features based on object spectral information (image DN) as well as object contextual information, such as relation to super-objects were used in the classification. The features based on object spectral information were: brightness and ratio B5/ratio B7 to level 2 and the Normalized Burn Ratio (NBR=B4-B7/B4+B7). Existence of super-objects was used as contextual feature. The object NBR was calculated from the NBR values of all *n* pixels forming an image object. Membership functions were adapted for each chosen classification feature. Aerial photos and field notes were used to help interpret the satellite image and select burn thresholds.

For the fourth approach (combined-based approach using SMA and OBIA) two different levels of image objects representing different scales were created also with the aim of capturing fire severity categories. Same class hierarchy as developed in third approach was also adopted (figure 7). Fraction images were used to extract features that were not well distinguishable in the multispectral image. Fuzzy membership functions, which are the knowledge-based part of the classification methodology in eCognition® software, were used to apply fuzzy range to the selected features (which separates a class from other classes, fire severity classes for instance). Because it is necessary to choose the feature to which to apply the membership function, it was explored the feature space to determine which feature(s) best separate the problem classes (fire severity classes). Features based on object information (from fraction image-abundance values) as well as object contextual information, such as neighbourhood and relation to super-objects were used in the classification (figure 8).

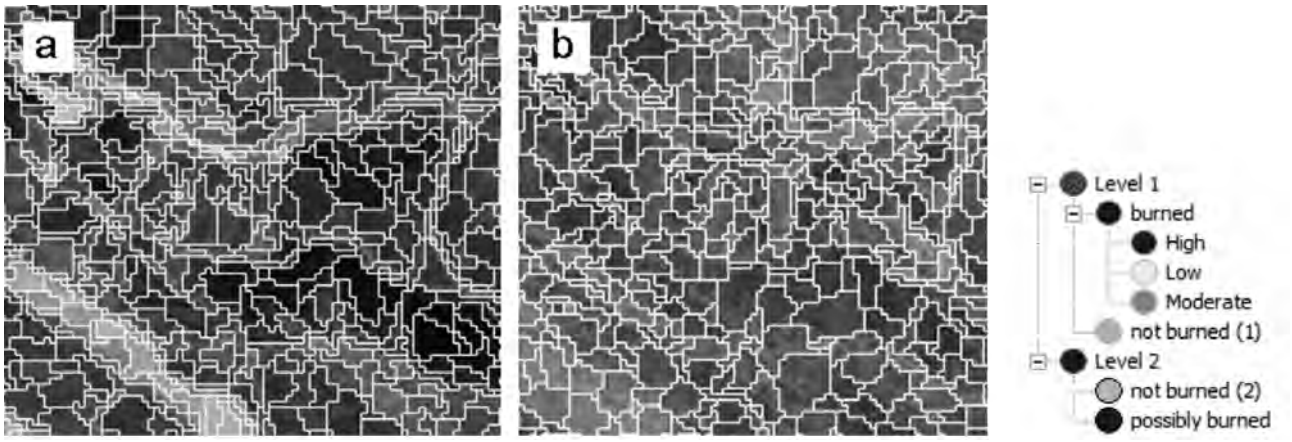

Figure 7. A section of the study area showing the segmentation results on level 1. (a) Approach 3rd. (b) Approach 4th. (c) Class hierarchy created for both approach 3rd and 4th.

The features mean burned vegetation, mean difference to scene burned vegetation and mean soil were useful at differentiating *possibly burned* and not burned from each other in level 2. At level 1, features such as existence of super-objects and mean burned vegetation were the best in separating fire severity classes (low, moderate and high) from each other. Membership functions were adapted for each chosen classification feature by interactively funding the lower and upper limits of the fuzzy ranges on segmentation level 1 for the classes Low, Moderate and High fire severity (figure 9).

Fire severity class areas

The area of fire severity categories varied among the fourth approaches analyzed in this study. Total areas of each approach depend on the combined ability of the classifier and the potential of each technique to separate

Level 2

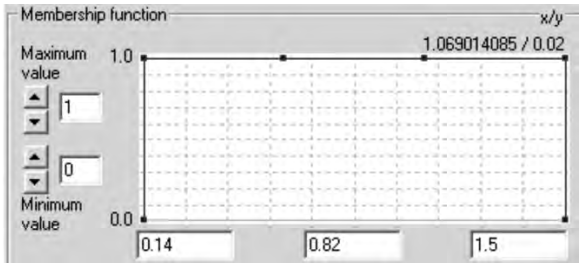

Feature: Mean burned vegetation

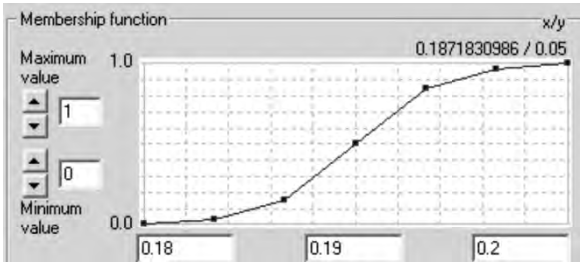

Feature: Mean diff. to scene burned veg.

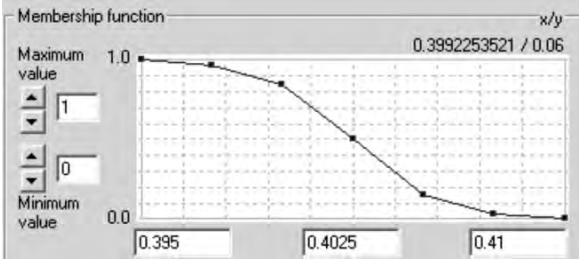

Feature: Mean soil

Figure 8. Membership functions of level 2 and 1 for fourth approach.

Level 1

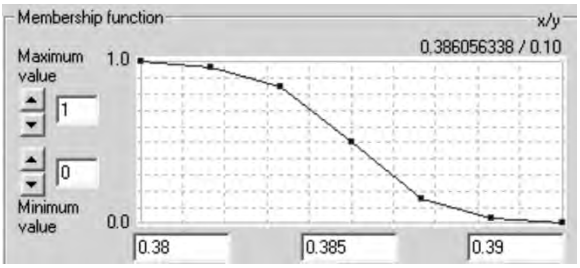

Feature: Mean burned veg for Low

Feature: Mean burned veg for Moderate

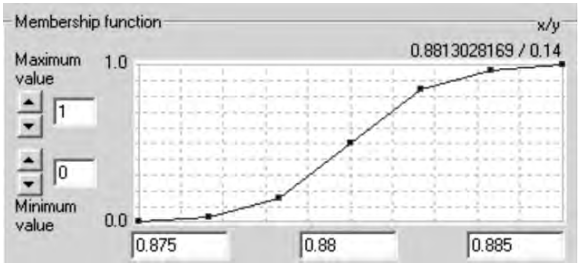

Feature: Mean burned veg for High

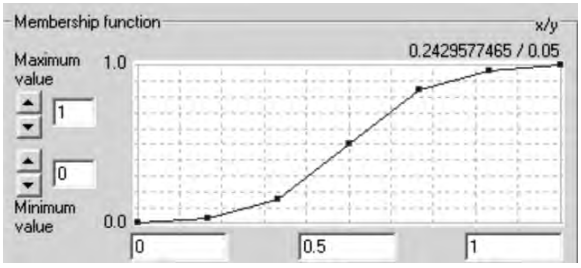

Existence of Possibly burned (L2)

Figure 9. Membership functions of level 1 for fourth approach.

among classes. Total areas of each class and their percentages are shown in table 1.

Accuracy assessments

The classification accuracy between sites visited on the ground and the final fire severity classification displayed different results (table 2). To ensure independence, no training data were used for validation. The remote sensing fire severity values at pixel-level of the plots were then compared to the field survey (100 m-diameter) fire severity classes (table 4).

Regarding the KIA (Kappa Index of Agreement) statistics, the highest values corroborated the overall accuracy (OA) results, with object-based approaches (3 and 4) showing the highest accuracies, in opposite relation with the pixel-based approaches. As happen in overall accuracy, KIA values displayed better values when fraction images were introduced.

A revision of significant differences among KIA statistics based on equation (3) was calculated and showed in table 3. It was apparent that the large differences in accuracy observed between the classifications expressed in terms of proportions of correctly allocated pixels were statistically significant at the 0.1% level of significance. This led to the conclusion that the classification accuracy derived from the four approaches was distinctively different, and the advantage of the approach 4 over the rest of approaches was significant.

An error matrix for each approach was also produced. Based on the User's, Producer's and KIA per class accuracy, individual class accuracies revealed diverse differences among methodologies (table 4).

Table 1. Severity area estimated for each approach

Approach	Methods		High	Moderate	Low	Total area
	Imagery	Classification	(ha)	(ha)	(ha)	(ha)
1	ETM+	ISODATA	686.68	1589.87	1045.15	3309.00
2	Fraction	ISODATA	1097.09	1306.63	917.98	3309.00
3	ETM+	OBIA	1366.65	1358.65	647.21	3309.00
4	Fraction	OBIA	1479.63	1200.87	691.92	3309.00

Table 2. Overall accuracies and KIA statistics for each considered approach

Approach	Methods		Overall accuracy (%)	KIA
	Imagery	Classification		
1	ETM+	ISODATA	59.37	0.3997
2	Fraction	ISODATA	77.67	0.6652
3	ETM+	OBIA	84.67	0.7685
4	Fraction	OBIA	97.32	0.9596

Discussion

Confusion among classes occurred for all approaches even though classes were supposedly quite different in their spectral responses. For the approaches that used ETM+ data instead of fraction imagery as input data for distinguishing among classes, the moderate and low severity classes were confused in the visible and NIR band, but displayed well in the SWIR range. In this regard, White *el al*. (1996) reported Landsat TM band 7 (SWIR) data is useful for distinguishing among different burn severity classes. Regarding approaches using fraction images, they displayed high severity areas characterized by a large amount of burned vegetation and low amount of vegetation and soil, the opposite trend for the low severity areas and an intermediate trend for the moderate severity areas (figure 10). The incorporation of the fraction image into the classification procedure increased the accuracy for both subpixel- and object-based approaches. By employing fraction image the overall accuracy of fire severity classification was improved by 18.30% in subpixel-based and by 12.65% in combined-based approaches (Table 2). Several authors have reported that using fraction images in a classification produces a higher accuracy than results produced by classifying the single sensor bands (Smith *et al*., 1990; Settle and Drake, 1993; Caetano *et al*., 1994; Ustin *et al*., 1996; Huguenin *et al*., 1997; Cochrane and Souza, 1998; Settle and Campbell, 1998; Aguiar *et al*., 1999; Elmore *et al*., 2000; Riaño *et al*., 2002; Theseira *et al*., 2002).

The methods that used ISODATA as classifier performed more moderate and low categories, whereas the OBIA methods (object-based classification), which classified more high and moderate classes. Approach 1 (pixel-based) displayed the highest values for the low severity class, being almost two times larger than the object-based approaches, and lowest values for the high severity class. This was because the ISODATA clustering algorithm only had a one-dimensional space to separate pixels into classes and the means of the classes

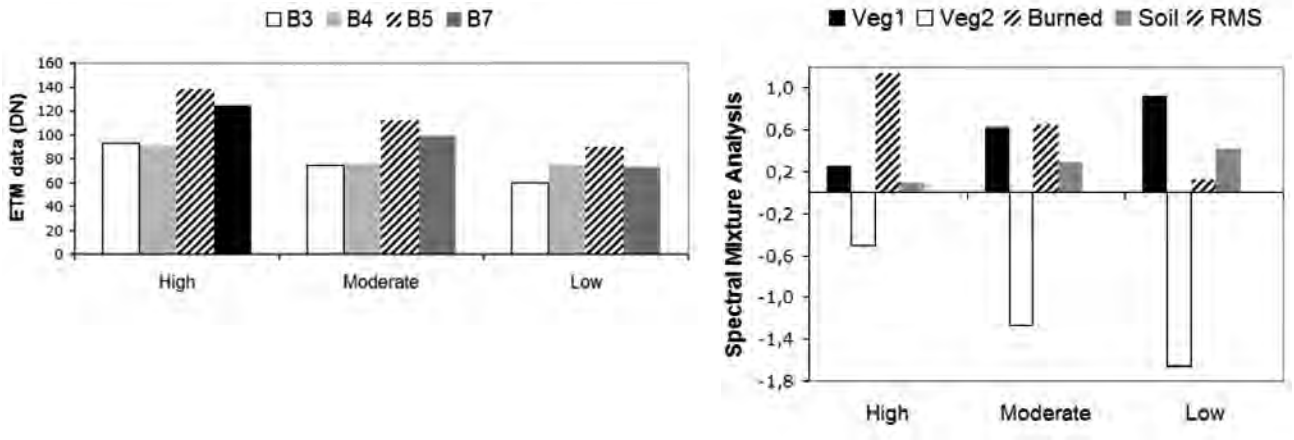

Figure 10. Mean values for each fire severity class (high, moderate and low), for approaches using ETM+ data (left) and for those using fraction imagery (right). Left graphic bars represent the utilized bands: B3, B4, B5 and B7. Right graphic bars represent the different endmembers: vegetation 1, vegetation 2, burned vegetation, soil and error term (RMS). Each sub-section in the right graphic shows the three selected classes: high, moderate and low severity.

Table 3. Significant Zeta statistics (Z=1.96) for all possible pair combinations of the considered approaches (1, 2, 3 and 4)

Approach	1	2	3	4
1		11.09	13.04	15.97
2	S		6.46	11.49
3	S	S		9.22
4	S	S	S	

S= significant. Z=1.96 significant at α=0.05

therefore tended to be uniformly distributed along the one-dimensional space (Miller and Yool, 2002). The better results obtained by approaches that included object-based image analysis into its process are mainly due to the ability of a context-based classification to reduce the speckle in the classification. Obviously, the object-based classification, which first extracts homogeneous regions and then classifies them, avoids the annoying salt-and-pepper effect of the spatially-fine classification results, which is typical of pixel-based analysis. Besides, combined-based approach (SMA/OBIA) performed better results at individual class level. It dealt satisfactory with the problems of classes confusion (burned vegetation and non-vegeted, slighty burned and unburned vegetation) using the information contained into the fraction imagery to the object-based classification and, it had an advantage over the rest of approaches tested by supplying the opportunity to combine contextual and subpixel information (contribution of each surface material in each mixed pixel) into classification which enhanced the accuracy. KIA per class, PA and UA reached high accuracy values, indicating that confusion between problematic classes such as moderate and high were minimized. This implies that introducing fraction image and object-based classification may helpful for improving separability between classes (Table 4).

The proposed method shows potential for further applications such as land cover changes, mining activities, etc. Despite future studies will examine alternative approaches to analyzing images of different resolutions.

Conclusions

Fire severity mapping is an important step by providing operational information for post-fire restoration. This paper investigated the utilization of satellite image and image processing techniques to derive fire severity information. Different approaches were tested in order to obtain accurate fire severity maps. Results showed that fraction images generated by unmixing of a Landsat ETM+ post-fire image can be used as input in an

Table 4. Error matrix and accuracy assessment by fire severity categories for each considered approach

User/Reference Class	High	Moderate	Low	Sum	User/Reference Class	High	Moderate	Low	Sum
Confusion Matrix					**Confusion Matrix**				
High	106	20	1	127	High	203	16	0	219
Moderate	116	94	10	220	Moderate	54	117	8	179
Low	35	91	199	325	Low	0	72	202	274
Sum	257	205	210		Sum	257	205	210	
Producer	0.413	0.459	0.948	**Approach**	Producer	0.789	0.571	0.962	**Approach**
User	0.835	0.427	0.612	**1**	User	0.927	0.654	0.737	**2**
KIA Per Class	0.277	0.191	0.921		KIA Per Class	0.742	0.362	0.941	
User/Reference Class	**High**	**Moderate**	**Low**	**Sum**	**User/Reference Class**	**High**	**Moderate**	**Low**	**Sum**
Confusion Matrix					**Confusion Matrix**				
High	222	44	0	266	High	255	8	0	263
Moderate	35	148	11	194	Moderate	2	197	8	207
Low	0	13	199	212	Low	0	0	202	202
Sum	257	205	210		Sum	257	205	210	
Producer	0.883	0.768	0.909	**Approach**	Producer	0.980	0.897	0.962	**Approach**
User	0.862	0.756	0.950	**3**	User	0.942	0.935	0.971	**4**
KIA Per Class	0.776	0.609	0.921		KIA Per Class	0.989	0.943	0.943	

object-based classification improving the result accuracy. Results complement the findings of a small number of previous studies that support the use of SMA in mapping fire severity due to its ability to produce fractions representative of subpixel components directly related to fire severity. The accuracy of fire severity categories was better combining SMA and OBIA than for the rest of approach tested. McNemar's test was used to evaluate the statistical significance of the difference between the four methods. The difference in accuracy expressed in terms of proportions of correctly allocated pixels was statistically significant at the 0.1% level, which meant that the thematic mapping result using the combined-approach (SMA/OBIA) achieved a much higher accuracy than the rest of approaches.

Acknowledgments

This work was carried out within the framework of the L25-04 project: *Application of new satellite image processing methodologies to estimate forest resources in Castilla y León, Spain*, which is supported by funding of Junta de Castilla y León (Spain).

References

ADAMS, J.B., SMITH, M.O. and GILLISPIE, A.R., 1993. Imaging spectroscopy: interpretations based on spectral mixture analysis. In: Remote Geochemical Analysis: Elemental and Mineralogical Composition (C. M. Pieters and P. A. Englert, Eds.), Cambridge University Press, Cambridge, UK, pp. 145-166.

ADAMS, J.B., SABOL, D.E., KAPOS, V., ALMEIDA, R., ROBERTS, D.A., SMITH, M.O. and GILLESPIE, A.R., 1995. Classification of multispectral images based on fractions of endmembers – Application to Land-Cover change in the Brazilian Amazon. Remote Sensing of Environment, 52 (2), pp. 137-154.

AGUIAR, A.P.D., SHIMABUKURO, Y.E., and MASCARENHAS, N.D.A., 1999. Use of synthetic bands derived from mixing models in the multispectral classification of remote sensing images. International Journal of Remote Sensing, 20 (4), pp. 647-657.

ARNO, S.F., and FIEDLER, C.E., 2005. Mimicking nature's fire: Restoring fireprone forests in the west. Washington, D.C.: Island Press 256 pp.

BAATZ, M. and SCHÄPE, A., 1999. Object-oriented and multi-scale image analysis in semantic networks. In: 2nd International Symposium on Operationalization of Remote Sensing, 16 August 1999 (Enshede: ITC), pp. 16-20.

BENZ, U.C., HOFFMAN, P., WILLHAUCK, G., LINGENFELDER, I. and HEYNEN, M., 2004. Multi-resolution, object-oriented fuzzy analysis of remote sensing data for GIS-ready information. ISPRS Journal of Photogrammetry and Remote Sensing, 58, pp. 239-258.

BOARDMAN, J.W., KNUSE, F.A., and GREEN, R.O., 1995. Mapping target signatures via partial unmixing of AVIRIS data. In: Proceedings of the Fifth JPL Airborne Earth Science Workshop (Pasadena: JPL Publication 95-1), pp. 23-26.

BOARDMAN, J.W. and KRUSE, F.A., 1994. Automated spectral analysis: A geological example using AVIRIS data, north Grapevine Mountains, Nevada. In: Proceedings, ERIM Tenth Thematic Conference on Geologic Remote Sensing, Ann Arbor, MI, pp. 407-418.

BREWER, C.K., WINNE, J.C., REDMOND, R.L., OPITZ, D.W., and MANGRICH, M.V., 2005. Classifying and mapping wildfire severity: A comparison of methods. Photogrammetric Engineering and Remote Sensing, 71, 1311−1320.

BROWN, J.K., and SMITH, J.K., 2000. Wildland fire in ecosystems: Effects of fire on flora. General Technical Report, RMRS-GTR-42-vol. 2. (pp.) Ogden, UT: USDA Forest Service, Rocky Mountain Research Station 257 pp.

CAETANO, M.S., 1995. Burned vegetation mapping in mountainous areas with satellite remote sensing. Master Thesis, University of California, Santa Barbara, pp. 328.

CAETANO, M.S., MERTES, L.A.K. and PEREIRA, J.M.C., 1994. Using spectral mixture analysis for fire severity mapping. In: Proceedings of the 2nd Conference on Forest Fire Research, 11, pp. 667-677.

CAETANO, M.S., MERTES, L.A.K., CADETE, L. and PEREIRA, J.M.C., 1996. Assessment of AVHRR data for characterising burned areas and post-fire vegetation recovery, In: EARSEL Advances on Remote Sensing, 4 (4-XI), pp. 124-134.

CALVO, L., TÁRREGA, R. and LUIS, E., 1998. Space-time distribution patterns of *Erica australis* L. subsp. *arogonensis* (Willk) after experimental burning, cutting, and ploughing. Plant Ecology, 137, pp. 1-12.

CHAFER, C.J., NOONAN, M. and MACNAUGHT, E., 2004. The Post-fire measurement of fire severity and intensity in the Christmas 2001 Sydney wildfires. International Journal of Wild land Fire, 33, pp. 227-240.

CHUVIECO, E. and CONGALTON, R.G., 1988. Using cluster analysis to improve the selection of training statistics in classifying remotely sensed data. Photogrammetric Engineering and Remote Sensing, 54, pp. 1275-1281.

CONGALTON, R., 1991. A review of assessing the accuracy of classifications of remotely sensed data. Remote Sensing of Environment, 37, pp. 35-46.

CONGALTON, R.G. and GREEN, J., 1999. Assessing the accuracy of remotely sensed data: principles and practice. New York, Lewis Publishers, pp. 137.

COCHRANE, M.A. and SOUZA, C.M., 1998. Linear mixture model classification of burned forests in the Eastern Amazon, International Journal of Remote Sensing, 19, pp. 3433-3440.

DEBANO, L.F., NEARY, D. G., and FFOLLIETT, P. F., 1998. Fire's effects on ecosystems. John Wiley & Sons, New York, New York, USA.

DE SANTIS, A. and CHUVIECO, E., 2007. Burn severity estimation from remotely sensed data: Performance of simulation versus empirical models, Remote Sensing of Environment, 108, pp. 422-435.

DÍAZ-DELGADO, R., PONS, X. and LLORET, F., 2001. Fire severity effects on vegetation recovery after fire. The Bigues i Riells wildfire case study. In: 3rd International Workshop on Remote Sensing and GIS applications for Forest Fires Management. New methods and sensors, Chuvieco, E. and Martín, M.P. (Eds.), pp. 152-155. Paris: EARSeL.

DÍAZ-DELGADO, R., LLORET, F. and PONS, X., 2003. Influence of fire severity on plant regeneration by means of remote sensing imagery. *International Journal of Remote Sensing*, 24, pp. 1751-1763.

DOERR, S.H., SHAKESBY, R.A., BLAKE, W.H., CHAFER, C.J., HUMPHREYS, G.S., and WALLBRINK, P.J., 2006. Effects of differing wildfire severities on soil wettability and implications for hydrological response. Journal of Hydrology, 319, 295−311.

ELMORE, A.J., MUSTARD, J.F., MANNING, S.J. and LOBELL, D.B., 2000. Quantifying vegetation change in semiarid environments: Precision and accuracy of Spectral Mixture Analysis and the Normalized Difference Vegetation Index. Remote Sensing of Environment, 73, pp. 86-102.

ENVI, 2000. ENVI User's Guide. Research Systems Inc., Boulder, Colorado, pp. 930.

EPTING, J., VERBYLA, D. and SORBEL, B., 2005. Evaluation of remotely sensed indices for assessing burn severity in interior Alaska using Landsat TM and ETM+. Remote Sensing of Environment, 96, pp. 328-339.

FOODY, G.M., 2004. Thematic map comparison: evaluating the statistical significance of differences in classification accuracy. Photogrammetric Engineering and Remote Sensing, 70, pp. 627–633.

GITAS, I.Z., MITRI, G.H. and VENTURA, G., 2004. Object-based image classification for burned area mapping of Creus Cape, Spain, using NOAA-AVHRR imagery. Remote Sensing of Environment, 92, pp. 409-413.

GONZÁLEZ-ALONSO, F., MERINO-DE-MIGUEL, S., ROLDÁN-ZAMARRÓN, A., GARCÍA-GIGORRO, S. and CUEVAS, J.M., 2007. MERIS Full Resolution data for mapping level-of-damage caused by forest fires: the Valencia de Alcántara event in August 2003. International Journal of Remote Sensing, 28 (3-4), pp. 797-809.

GARCIA-HARO, F.J., GILABERT, M.A. and MELIA, J., 1996. Linear spectral mixture modelling to estimate vegetation amount from optical spectral data. International Journal of Remote Sensing, 17 (17), pp. 3373-3400.

GOODWIN, N., COOPS, N.C. and STONE, C., 2005. Assessing plantation canopy condition from airborne imagery using spectral mixture analysis and fractional abundances. International Journal of Applied Earth Observation and Geoinformation, 7, pp. 11-28.

GREEN, A.A., BERMAN, M., SWITZER, P., and CRAIG, M.D., 1988. A transformation for ordering multispectral data in terms of image quality with implications for noise removal. IEEE Transactions on Geoscience and Remote Sensing, 26, 65-74.

HILL, J., 1993. High precision land cover mapping and inventory with multi-temporal Herat observation data. European Comision, EUR 15271.

HOY, E.E., FRENCH, N.H.F., TURETSKY, M.R., TRIGG, S.N., and KASISCHKE, E.S., 2008. Evaluating the potential of Landsat TM/ETM+ imagery for assessing fire severity in Alaskan black spruce forests. International Journal of Wildland Fire, 17, pp. 500-514.

HUGUENIN, R.L., KARASKA, M.A., BRALICOM, D.V. and JENSEN, J.R., 1997. Subpixel classification of bald cypress and tupelo gum trees in Thematic Mapper imagery. Photogrammetric Engineering and Remote Sensing, 63, pp. 717-725.

JAKUBAUSKAS, M.E., LULLA, K.P. and MAUSEL, P.W., 1990. Assessment of vegetation change in a fire-altered forest landscape. Photogrammetric Engineering and Remote Sensing, 56, pp. 371-377.

JENSEN, J.R., 1996. Introductory digital processing: a remote sensing perspective. Englewood cliffs, New Jersey: Prentice-Hall, pp. 315.

JUSTICE, C.O., MALINGREAU, J.P. and SETZER, A.W., 1993. Satellite remote sensing of fires: potentials and limitations. In: Fire in he Environment: the Ecological, Atmospheric and Climatic Importance of Vegetation Fires, P.J. Crutzen and J.G. Goldammer (Eds), pp. 77-88 (New York: John Wiley and Sons).

KEY, C.H., 2005. Remote sensing sensitivity to fire severity and fire recovery. In: Proceedings of the 5th International

Workshop on Remote Sensing and GIS Applications to Forest Fire Management: Fire Effects Assessment, De la Riva, J., Pérez-Cabello, F. and Chuvieco, E. (Eds): 29-39. Universidad de Zaragoza.

KEY, C.H. and BENSON, N.C., 1999. Measuring and remote sensing of burn severity. In: Proceedings Joint Fire Science Conference and Workshop, vol. II (p. 284), L.F. Neuenschwander, and K.C. Ryan (Eds.). Moscow, ID: University of Idaho and International Association of Wildland Fire.

KEY, C.H, and BENSON, N.C., 2002. Landscape assessment, in fire effects monitoring (FireMon) and inventory protocol: Integration of standardized field data collection techniques and sampling design with remote sensing to assess fire effects. NPS-USGS National Burn Severity Mapping Project.

KEY, C.H., BENSON, N.C., SORBEL, B., ZHU, Z., OHLEN, D., HOWARD, S. and CLEMENT, B., 2002. National Park Service-U.S. Geological Survey National Burn Severity Mapping Project. Retrieved September 30, 2002 from USGS EROS Data Center archive and web site: http://edc2.usgs.gov/fsp/severity/fire_main.asp.

KEY, C.H. and BENSON, N.C., 2004. Ground Measure of Severity, The Composite Burn Index. In: FIREMON: Fire Effects Monitoring and Inventory System, Lutes, R.E. Keane, J.F. Caratti, C.H. Key, N.C. Benson, and L.J. Gangi (Eds.). Gen. Tech Rep. RMRS-GTR-XXX, Ogden, UT: U.S. Department of Agriculture, Forest Service, Rocky Mountain Research Station.

KOUTSIAS, N., KARTERIS, M., FERNÁNDEZ-PALACIOS, A., NAVARRO, C., JURADO, J. NAVARRO, R. and LOBO, A., 1999. Burned land mapping at local scale. In: E. Chuvieco (Ed) Remote Sensing of Large Fires, pp. 157-187, Spring-Verlag, Berlin.

LEONE, V. and LOVREGLIO, R., 2005. Pre and post-fire treatments in Aleppo pine stands: prevention sylviculture and restoration. In: Proceedings II International Conference on prevention strategies of fires in Southern Europe: forest management as a tool for fire prevention. Barcelona, 9-11 may 2005.

LILLESAND, T.M. and KIEFER, R.W., 2000. Remote sensing and image interpretation. 4th ed. New York: Wiley, pp. 724.

LU, D. and WENG, Q., 2004. Spectral mixture analysis of the urban landscape in Indianapolis with Landsat ETM+ imagery. Photogrammetric engineering and remote sensing, 70 (9), pp. 1053-1062.

McCARRON, J.K. and KNAPP, A.K., 2003. C3 shrub expansion in a C4 grassland: positive post-fire responses in resources and shoot growth. American Journal of Botany, 90 (10), pp. 1496-1501.

MILLER, J.D. and THODE, A.E., 2007. Quantifying burn severity in a heterogeneous landscape with a relative version of the delta Normalized Burn Ratio (dNBR). Remote Sensing of Environment, 109 (1), pp. 66-80.

MILLER, J.D. and YOOL, S.R., 2002. Mapping forest post-fire canopy consumption in several overstory types using multi-temporal Landsat TM and ETM data. Remote Sensing of Environment, 82, pp. 481– 496.

MILNE, A.K., 1986. The use of remote sensing in mapping and monitoring vegetational change associated with bush-fire events in eastern Australia. Geocarto International, 1: 25-32.

MITRI, G.H. and GITAS, . ., 2002. The development of an object-oriented classification model for operational burned area mapping on the Mediterranean island of Thasos using LANDSAT TM images. In Forest Fire Research and Wildland Fire safety, Viegas (ed.). Milpress, Rotterdam.

MITRI, G.H. and GITAS, I.Z., 2004a. A performance evaluation of a burned area object-based classification model when applied to topographically and non-topographically corrected TM imagery. International Journal of Remote Sensing, 25, pp. 2863-2870.

MITRI, G.H. and GITAS, I.Z., 2004b. A semi-automated object-oriented model for burned area mapping in the Mediterranean region using Landsat-TM imagery. International Journal of Wildland Fire, 13, pp. 367-376.

MITRI, G.H. and GITAS, I.Z., 2006. Fire type mapping using object-based classification of Ikonos imagery. International Journal of Wildland Fire, 15, pp. 457-462.

MITRI, G.H. and GITAS, I.Z., 2008. Mapping the severity of fire using object-based classification of IKONOS imagery. International Journal of Wildland Fire, 17, pp. 431-442.

MORGAN, P., HARDY, C.C., SWETNAM, T., ROLLINS, M.G. and LONG, L.G., 2001. Mapping fire regimes across time and space: Understanding coarse and fine-scale fire patterns. International Journal of Wildland Fire, 10, pp. 329-342.

NAVULUR, K., 2007. Multispectral image analysis using the object-oriented paradigm. Taylor & Francis group, NW, pp. 165.

NORTON, J., GLENN, N., GERMINO, M., WEBER, K. and SEEFELDT, S., 2009. Relative suitability of indices derived from Landsat ETM+ and SPOT 5 for detecting fire severity in sagebrush steppe. International Journal of Applied Earth Observation and Geoinformation, 11, pp. 360-367.

PATTERSON, M.W. and YOOL S.R., 1998. Mapping fire-induced vegetation mortality using Landsat Thematic Mapper data: a comparison of linear transformation techniques. Remote Sensing of Environment, 65, pp. 132-142.

QUINTANO, C., SHIMABUKURO, Y.E., FERNÁNDEZ, A., and DELGADO, J.A., 2005. A spectral unmixing approach for mapping burned areas in Mediterranean countries. International Journal of Remote Sensing, 26 (7), pp. 1493-1498.

RAMÓN, R.M., RETANA, J., GRACIA, M. and RODRÍGUEZ, R., 2005. A quantitative comparison of methods for classifying burned areas with LISS-III imagery. International Journal of Remote Sensing, 26 (9), pp. 1979-2003.

RIAÑO, D., CHUVIECO, E., USTIN, S., ZOMER, R., DENNISON, P., ROBERTS, D. and SALAS, J., 2002. Assessment of vegetation regeneration after fire through multitemporal analysis of AVIRIS images in the Santo Mountains. Remote Sensing of Environment, 79, pp. 60-71.

ROBERTS, D.A., ADAMS, J.B. and SMITH, M.O., 1993. Discriminating green vegetation, non-photosynthetic vegetation and soils in AVIRIS data. Remote Sensing of Environment, 44, pp. 255-269.

ROBERTS, D.A., BATISTA, G.T., PEREIRA, J.L.G., WALLER, E.K. and NELSON, B.W., 1998a. Change identification using multitemporal spectral mixture analysis: Applications is eastern Amazonia, Remote Sensing Change Detection: Environmental Monitoring Methods and Applications (R. S. Lunetta and C. D. Elvidge, editors). Ann Arbor Press, Ann Arbor, Mich., pp. 137-161.

ROBERTS, D.A., GARDNER, M., and GREEN, R.O., 1998b. Mapping chaparral in the Santa Monica Mountains using multiple endmember spectral mixture models. Remote Sensing of Environment, 65, 267–279.

ROGAN, J. and FRANKLIN, J., 2001. Mapping burn severity in Southern California using spectral mixture analysis. In: Proceedings of the International Geoscience and Remote Sensing Symposium (IGARRS 01), Sydney, Australia, 9-13 July.

ROGAN, J. and YOOL, S.R., 2001. Mapping fire-induced vegetation depletion in the Peloncillo Mountains, Arizona and New Mexico. International Journal of Remote Sensing, 22 (16), pp. 3101-3121.

ROGAN, J., FRANKLIN, J. and ROBERTS, D.A., 2002. A comparison of methods for monitoring multitemporal vegetation change using thematic mapper imagery. Remote Sensing of Environment, 80, pp. 143-156.

ROLDÁN-ZAMARRÓN, A., MERINO-DE-MIGUEL, S., GONZÁLEZ-ALONSO, F., GARCÍA-GIGORRO, S. and CUEVAS, J.M., 2006. Minas de Riotinto (south Spain) forest fire: Burned area assessment and fire severity mapping using Landsat 5-TM, Envisat-MERIS, and Terra-MODIS postfire images. Journal of geophysical research-biogeosciences, 111, G04S11, doi: 10.1029/2005JG000136.

RYAN, K.C., and NOSTE, N.V., 1985. Evaluating prescribed fires. In: USDA (Ed.), Workshop on wildness fires, pp. 230-238.

SAFFORD, H.D., 2004. Fire effects on plant diversity in serpentine vs. sandstone chaparral. Ecology, 85, pp. 539-548.

SETTLE, J. and CAMPBELL, N., 1998. On the errors of two estimators of sub-pixel fractional cove when mixing is linear. IEEE Geoscience and Remote Sensing, 36, pp. 163-170.

SETTLE, J.J. and DRAKE, N.A., 1993. Linear mixing and the estimation of ground cover proportions. International Journal of Remote Sensing, 14, pp. 1159-1177.

SHIMABUKURO, Y.E. and SMITH, J.A., 1991. The least-squares mixing models to generate fraction images derived from remote sensing multispectral data. IEEE Transactions on Geoscience and Remote Sensing, 29, pp. 16-20.

SMALL, C., 2004. The Landsat ETM+ spectral mixing space. Remote Sensing of Environment, 93, pp. 1-17.

SMITH, M.O., USTIN, S.L., ADAMS, J.B. and GILLESPIE, A.R., 1990. Vegetation in deserts: I. A regional measure of abundance from multispectral images. Remote Sensing of Environment, 31, pp. 1-26.

SMITH, A.M.S., WOOSTER M.J., DRAKE, N.A., DIPOTSO, F.M., FALKOWSKI, M.J. and HUDAK, A.T., 2005. Testing the potential of multi-spectral remote sensing for retrospectively estimating fire severity in African savanna environments. Remote Sensing of Environment, 97 (1), pp. 92-115.

SOUZA JR., C., FIRESTONE, L., MOREIRA SILVA, L. and ROBERTS, D., 2003. Mapping forest degradation in the Eastern Amazon from SPOT 4 through spectral mixture models. Remote Sensing of Environment, 87, pp. 494-506.

SUNAR, F., and ÖZKAN, C., 2001. Forest fire analysis with remote sensing data. International Journal of Remote Sensing, 22, 2265−2277.

TEILLET, P.M., GUINDON, B. and GOODENOUGH, D.G., 1982. On the slope-aspect correction of multispectral scanner data. Can. J. Remote Sens. 8, 84-106.

THESEIRA, M.A., THOMAS, G. and SANNIER, C.A.D., 2002. An evaluation of spectral mixture modeling applied to a semi-arid environment. International Journal of Remote Sensing, 23, pp. 687-700.

TURNER, M.G., HARGROVE, W.W., GARDNER, R.H. and ROMME, W.H., 1994. Effects of fire on landscape heterogeneity in Yellowstone National Park, Wyoming. Journal of Vegetation Science, 5, pp. 731-742.

USTIN, S.L., HART, Q.J., DUAN, L. and SCHEER, G., 1996. Vegetation mapping on hardwood rangelands in California. International Journal of Remote Sensing, 17, pp. 3015-3036.

VAN WAGTENDONK, J.W., ROOT, R.R. and KEY, C.H., 2004. Comparison of AVIRIS and Landsat ETM+ detection capabilities for burn severity. Remote Sensing of Environment, 92, pp. 397-408.

VERBYLA, D.L., KASISCHKE, E.S. and HOY, E.E., 2008. Seasonal and topographic effects on estimating fire severity from Landsat TM/ETM+ data. International Journal of Wildland Fire, 17, pp. 527-534.

WHITE, J.D., RYAN, K.C., KEY, C.C. and RUNNINGS, S.W., 1996. Remote sensing of forest fire severity and vegetation recovery. International Journal of Remote Sensing, 6, pp. 125-136.

WIMBERLY, M.C. and REILLY, M.J., 2007. Assessment of fire severity and species diversity in the southern Appalachians using Landsat TM and ETM+ imagery. Remote Sensing of Environment, 108 (2), pp. 189-197.

Chapter III

Óscar Fernández-Manso, Alfonso Fernández-Manso, Carmen Quintano Pastor, Flor Álvarez Taboada, 2005. **Mapping forest cover changes caused by mining activities using spectral mixture analysis and object oriented classification**. In Håkan Olsson (Ed.) *Proceedings of ForestSat 2005 -Scientific workshop in operational tools in forestry using remote sensing techniques*, 8c: 77-81

Resumen

Cartografía de cambios en la cobertura forestal causados por minería a cielo abierto usando análisis de mezclas espectrales y clasificación orientada a objetos

La información relativa a la localización de actividades mineras es esencial en aplicaciones medio ambientales y en la gestión forestal sostenible. Los avances en el análisis de imágenes de satélite proporciona la posibilidad de investigar nuevos enfoques a la hora de detectar los cambios en la cobertura forestal causados por la minería a cielo abierto (carbón, pizarra y caliza). La clasificación de imágenes de satélite basadas puramente en los valores espectrales de los píxeles tiene sus limitaciones y ha creado alguna confusión entre las zonas afectadas por la minería a cielo abierto y otras zonas tales como las áreas urbanas y las masas de agua. Estas confusiones están relacionadas con el problema de la mezcla de coberturas a nivel píxel. Con el objetivo de dar una solución a este problema, se testó en el la comarca de El Bierzo (León) las sinergias que proporcina un método que combina el análisis lineal de mezclas espectrales junto a la clasificación orientada a objetos. Con ello se pretende localizar lugares para llevar a cabo una restauración y el seguimiento de futuras minas (especial interés en explotaciones ilegales). En este trabajo se desarrolló un modelo en el que se segmentó la imagen fracción sombra en objetos los cuales fueron clasificados utilizando funciones de pertenencia. La combinación de ambas técnicas mostró resultados muy prometedores.

Palabras clave: segmentación, clasificación orientada a objetos, descomposición espectral, minería

Methods for estimation and change detection

MAPPING FOREST COVER CHANGES CAUSED BY MINING ACTIVITIES USING SPECTRAL MIXTURE ANALYSIS AND OBJECT-ORIENTED CLASSIFICATION

O. Fernández-Manso[a], A. Fernández-Manso[a], C. Quintano-Pastor[b] and M.F. Álvarez[a]

[a] Grupo de investigación IPR-Ingeniería y Planificación Rural. University of León. EST. Ingeniería Agraria, Av. Astorga sn, 24400 Ponferrada (Spain), email: oscar.manso@gmail.com
[b] Departamento de Tecnología Electrónica. University of Valladolid

ABSTRACT

Information about mining activities location is essential for environmental applications and sustainable forest management. Advancements in satellite imagery analysis provide possibilities to investigate new approaches for forest cover changes detection caused by mining activities (coal contour surface, slate and limestone mining). Classification based purely on spectral values of pixels has its limitations and has reported to create confusion between mining affectation areas and other like urban areas or those with water bodies. These confusions are related to the problem of the mixed pixel. To provide a solution the synergy between a subpixel technique (linear spectral mixture analysis) and objected-oriented image classification was tested in El Bierzo County (Spain) with the aim to locate sites for restoration and to monitor future mines (special interest at illegal exploitations). A model was developed for this study involving the segmentation of shade fraction image into objects at once level and classification based in membership functions as classifier. The combination of both techniques showed very promising results.

Keywords: segmentation, object-oriented classification, unmixing, mining activities

1 INTRODUCTION

Remote sensing plays an important role in identifying forest areas associated with mines or older operating mine sites. Improvements in the spatial and spectral resolution of remote sensing data and new image analysis techniques have provided a wider scope for studying environmental attributes affected by mining, which include forest cover change, land and water. Mining brings about significant geomorphological changes in the mine site as well as in the surroundings. To monitor the changes in these attributes, remote sensing acts as an essential tool. Remote sensing provides the basic data to undertake inventory of land use, water resources as well as the temporal information required to monitor sustainable land management practices.

The traditional satellite image classification has been performed by pixel-based classification (unsupervised and supervised). Alternatives to this are being currently developed for instance the spectral mixture analysis (SMA) approach that takes subpixel classification techniques (i.e. SMA) on remotely sensed data and the object-oriented (OOIC) approach which is based fuzzy logic, allows the integration of a broad spectrum of different object features, such spectral, form, shape and texture.

Although SMA have been extensively used in different applications during the last decade (Cross *et al*., 1991; Ustin *et al*., 1993; Caetano *et al*., 1994; Novo and Shimabukuro, 1994), it was first proposed in the early seventies (Horwitz *et al*., 1971; Marsh *et al*., 1980; Adams *et al*., 1986). The SMA intends to derive the proportions of different basic land cover types that compose a mixed pixel. As a result, this technique is very appropriate to monitor cover change processes, since the mixture of vegetation and soil is very common in forest areas.

The objectives of this paper were: (a) to evaluate the potential of SMA and OOIC techniques using Landsat ETM+ images in the discriminating of mining activities in a forestry context; (b) to determinate the exploitation size that is capable to discriminate the model keeping in mind the complexity of the territory (El Bierzo); and (c) to map the areas affected by mining exploitations.

2 MATERIAL AND METHODS

2.1 SITE DESCRIPTION

The study was carried out in El Bierzo County (Figure 1). It is in a sheltered mountain valley on the north-western boundary of the province of León, in the autonomous region of Castilla y León (Spain) and defined by: 7º5'23"-6º6'6"W longitude and 42º54'23"-42º24'10"N latitude. The area is sandwiched between the Cordillera Cantábrica and the Montes de León, its natural limits being the Sierras de Caurel and Ancares, the Aquilanos mountains and the Sierra de Gistredo, and is irrigated by the rivers Sil, Ancares and Burdia. The mountain ranges shelter it from the excesses of both continental and temperate climate and produce some of the most exciting landscapes (i.e. Las Médulas) in Continental Spain. The altitudes are between 359 to 2,110 m a.s.l, and the mean slope is 17%. Annual rainfall is among 670 to 720 mm and temperatures range from a summer high of 32º C to a winter low of 1º C with a year- round average of 13º C. The proximity to Asturias and Galicia make it an area with its own characteristic vegetation, different to the rest of Castilla y León. It contains a microclimate where vineyards coexist with fruit trees, pastures and immense oak and chestnut forests.

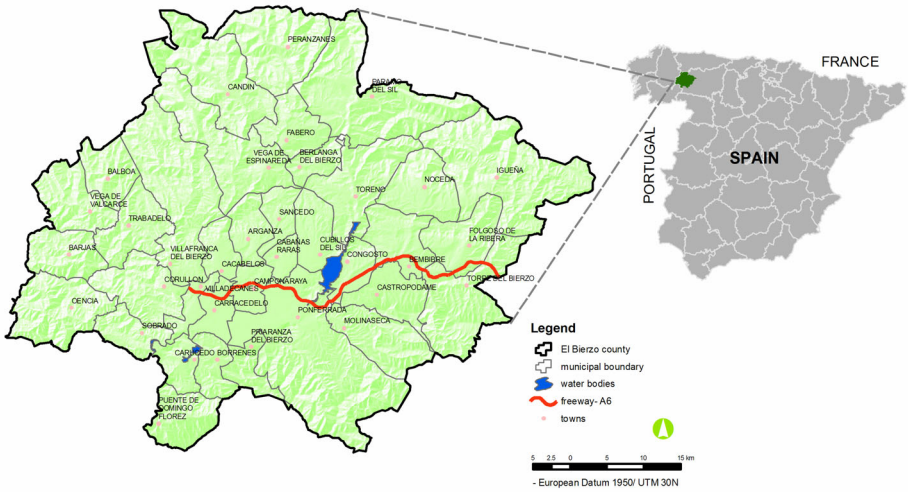

Figure 1. Location of the study area

2.2 MATERIAL

Two Landsat-7 ETM+ satellite images acquired on 20 June 2001 and 17 June 2000 were used for this research. The other datasets used in this study were: orthophoto mosaic of the area (Sept-Oct. 2000) and cadastral map.

2.3 METHODOLOGY

Prior to the SMA and OOC image analysis the Landsat image was pre-processed. Pre-processing of the remotely sensed data included his radiometric and geometric correction. Reflectivity conversion was un-necessary because linear SMA can be applied directly to the original digital numbers (DN). A mosaic of the two satellite imagery was performed as well.

Subsequently, spectral mixture analysis was applied to the image. It is generally defined as the calculation of area land cover fractions within a pixel (Roberts et al., 1998). The process involves the selection of representative pure land cover spectra (endmembers) and the unmixing of the spectral information of a pixel. The unmixing considers that each pixel can be represented as a weighted linear combination of the selected endmembers, with the weight being the endmember fractions, and a residual that all sum to one. A MNF (Minimum noise fraction) transformation was applied to the data to reduce the noise in the data and to focus the spectral unmixing on the image information with most thematic content. The final end-members used for the spectral unmixing were determined by a pixel purity analysis (PPI) that identifies the purest pixels on the edges of the multi-dimensional point cloud of pixel vectors. The PPI selected candidate pixels were evaluated and the four final endmembers (dark soil, light soil, shade and vegetation) were selected to subsequently perform the spectral mixture analysis. The next two steps: endmembers spectra definition and unmixing of bands number 3, 4, 5, and 7, were remade till de RMS

error was inferior to 1. After the purest pixels were identified in the n-dimensional scatter plot, an inverse MNF transform was applied to obtain the endmembers spectra and their spectral response was visually verified. The fractions derived from these endmembers (Figure 2) then will be used as inputs in the OOIC model.

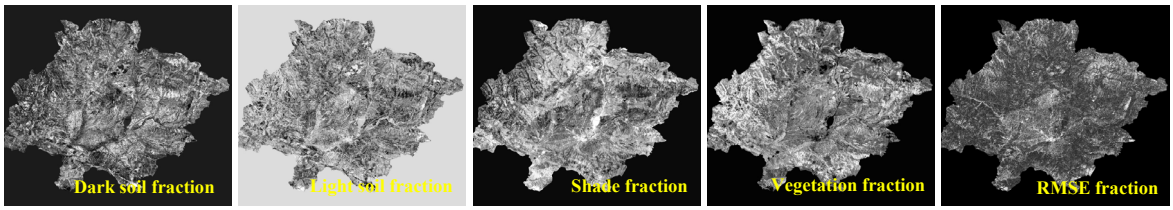

Figure 2. Fraction imagery

In contrast to classic image processing methods, the basic processing units of object-oriented image analysis (OOIC) are image objects or segments and not single pixels, moreover, classification acts on image objects. One motivation for the object-oriented approach is the fact that, in many cases, the expected result of most image analysis tasks is the extraction of real world objects, proper in shape and proper in classification. This expectation cannot be fulfilled by traditional, pixel-based approaches (Baatz, 1999).

Analysis of an image in the object-oriented approach involved classifying the image objects according to class descriptions organized in an appropriate knowledge base. The knowledge base itself was created by means of inheritance mechanisms, concepts and methods of fuzzy logic and semantic modeling. The development of the object-oriented model involved two steps, namely segmentation and classification (Mitri and Gitas, 2002).

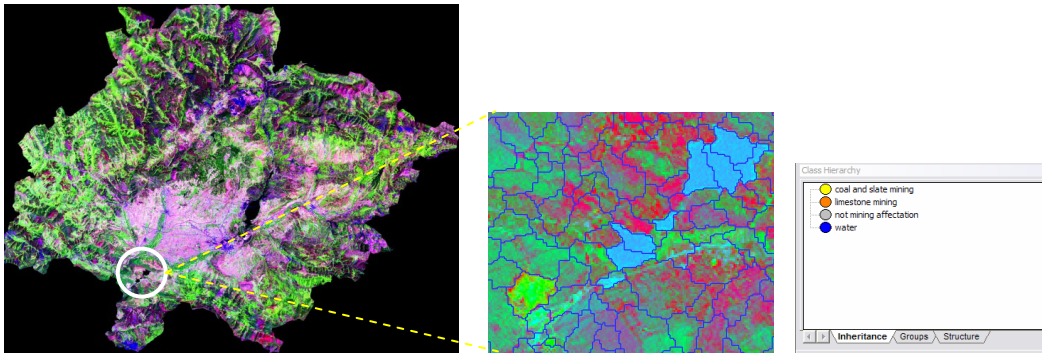

Figure 3. A section of the study area showing the segmentation and the classes

The shade fraction image was segmented into objects on once scale level (Figure 3). After segmentation, all image objects were automatically linked to a network in which each image object knows its neighbors, thus affording important context information for later analysis. Subsequently, repetition of segmentation with different scale parameter creates a hierarchical network of image objects. The better segmentation results were given out with a scale parameter of 4 and composition of homogeneity criterion (color=0.9 and compactness=0.23).

It was enough once segmentation level in discriminating between mining affectation and the other classes of confusion. We tried a multiresolution segmentation approach with two segmentation levels but were not possible to distinguish among kinds of mining activities. Anyway, our first goal was to detect these impacts and not to discriminate the type.

The objects were classified as coal and slate mining, limestone mining, not mining affectation and water without related classes. This level provided a context to detect the places with mining affectation. In the classification membership functions (fuzzy rules) was used as classifier.

3 RESULTS AND DISCUSSIONS

The map resulting from the object-oriented classification is shown in Figure 4. According to the classification the mining class occupying the largest area is coal and slate mining (1,128.62 ha) with the

number of objects identified as belonging in that class being 66. The total area affected by mining detected was 1,174.84 (SD= 14.15 ha).

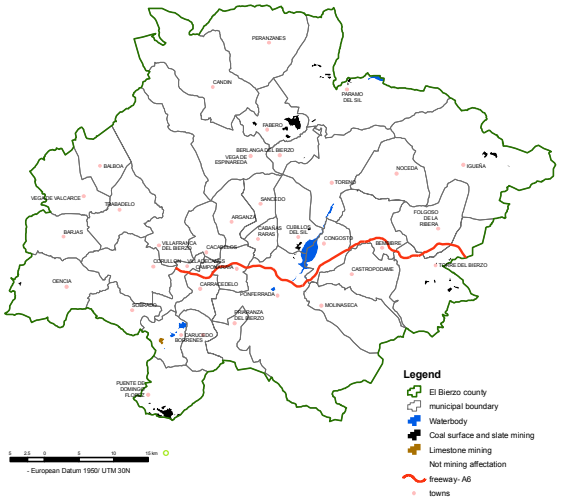

Figure 4. Mining activities detected by the model

Figure 5. Site of Community Importance affected by mining

By crossing the map of classification result with the Site of Community Importance (included in the network of protected areas "Natura 2000" of the European Union-according to the Habitats Directive 92/43/EEC) was possible to observe that some of the mines detected are into or very close to cited sites (Figure 5).

Regarding to the land use affected by mining activity it was possible to determine that the largest areas influenced were shrubs and broadleaved forests (Table 1).

Table 1. Types of land use affected by mining activities

Land use	Mining type	Area (ha)	Area (%)
Broadleaved forests	coal surface; limestone; slate	288.39	24.55
Coniferous forests	coal surface; slate	59.75	5.09
Mixed forest	coal surface; slate	11.71	1.00
Shrubs	coal surface; slate	672.42	57.23
Natural grassland	coal surface; slate	129.76	11.05
Crops	coal surface; slate	7.47	0.64
Others	coal surface; slate	5.34	0.45
	Total	**1,174.84**	**100.00**

It was necessary to obtain information about the classification stability (Figure 6) and about how capable the classes were of extracting the desired image information. Besides the classical methods of accuracy assessment, special methods, based upon fuzzy concepts, were used. The accuracy of the classified image was the assessed using test areas collected in the orthophotos (pixel size of 0.7 m) and imported into the project by means of a TTA mask to compare the classification with ground truth based on pixels. Producer, user and overall accuracies were calculated along with the Kappa statistic (Congalton and Green, 1999).

The biggest error source in the classification comes mainly from the confusion with the class urban area. This problem can be solved with simplicity using a mask (cadastral map) that includes these surfaces. As for the type of extracted mineral the pattern allows to differentiate groups between two: exploitations of limestone and those of coal-slate, although it can be discriminated against later on by means of the use of the geologic map.

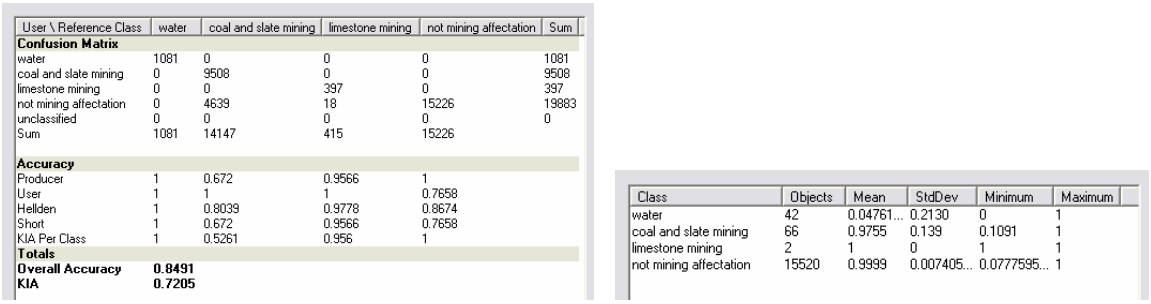

User \ Reference Class	water	coal and slate mining	limestone mining	not mining affectation	Sum
Confusion Matrix					
water	1081	0	0	0	1081
coal and slate mining	0	9508	0	0	9508
limestone mining	0	0	397	0	397
not mining affectation	0	4639	18	15226	19883
unclassified	0	0	0	0	0
Sum	1081	14147	415	15226	
Accuracy					
Producer	1	0.672	0.9566	1	
User	1	1	1	0.7658	
Hellden	1	0.8039	0.9778	0.8674	
Short	1	0.672	0.9566	0.7658	
KIA Per Class	1	0.5261	0.956	1	
Totals					
Overall Accuracy	**0.8491**				
KIA	**0.7205**				

Class	Objects	Mean	StdDev	Minimum	Maximum
water	42	0.04761...	0.2130	0	1
coal and slate mining	66	0.9755	0.139	0.1091	1
limestone mining	2	1	0	1	1
not mining affectation	15520	0.9999	0.007405...	0.0777595...	1

Figure 6. Accuracy assessment for the final classification/Classification stability (fuzzy accuracy assessment)

The result of the classification confusion matrix is showed in Figure 6. The overall classification accuracy was estimated to be 84.91 %. Kappa statistic was 72.05 %.

4 CONCLUSIONS

The proposed methodology allows the elaboration of forest cover change maps in the current moment in one of the main mining regions of the European Union in the obtaining of non metallic minerals.

The model works optimally for mining impacts largest than 5 ha. The tessellation and complexity of the land uses make that the smallest impacts are of difficult segregation. This apparent problem, in the practice, is resolved since the type of exploitation of more impact, surface mining, generally occupies large surfaces.

The obtained maps have a great utility for the analysis of the regressive changes in the forest since these activities correspond to the main genesis of changes.

The synergies of SMA and OOIC to map forest cover changes caused by mining activity have been demonstrated. Although this work is only in its preliminary stages the results indicate a great potential for extracting information from multispectral satellite imagery.

REFERENCES

Adams, J.B., Smith, M.O. and Johnson, P.E. 1986. Spectral mixture modelling: a new analysis of rock and soil types at the Viking Lander I site. *Journal of Geophysical Research*. 91: 8098–8112.

Baatz, M.A.S. 1999. Object-Oriented and Multi-Scale Image Analysis in Semantic Networks. *In Proc. of the 2nd International Symposium on Operationalization of Remote Sensing*, Enschede. ITC.

Caetano, M.S., Mertes, L.A.K. and Pereira, J.M.C. 1994. Using spectral mixture analysis for fire severity mapping. Second International Conference on Forest Fire Research, Coimbra;

Congalton, R.G. and Green, J. 1999. Assessing the accuracy of remotely sensed data: principles and practice. NY: Lewis publishers.

Cross, A.M., Settle, J.J., Drake, N.A. and Paivinen, R.T.M. 1991. Subpixel measurement of tropical forest cover using AVHRR data. *International Journal Remote Sensing*. 12: 1119–1129.

Horwitz, H.M., Nalepka, R.F., Hyde, P.D. and Morgenstern, J.P. 1971. Estimating the proportion of objects within a single resolution element of a multispectral scanner. *In Seventh International Symposium on Remote Sensing of Environment*, pp. 1307–1320.

Marsh, S.E., Switzer, P., Kowalick, W.S. and Lyon, R.J.P. 1980. Resolving the percentage of component terrains within single resolution elements. *Photogrammetric Engineering and Remote Sensing*. 46: 1079–1086.

Mitri, G.H. and Gitas, I.Z. 2002. The development of an object-oriented classification model for operational burned are mapping on the Mediterranean island of Thasos using Landsat TM images. *Forest Fire & Wildland Fire Safety*, Viegas (ed.) Millpress, Rotterdam, ISBN 90-77017-72-0.

Novo, E.M. and Shimabukuro, Y.E. 1994. Spectral mixture analysis of Inland tropical waters. *International Journal of Remote Sensing*. 15: 1351–1356. pp.

Roberts, D.A., Gardner, M., Church, R., Ustin, S., Scheer, G., and Green, R.O. 1998. Mapping chaparral in the Santa Monica Mountains using multiple endmember spectral mixture models. *Remote Sensing of Environment*. 65, 267-279.

Ustin, S.L., Smith, M.O. and Adams, J.B. 1993. Remote sensing of ecological processes: a strategy for developing and testing ecological models using spectral mixture analysis. In Ehrlinger, J. R. & Field, C. B. (Eds), *Scaling Physiological Processes. Leaf to Globe*, 339–357. San Diego: Academic Press.

Chapter IV

Fernández-Manso, A., Quintano, C., Fernández-Manso, O., dos Santos, J.R., Maldonado, F.D., 2005. **Spectral Mixture Modeling to estimate wood volume in the north of Spain from optical satellite data**. *Ambiência*, 1 (2), 213-222.

Resumen

Cartografía del volumen de masas de coníferas usando análisis de mezclas espectrales y datos del satélite Landsat Thematic Mapper

La información obtenida a partir de imágenes de satélite es una importante fuente de datos para la gestión forestal. Las técnicas de teledetección aportan información acerca del volumen, biomasa y otros parámetros biofísicos de las masas forestales. El principal objetivo de este estudio es cartografiar el volumen de masas forestales de coníferas utilizando el análisis de mezclas espectrales (LSMA) en imágenes de satélite Landsat Thematic Mapper (TM). Las imágenes fracción obtenidas a partir de descomposión espectral muestran más facilmente las propiedades biofísicas que las bandas originales de la imágen de satélite, ya que representan aspectos físicos de la cobertura del terreno. El estudio se realizó en El Alto Valle del Ebro (España). Se emplearon dos mini-escenas (50x50 km) adquiridas el 12 de marzo y el 13 de julio de 1996. El metodología aplicada se llevó a cabo en los tres pasos siguientes: 1) descomposición espectral de las bandas originales, bandas 3, 4, 5 y 7 (las más empleadas en estudios de vegetación) fueron utilizadas en LSMA; 2) correlación entre las imágenes fracción, obtenidas en el paso anterior, y el volume con corteza (extraído del Segundo Inventario Forestal Nacional) por medio de técnicas de regresión y análisis multivariante; 3) obtención de cartografía de volumen de masas forestales mediante técnicas de interpolación, utilizando el modelo alométrico, obtenido en el paso anterior, y como variable independiente, el área basimétrica (AB). La conclusión principal de este trabajo fue la posibilidad de obtener un modelo ($R^2_{ajustado}$=0,75) que permitió estimar el volumen de una masa forestal a partir de datos de satélite de resolución espacial media. Además, se pudo obtener un mapa con del volume estimado empleando el modelo y la ayuda de ortofotografías digitales.

Palabras clave: inventario forestal, teledetección, cartografía de volumen, descomposición espectral

SPECTRAL MIXTURE MODELING TO ESTIMATE WOOD VOLUME IN NORTH OF SPAIN FROM OPTICAL SATELLITE DATA

MAPEAMENTO DE VOLUME EM POVOAMENTO DE CONÍFERAS USANDO A MISTURA ESPECTRAL DE IMAGENS TM/LANDSAT

Alfonso Fernández Manso[1]
Carmen Quintano Pastor[2]
Óscar Fernández Manso[1]
João Roberto dos Santos[3]
Francisco Darío Maldonado[3]

ABSTRACT

Information from satellite imagery is an important data source to forest management. Remote sensing techniques provide information about volume, biomass and other biophysical parameters of forest stands. The main goal of this work is to map the conifer stand volume from Landsat Thematic Mapper (TM) data using Spectral Mixture Analysis (SMA). Fraction images from spectral unmixing show biophysics properties more easily than original bands because they represent physics aspects of ground covers. The work area was El Alto Valle del Ebro (Spain). Two mini-scenes, (50x50km) acquired on March 12th 1996 and July 13th 1996, were used. The applied methodology had three main steps: 1) unmixing the original imagery, the bands 3, 4, 5 and 7 (the most employed in vegetation studies) were used in SMA; 2) these fraction images were related with the over bark volume (OBV) variable (extracted from Second Spanish National Forest Inventory NFI2) by means of regression techniques and multivariate analysis; 3) a volume map was obtained using interpolation techniques from the obtained allometric model

[1] Universidad de León - Ingeniería Agraria, Escuela Superior y Técnica de Ingeniería Agraria, Avenida de Astorga s/n, 24400 Ponferrada - León, España. Email: alfonso@unileon.es; oscar.manso@gmail.com
[2] Universidad de Valladolid - Tecnología Electrónica, Escuela Universitaria Politécnica, Francisco Mendizábal, 1, 47014 - Valladolid, España. Email: menchu@tele.uva.es
[3] INPE - Instituto Nacional de Pesquisas Espaciais - Av. dos Astronautas, 1758 CEP.: 12.227-010São José dos Campos - SP, Brasil. Email: jroberto@dsr.inpe.br; francis@dsr.inpe.br

Recebido para publicação em 29/09/2005 e aceito em 31/10/2005

and the basal area (BA), of considered stand. The main conclusion of this work was the possibility to obtain a model (adjusted R^2=0.75) which permitted to estimate the stand volume from medium spatial resolution satellite data. Moreover, the use of this model and with the support of digital ortophotographs allowed an estimated volume map to be obtained.

Key words: Forest inventory; remote sensing; conifer stand; volume mapping; unmixing

RESUMO

Informação advinda de imagens de satélite é uma importante fonte de dados para subsidiar o manejo dos recursos florestais.Técnicas de sensoriamento remoto têm propiciado informações de volume, biomassa e outros parâmetros biofísicos de povoamentos florestais. Nesse contexto, o principal objetivo deste trabalho é mapear, a partir de dados do sensor Thematic Mapper/ LANDSAT, o volume contido em povoamentos de coníferas, utilizando para tal a técnica de modelo de mistura espectral (SMA). Imagens-fração derivadas do modelo de mistura espectral mostram propriedades biofísicas mais facilmente que as bandas originais por representar melhor os aspectos físicos da cobertura do terreno. A área de estudo selecionada corresponde a região de El Alto Valle del Ebro (Espanha), com dimensão de 50km x 50km,cuja imagem de satélite é datada de 13/07/1996. No procedimento metodológico foram adotados três principais passos: 1) a aplicação do modelo de mistura espectral a partir das bandas originais TM 3, 4, 5 e 7 (as mais empregadas em estudos de vegetação) gerando imagens sintéticas;2) as componentes-fração “vegetação”, “solo”e “sombra” dessas imagens sintéticas foram relacionadas com a variável de volume com casca (OBV), cujos dados foram extraídos do II Inventário Florestal Nacional da Espanha – NFI2-, a partir de técnicas de regressão e análise multivariada; 3) um mapa de volume foi obtido através de técnicas de interpolação, usando dados de modelo alométrico e de área basal. A principal conclusão desse trabalho relata a possibilidade de obtenção de um modelo matemático (R2 ajustado de 0,75) que permite estimar o volume florestal a partir de imagens satelitárias de média resolução espacial. A utilização do modelo desenvolvido com subsídio de informações derivadas de ortofotos digitais permitiu elaborar um mapa de volume estimado.

Palavras-chave: Inventário florestal; sensoriamento remoto; povoamento de coníferas; mapeamento de volume; mistura espectral

INTRODUCTION

The woody volume of a forest stand is such an important parameter that any extraction without this being known is simply not viable and the sustainable management of forests would be impossible. (STELLINGWERF e HUSSIN, 1997). The classical way to quantify forest stand volume was by using volume tables with one or more entries. However, in the last few decades, the stand volume has been quantified by regression models based on aerial photographs. At present various forestry agencies use remote sensed images, in addition to aerial photographs, to detect, identify, classify, evaluate and measure the different forest covers and the changes produced in them.

Traditionally, spectral vegetation indices (Normalized Difference Vegetation Index, NDVI, specially) have been used to infer biophysical vegetation properties. For instance, Gong et al. (1995) found that NDVI and Leaf Area Index (LAI) were positively correlated with coniferous forest. However, other studies found that NDVI was not the best indicator: Elundh et al. (2001) found a weak correlation between LAI and NDVI; and Huete et al. (1997) indicated that NDVI spectrally saturated over forested areas and was sensitive to canopy background reflectance change. The use of fraction images, derived from Spectral Mixture Analysis (SMA), can offer an alternative to applying a variety of spectral indices and correlations with measured leaf and crown-based attributes.

SMA procedure was used in this study to transform the original image and then regression analysis was used to relate the obtained fraction images with the Over Bark Volume OBV (m3/ha.) extracted from the data of the Second Spanish National Forest Inventory (NFI2). Fraction images from spectral unmixing show biophysics properties more easily than original bands because they represent physics aspects of ground covers. Thus, the main objective of this study was to evaluate the utility of SMA and to quantify the volume of a stand of *Pinus sylvestris* L. from Landsat Thematic Mapper (TM) images in Mediterranean areas.

STUDY AREA

The study area was the Upper Ebro Valley Burgos and Álava (Spain), and the surface area studied was 952 km2. The climate in the Upper Ebro Valley corresponds to inland mid-mountain areas, and is characteristic of transition zones between the Atlantic and the Mediterranean with hot, dry summers and winters with abundant snowfall. The tree covered area constitutes more than 58% of the total forest area, highlighting Scots pine stands (*Pinus sylvestris* L.)

METHODOLOGICAL APPROACH

The satellite information used in this study came from a Landsat TM mini-scenes, (50x50 km), acquired on 13th July 1996. The relationships between forest stand parameters and Landsat TM spectral responses were showed in different scientific publications as Dengsheng et al. (2004), Mäkelä e Perkkarinen (2004), Santos et al. (1999), Magnusson e Fransson (2004).

The information on stand volume was taken from the Spanish NFI2 in the study area. The advantages of using the NFI2 plots instead of experimental ones are mainly: 1) the objectivity of the sampling of the forest stands; 2) the existence of a large quantity of data; 3) their homogeneity; and 4) the uniformity of their geographical distribution. Figure 1 shows the location of considered NFI2 plots.

Figure 1. Location of considered NFI2 plots

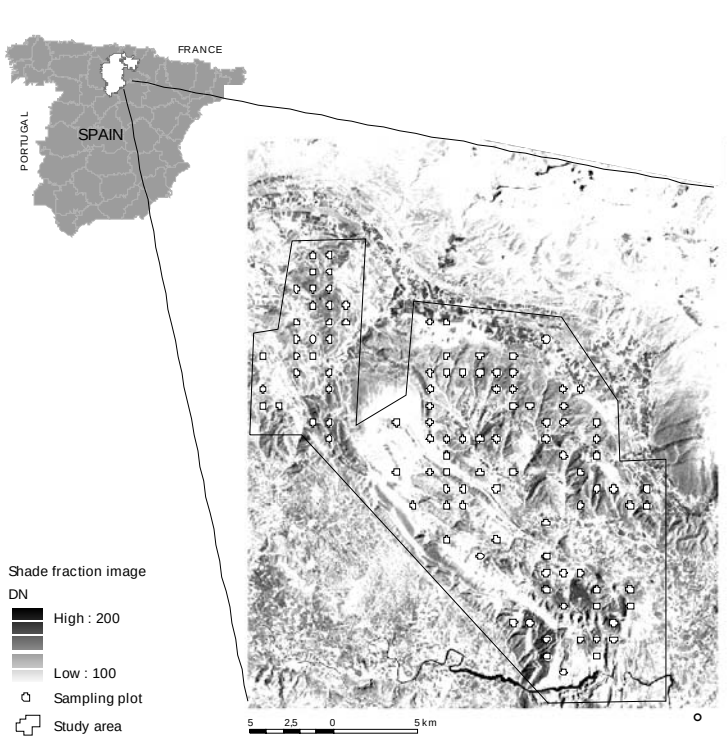

First at all, it was necessary to correct the images radiometrically and geometrically. Geometric correction needed Ground Points (GP) to be located on 1: 50 000 maps. A sampling linear transformation and the nearest neighbour were also used to obtain a geometrically corrected image with error < 1.5 pixels.

The conversion to reflectance values was considered unnecessary since an important behaviour of SMA is its invariance under linear transformations. Linear SMA assumes that pixel values are linear combinations of reflectances from a limited set of constituent elements, called endmembers. Each field on the scene contributes with a quantity of signal received on the sensor characteristic of the type of field cover and proportional to the area occupied within the pixel. In addition, the sum of these basic cover proportions must be the unit for each pixel. In this way the linear model is defined for each pixel of the image by the following equation:

$$x = Mf + e$$

where,

x: n-dimension digital-number vector;
M: n x c endmember spectra matrix;
n:is the number of bands used;
c:the number of endmembers;
f: c-dimension fraction vector;
e: n-dimension error vector, representing residual error.

On resolving the previously posed system of equations, a fraction image is obtained for each endmember defined which represents an estimate of the proportion of pixel occupied by that endmember. An image of error made in the transformation is also obtained.

The NFI2 data of interest for the work database were extracted using the BASIFOR program. This program allows the plot data complying with certain requisites established by the user to be extracted easily. (DEL RIO et al., 2001). The database was prepared for locating the relations between the satellite images and the forest stand parameters.

The analysis of multiple regression tries to establish an equation to define the existing relation between the dependent variable, 'y', (Over Bark Volume, OBV), and a set of independent variables, 'x1', 'x2', ..., 'xp', (fraction images). After defining the equations of regression, the R2 coefficient obtained was revised and an analysis of the residuals was carried out. In order to define the equation of regression only half of the available plots were used, reserving the other half for evaluating the equation obtained. Once the estimation model had been validated, it was applied to produce an estimated volume map.

RESULTS AND DISCUSSION

Before applying SMA, it was necessary to identify the endmember signatures, which had been extracted directly from the image (called image endmembers). Starting from the scatter plot it was possible to select the radiance intervals of the vegetation, shade and soil endmembers, identifying the purest pixels. (QUINTANO et al., 2005; QUINTANO et al., *in press*).

Once the unmixing was correctly performed and the fraction images were obtained (see Figure 2) a mean filter was applied (to minimize the possible registration error between the plots considered and the satellite image) and its digital value in the considered plots was extracted. A total of 107 plots in the July image were considered valid (53 for obtaining the estimate and 54 for verifying it).

Figure 2. Fraction images (13th July 1996)

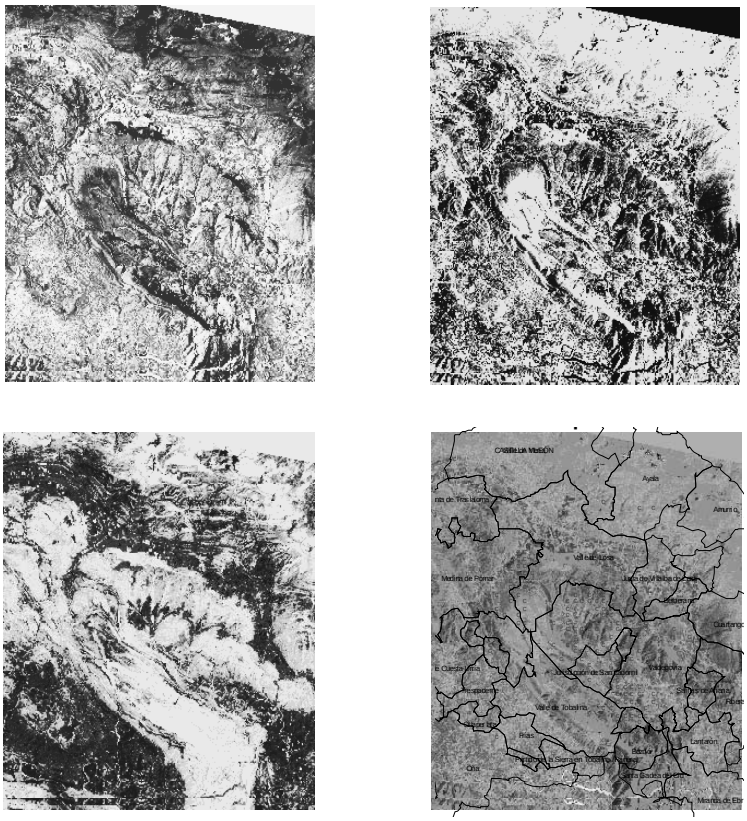

On analyzing the relationship between the fraction images and the OBV variable was observed a low correlation index (R2 = 0.34) between the shade image and OBV, but of great significance. The problem of the low correlation between satellite data

and forest parameters had already been recorded by other researchers. (AHERN et al., 1991; HYPPÄ et al., 2000). Trying to solve this problem, the data were first grouped depending on the OBV variable, as suggested by Ardö (1992), but on considering the rest of the plots not previously used, the estimation was seen to be not valid. Finally, an attempt was made to define the relation between these variables considering the different levels of volume existing, analyzing the behavior of each volume group defined independently. For a faster and clearer visualization these groups were defined by percentiles of 25%, 50%, 75% and 99% (low volume, medium volume, high volume, and very high volume, respectively) instead of by cluster analysis (Table 1 shows the considered volume groups).

Table 1. Volume groups

Volume Group	Average volume (m^3/ha)	Plots considered
Low volume	55.3	13
Médium volume	93.7	13
High volume	130.6	13
Very high volume	221.9	14

After this stage the regression between the stand volume and the fraction images was done group by group, obtaining a R2 equal to 0.913 and an adjusted R2 equal to 90.51 (p-value < 0.001).

In order to validate the analysis carried out, the 54 plots not used so far were employed. On this occasion, the Pearson coefficient of correlation between the observed and estimated volumes was 0.89 with a high level of significance (p-value < 0.0001). Figure 3 shows the results on applying the expression obtained in the verification plots. The equation of regression finally obtained was:

$$\begin{aligned} OBV = & - 4.12 + 0.44 * shade \\ & + 33.14 * (GROUP\_OBV = \text{'medium volume group'}) \\ & + 70.06 * (GROUP\_OBV = \text{'high volume group'}) \\ & + 154.96 * (GROUP\_OBV = \text{'very high volume group'}) \end{aligned}$$

where,

GROUP_OBV = x is a logical variable which takes the value '1' when the value of considered OBV belongs to group 'x', and value '0' when it does not belong to that group.

Considering these results, it was possible to remark that: (1) there were good estimations when the volume not exceeded 200 m3/ha (very high volume); and (2) the

worst estimations were observed when the volume belonged to the "very high" volume group. These affirmations agree with the results obtained by researchers as Ardö (1992).

Figure 3. Observed vs. estimated volume

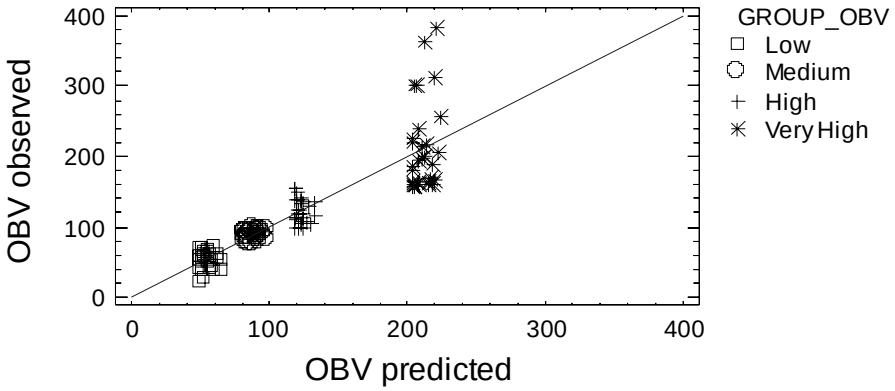

Figure 4. Estimated volume map

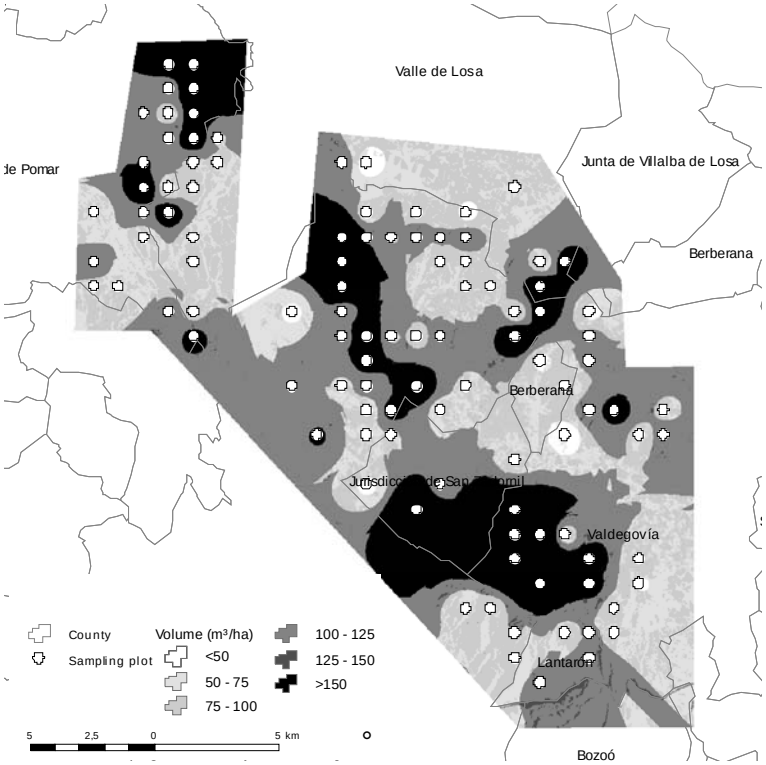

However, in spite of the good results obtained, this expression has practical limits as it does not allow the volume of a specific forest stand to be estimated unless certain knowledge of it is available. To minimize this problem, three steps were carried out:

1) the mass was stratified (considering the four volume groups before defined) by identification of different development levels on digital orthophotographs; 2) the model was applied to the shade fraction image to obtain the estimated volume, considering the volume groups defined in step 1; and 3) the estimated volume image was reclassified considering six volume classes with 25m3/ha intervals (Figure 4) (these classes are the common classes used by the Spanish Forestry System.

CONCLUSIONS

Bearing in mind the results obtained, the main conclusion of this study was to validate the utility of using SMA and regression techniques for quantifying the volume of a stand of *Pinus sylvestris* L. from Landsat TM images working in Mediterranean environments. To improve the way of obtaining the volume map, we are working in automating the digital orthophotographs stratification process by means of object oriented classification. The digital map produced can be integrated as a new source of data in the Information System of the regional forestry administrative authority.

REFERENCES

AHERN, F.J.; ERDLE, T.; MACLEAN, D.A.;KNEPPECK, I.D.A quantitative relationship between forest growth rates and Thematic Mapper reflectance measurements. *International Journal of Remote Sensing*, v.12, n.3, p. 387 400, 1991.

ARDÖ, J. Volume quantification of coniferous forest compartments using spectral radiance recorded by Landsat Thematic Mapper. *International Journal of Remote Sensing*,v. 13, p. 1779 1786, 1992.

DEL RIO, M.; RIVAS, J.; CONDES, S.; MARTÍNEZ MILLÁN, J.; MONTERO, G.; CAÑELLAS, I.; ORDÓÑEZ, C.; PANDO, V.; SAN MARTÍN, R.; BRAVO, F.BASIFOR: Aplicación informática para el manejo de bases de datos del segundo inventario forestal nacional. In: III CONGRESO FORESTAL ESPAÑOL, Granada, Spain, 25-28 Sept., 2001. Proceedings.[CD-ROM]

DENGSHENG, L.; MAUSEL, P.; BRONDÍZIO, E.; MORAN, E. Relationships between forest stand parameters and Landsat TM spectral responses in the Brazilian Amazon Basin. *Forest Ecology and Management*, v. 198, p. 149–167, 2004

EKLUNDH, L.; HARRIE, L.; KUUSK, A. Investigating relationships between Landsat ETM+ sensor data and leaf area index in a Boreal conifer forest. *Remote Sensing of Environment*, v. 78, p. 39–251, 2001

GONG, P.; PU, R.; MILLER, J.R. Coniferous forest leaf area index estimation along the Oregon transect using Compact Airborne Spectrographic Imager Data. *Photogrammetric Engineering and Remote Sensing*, v. 61, p. 1107–1117, 1995

HUETE, A.R.; LIU, H.Q.; BATCHILY, K.; VAN LEEUWEN, W. A. Comparison of vegetation indices over a global set of TM images for EOS-MODIS. *Remote Sensing of Environment*,v. 59, p. 440–451, 1997.

HYPPÄ, J.; HYPPÄ, H.; INKINEN, M.; ENGDHL, M.; LINKO, S.; ZHU, Y. Accuracy comparison of various remote sensing data sources in the retrieval of forest stand attributes. *Forest Ecology and Management*,v. 128, p. 109 120, 2000.

MAGNUSSON, M.; FRANSSON, J.E.S. Combining CARABAS-II VHF SAR and Landsat TM satellite data for estimation of forest stem volume. In: INTERNATIONAL GEOSCIENCE AND REMOTE SENSING SYMPOSIUM – IGARSS'04, Anchorage, Alaska, 20-24 Sept., 2004. Proceedings, p. 2327-2331. [CD-ROM]

MÄKELÄ, H.; PEKKARINEN, A.Estimation of forest stand volumes by Landsat TM imagery and stand-level field - Inventory data. *Forest Ecology and Management*, v. 196, p. 245–255, 2004

QUINTANO, C.; SHIMABUKURO, Y.E.; FERNÁNDEZ-MANSO, A.; DELGADO, J.A. A spectral unmixing approach for mapping burned areas in Mediterranean countries. *International Journal of Remote Sensing*. v. 26, p.1493-1498, 2005.

QUINTANO, C., FERNÁNDEZ-MANSO, A., FERNÁNDEZ-MANSO, O., SHIMABUKURO, Y.E.Mapping burned areas in Mediterranean countries using Spectral Mixture Analysis from a unitemporal perspective. *International Journal of Remote Sensing*, (*in press*).

SANTOS, J.R.; PARDILACRUZ, M. S.; KEIL, M.; KRAMER, J.M.C.A lineal spectral mixture model to estimate forest and savanna biomass at transition areas in Amazonia. In: INTERNATIONAL GEOSCIENCE AND REMOTE SENSING SYMPOSIUM – IGARSS'99, Hamburg, Germany, 28 June - 2 July, 1999. Proceedings, p.753-755.[CDROM].

STELLINGWERF, D.A.; HUSSIN, A. *Measurements and estimations of forest stand parameters using remote sensing*. Ed. VPS; Utrecht, The Netherlands, 1997. pp. 273. (ISBN 90-6764-251-7)